

**SPATIOTEMPORAL DYNAMICS OF BIOGEOCHEMICAL REACTIONS
IN AN INTERTIDAL BEACH AQUIFER:
A FIELD, LABORATORY, AND NUMERICAL MODELING STUDY**

by

Kyra Han Kyul Kim

A dissertation submitted to the Faculty of the University of Delaware in partial fulfillment of the requirements for the degree of Doctor of Philosophy in Geology

Summer 2019

© 2019 Kyra Han Kyul Kim
All Rights Reserved

ProQuest Number:22583485

All rights reserved

INFORMATION TO ALL USERS

The quality of this reproduction is dependent upon the quality of the copy submitted.

In the unlikely event that the author did not send a complete manuscript and there are missing pages, these will be noted. Also, if material had to be removed, a note will indicate the deletion.



ProQuest 22583485

Published by ProQuest LLC (2019). Copyright of the Dissertation is held by the Author.

All rights reserved.

This work is protected against unauthorized copying under Title 17, United States Code
Microform Edition © ProQuest LLC.

ProQuest LLC.
789 East Eisenhower Parkway
P.O. Box 1346
Ann Arbor, MI 48106 – 1346

**SPATIOTEMPORAL DYNAMICS OF BIOGEOCHEMICAL REACTIONS
IN AN INTERTIDAL BEACH AQUIFER:
A FIELD, LABORATORY, AND NUMERICAL MODELING STUDY**

by

Kyra Han Kyul Kim

Approved: _____
Neil C. Sturchio, Ph.D.
Chair of the Department of Geological Sciences

Approved: _____
Estella A. Atekwana, Ph.D.
Dean of the College of Earth, Ocean, and Environment

Approved: _____
Douglas J. Doren, Ph.D.
Interim Vice Provost for the Office of Graduate and Professional
Education and Dean of the Graduate College

I certify that I have read this dissertation and that in my opinion it meets the academic and professional standard required by the University as a dissertation for the degree of Doctor of Philosophy.

Signed:

Holly A. Michael, Ph.D.
Professor in charge of dissertation

I certify that I have read this dissertation and that in my opinion it meets the academic and professional standard required by the University as a dissertation for the degree of Doctor of Philosophy.

Signed:

William J. Ullman, Ph.D.
Member of dissertation committee

I certify that I have read this dissertation and that in my opinion it meets the academic and professional standard required by the University as a dissertation for the degree of Doctor of Philosophy.

Signed:

Wei-Jun Cai, Ph.D.
Member of dissertation committee

I certify that I have read this dissertation and that in my opinion it meets the academic and professional standard required by the University as a dissertation for the degree of Doctor of Philosophy.

Signed:

Scott D. Wankel, Ph.D.
Member of dissertation committee

ACKNOWLEDGMENTS

The writing of this dissertation and completion of this degree would not have been possible without the help of many people along the way.

Holly, I am very lucky and grateful that you were my advisor. You have led-by example on how to be hard-working, creative, and patient. I have come to you with many problems and you have always dealt them with grace, whether academic- or life-related. I hope to become a scientist like you someday, with the same brilliance, professionalism, and warmth.

Bill, you have truly been my parent away from home. I was blessed to have your enthusiasm and care during my degree. Your countless hours in the field saying, “Kyra is the real boss here, I just do what she tells me to do,” has taught me to be a fun, self-less, and fully-serving academic for my future students.

Thank you to my committee members Drs. Wei-Jun Cai and Scott Wankel – thank you for your scientific inputs and your willingness to participate in this journey. Dr. Cai, thank you for all the opportunities you have offered my way and for always being so responsive to my ideas. Scott, I am glad to have you as my committee member, for even over our short interactions, your personality always challenged me to be an understanding, kind person.

Fieldwork for my dissertation was physically taxing, and many volunteered to help ease the load – without your help, it would have been so much tougher on the field and certainly less enjoyable: Haley Glos, Christopher Russoniello, Kaileigh Scott, James Heiss, Carlos Duque, Katie Li, James Hanes, Sam Dever, Eric Lunn,

Fang Tan, Veronique Oldham, Chris Grasso, Emily Ruhl, Corie Charpentier, Mikaela Kropp, Luke Frankel, Harrison Smith, Matthew Dunn, Tobias Hasse, Trevor Metz, Tye Pettay, Julia Guimond, Gengxiao (Leo) Leng, Lane Johnston, Shae Timmons, Matthew Doelp, Mark Lundine, Timothy Pilegard, Joe Gradone, and Zac Duval.

Thank you for volunteering so much of your time.

I am also indebted to the scientific input, training, and help of many, especially those who went above and beyond what they were asked to do: Janis Lopez, Jeanette Miller, Tye Pettay, Chris Sommerfield, Joanna York, Clara Chan, Jennifer Biddle, Todd Kana, Timothy Deering, Matt Cottrell, Mark Jolly, and Estella & Eliot Atekwana. James, Chris, Leo, and Asia – thank you for being such a great friend, mentor, and collaborator, with your brilliance, patience, and sense of humor. Matt Oliver – you have been the most inspiring mentor in my life, often challenging my ideas, attitude, and vision on life and human relationships. I truly cannot wait to become a thought giant like you.

My work and responsibilities were split between two cities, and I could not have continued my work without the generosity of friends that helped in various ways: Asia Downtin, Mei Johnson, Guy Fox, Joe Brodie & Yiben Wang, James Heiss, Veronica & Donald, and Julia Guimond. A special thanks goes to Gideon & Sara for being so reliable during all the countless trips I made up and down DE Route 1.

There are many friends that listened to me in distress, celebrated and grieved with me, came to support my singing, and made me laugh throughout troubles small and large – I thank you all: Corie Charpentier, Andrew Joesoef, Veronique Oldham, Julia Hagemeyer, Danielle Haulsee, Heather Cronin, Jason Button, Timothy Pilegard, Chris Grasso, Andrew Franca, Cassandra Harris, Matthew Vaughan, Taylor Deemer,

Kate Hudson & Walt Greydan, Guy Fox, Nikodimos Gebreselassie, Tianhang Gao, Quontana Clarke, Keith & Autumn Straume, Ashlee & Eric Rolkowski, Jaime & Greg Welch, Katie & Burt Miller, Colleen & Andy Maglione, Brittany & Mark Dickey, Zack & Marissa Murr, and many others from the Daiberhood, BGSA, GSG, and Solid Ground. I also thank the families that taught me more about life by letting me into theirs: Lori & Mike, the Rodis, the Olivers, the Cohens, the Petrones, the Biddles.

The legacy that I build mine upon was not free nor easy. I think often to how my dad finished his Ph.D., not long after the recent passing of his father and my newborn-self tugging him away from his professorial dreams. Thank you to my parents for being silently patient, loving, and self-less from afar during my moments of impatience and immaturity. Appa, I truly hope that I grow to be a person of the same integrity, inner strength, endurance, and wisdom as you are. Umma, you challenge me to always seek truth, and be creative and zealous in its approach. Han Young, you are the greatest source of my laughter and I am blessed to have you as a friend and sister. Pyeong-gang, though you are no longer with us, you've shown us how to love unconditionally, trust loyally, and enjoy wholeheartedly. We all miss you very much.

This dissertation is dedicated to my two grandfathers, one that I never met, and one that departed the world in 2018, after loving me very much even through the battles of Alzheimer's.

TABLE OF CONTENTS

LIST OF TABLES	x
LIST OF FIGURES	xi
ABSTRACT	xvi
Chapter	
1 INTRODUCTION	1
1.1 Hydrogeochemical Dynamics of Coastal Aquifer Intertidal Zones	1
1.2 Spatiotemporal Characteristics of Intertidal Biogeochemical Reactions ..	3
1.3 Broader Significance	5
REFERENCES	7
2 SPATIAL PATTERNS OF GROUNDWATER BIOGEOCHEMICAL REACTIVITY IN AN INTERTIDAL BEACH AQUIFER	14
2.1 Introduction	16
2.2 Study Area Description and Methodology	20
2.2.1 Study Area	20
2.2.2 Pore water and Particulate Analysis	21
2.2.3 Spatial Characterization of Pore water Reactivity.....	23
2.2.4 Groundwater Flow and Reactive Transport Model	25
2.3 Results	28
2.3.1 In Situ Pore Water Measurements.....	28
2.3.2 Incubation O ₂ , N ₂ Measurements	35
2.3.3 Reactive Transport Model Results	36
2.4 Discussion.....	40
2.5 Conclusions	45
REFERENCES	46

3	HYDROLOGIC SHIFTS CREATE COMPLEX TRANSIENT DISTRIBUTIONS OF PARTICULATE ORGANIC CARBON AND BIOGEOCHEMICAL RESPONSES IN BEACH AQUIFERS.....	53
3.1	Introduction	55
3.2	Field site and Methods.....	59
3.2.1	Field Site.....	59
3.2.2	Porewater Sampling and Incubation Experiments	60
3.2.3	Sediment Vibracores	62
3.2.4	Sand Column Deployments	62
3.3	Results	63
3.3.1	Physicochemical Parameters	63
3.3.2	Dissolved Nutrients	65
3.3.3	Porewater Reaction Rates.....	67
3.3.4	Spatial Distributions of Porewater POC, DOC, and Sedimentary Carbon	69
3.4	Discussion.....	75
3.4.1	Seasonal Dynamics of Salinity, Nutrient Distributions, and Reaction Characteristics	75
3.4.2	Carbon Pool Distributions and Dynamics	76
3.4.3	Nutrient Release and Leaching Dynamics	81
3.5	Conclusions	83
	REFERENCES	85
4	TRANSIENT CONTRIBUTIONS OF RETARDED PARTICULATE ORGANIC CARBON TO NITRATE REMOVAL IN BEACH AQUIFERS. 92	
4.1	Introduction	94
4.2	Numerical Simulations	98
4.2.1	Phase I: Groundwater Flow, Salt Transport, and Retarded POC Transport Model	99
4.2.2	Phase II: Reactive Transport Model	101
4.2.3	Sensitivity Analysis	102
4.2.4	Spring-Neap Transience Model.....	104
4.3	Results	104

4.3.1	POC and Reactivity Distribution – Base Case	104
4.3.2	Phase I: Spatial Distributions of POC and Nitrate Removal	106
4.3.3	Temporal Variations in POC Contributions	108
4.3.4	Phase II: Carbon Characteristics and their Impacts on Nitrate Removal.....	110
4.3.5	Phase II: Hydraulic Conductivity and Tidal Amplitude on POC Utilization	112
4.4	Discussion.....	115
4.4.1	Contributions of POC in a Dynamic Beach Environment.....	115
4.4.2	Model Assumptions of POC Chemical Characteristics.....	117
4.5	Conclusions	119
REFERENCES		121
5	CONCLUSIONS	129
5.1	Spatial Characteristics of Beach Aquifer Reactions.....	129
5.2	Reactive Particulate Organic Carbon Dynamics within Beach Aquifers	131
5.3	Particulate Carbon Contributions to Beach Biogeochemical Reactions	131
5.4	Implications	132
5.5	Recommendations for Future Work	134
REFERENCES		139
Appendix		
A	SUPPLEMENTARY MATERIALS FOR CHAPTER 2	142
B	SUPPLEMENTARY MATERIALS FOR CHAPTER 3	145
C	SUPPLEMENTARY MATERIALS FOR CHAPTER 4	148
D	COPYRIGHT INFORMATION	152

LIST OF TABLES

Table 2.1	Reaction Network and Kinetic Rate Expressions (Adopted from Bardini et al. [2012])	38
Table 2.2	Reaction Parameter Values	38
Table 4.1	Reaction network and kinetic rate expressions (adopted from Bardini et al., 2012 & Heiss et al., 2019)	101
Table 4.2	Parameter values used for the Base Case model and range of parameter values used for sensitivity analyses.....	102
Table A-1.	Data from the Cape Shores, Lewes, DE site, collected 08 and 10 September 2014. Data is organized by multi-level porewater sampler locations (A~G, refer to Figure 2.1), numbered by depth. x indicates distance from benchmark, y height above mean sea level. Abbreviated parameters are as follows: oxidation-reduction potential (ORP), dissolved oxygen (DO), particulate carbon (PC), dissolved inorganic carbon (DIC), particulate nitrogen (PN), and particulate phosphorus (PP). Refer to Section 2. Methods for details on data collection.	143
Table B-1.	Grainsize, D10 grainsize (10% percentile particle diameter), organic matter content, and oxygen consumption rates for Core C and Core F samples from July 2015 (location highlighted in Figure 3.3). Grainsize description from: Folk, R. L., and W. C. Ward [1957], Brazos River bar (Texas); a study in the significance of grain size parameters, Journal of Sedimentary Research, 27(1), 3-26, https://doi.org/10.1306/74D70646-2B21-11D7-8648000102C1865D .	146
Table C-1.	Tidal constituents used for fully transient circulation cell case.	149
Table C-2.	Parameters used for retardation equation. $K_d = 0.1$ is used in the base case simulation, but is varied across cases to increase the retardation factor.....	149

LIST OF FIGURES

- Figure 2.1 Schematic diagram of the intertidal circulation cell and the positions of multilevel pore water samplers (A–G) at Cape Shores. Each gray line indicates location of sampler and dark gray boxes indicate the approximate position and spacing of water sampling ports. Infiltration of saline seawater into the fresh groundwater creates a reactive intertidal circulation cell. Biogeochemical activity within this cell is supported by reactive organic carbon and oxygen originating from the infiltrating seawater. 16
- Figure 2.2 Map of the field site and sampling transect, Cape Shores, Lewes, Delaware, USA. 20
- Figure 2.3 Cross-sectional distributions of measured constituents. Black solid lines delineate surface topography. Dashed lines indicate mean high water, mean sea level, and mean low water (flush with topography). Multilevel pore water samplers are labeled in Figure 2.3a, with black dots indicating sampling locations. Yellow contours in Figures 3d, 3f–3i, 3k, and 3l (black in Figure 2.3h) are salinity (5, 15, and 20, labeled in Figure 2.3d), while white contours (Figures 2.3b, 2.3j, 2.3m, and 2.3n) show chlorophyll a (Figure 3e). Hot spot of chlorophyll is indicated with a star. Figures 2.3i and 2.3l (in bold) are from incubation results, while Figures 2.3a–2.3h, 2.3j, 2.3k, and 2.3m–2.3o are in situ measurements or calculations. 29
- Figure 2.4 Dissolved oxygen deficit from in situ measurements. All measured DO values are less than the normal atmospheric equilibrium concentration (NAEC) values of DO at its respective salinity and temperature and fall below the zero line (blue solid line). Measurements also all fall below the conservative mixing curve (gray dotted line), except for one sample that was taken from the most landward edge of the intertidal circulation cell at Sampler C. Black vertical arrow highlights rapid depletion of oxygen at high salinities. ... 31
- Figure 2.5 Salinity versus dissolved inorganic carbon. Dotted line indicates conservative mixing curve. 33

Figure 2.6	Total alkalinity versus dissolved inorganic carbon, in $\mu\text{mol/kg}$. Dotted line indicates a 1:1 line.....	34
Figure 2.7	Measured (1) and modeled (2) distributions for (a) salinity, (b) dissolved oxygen, (c) nitrate, and (d) N_2 in the intertidal beach aquifer at Cape Shores, DE. The flow vectors in Figure 2.7a-2 show the tidally averaged flow direction and magnitude. The horizontal dotted lines in both panels are MHHW and MSL. MLLW is contiguous with the topography at the base of the beachface. The modeled 1, 10, and 20 salinity contours are shown in Figures 2.7b-2, 7c-2, and 7d-2.	36
Figure 2.8	Relationship between chlorophyll and particulate carbon (PC) concentrations, and dissolved oxygen saturation.	41
Figure 3.1	Cross-sectional schematic of a coastal beach aquifer. Fresh groundwater discharges seaward, meeting the convectively-circulating seawater at the lower interface. Wave and tide action deliver seawater to the beachface, which then infiltrates into the aquifer creating and sustaining the intertidal circulation cell. Porewater sampling ports are indicated in black squares on the multi-level samplers (A-G). Fresh groundwater transports terrestrial nutrients (NO_3^- , PO_4^{3-} , and Si) while seawater delivers reactive organic carbon and oxygen. Modified from Kim et al. [2017].	55
Figure 3.2	Time-series of hourly tide levels, freshwater head, and precipitation. Grey lines indicate recorded tides at the nearby NOAA tidal station 8557830, with full moon indicated by open circles. Precipitation from NOAA Georgetown Sussex County Airport Station (GHCND: USW00013764) is marked in blue bar graph, and sampling events are indicated in red.	60
Figure 3.3	Cross-sectional interpolations of measurements of salinity, dissolved oxygen saturation (%), and oxidation-reduction potential (mV). Black dots indicate sampling locations. Salinity contours (15, 20, 25) are overlain in yellow or black to show position of the intertidal circulation cell. Zones of seawater infiltration are indicated with black arrows. Locations of vibracores (C, F) taken in July 2015 are indicated with a rectangle. Note colorbar variation for ORP.....	65
Figure 3.4	Cross-sectional distributions of dissolved nutrients. Salinity contours (15, 20, 25) are overlain in yellow for reference. Note changing colorbar for phosphate.....	67

Figure 3.5	Distribution of oxygen consumption rates and denitrification rates. Note changing colorbar.	68
Figure 3.6	Distributions of porewater POC and DOC. Note that DOC scale is % seawater DOC and goes above 100%. DOC was not measured for September 2014.	71
Figure 3.7	Retrieved sand column sediments with a fine layer of grey particles (left column, control on left and retrieved sample on right) and microscopic images of cells and algal fragments found (right column). Green autofluorescence (520~560 nm) was observed in the material (right column, bottom).	72
Figure 3.8	Cross-sectional distribution of oxygen consumption rates from i) vibracore sediment samples, in green circles (samples taken 16 July 2015); and ii) sand column deployment samples, in red circles (samples deployed 31 July 2015 and retrieved 13 October 2015). Circle sizes reflect the magnitude of respiration rates, indicated in numbers. Porewater POC distribution from 08 July 2015 is shown in greyscale for reference, with open circles indicating porewater sampling locations.	74
Figure 3.9	Conceptual diagram of carbon movement within the intertidal beach aquifer. Groundwater flow in the current hydrologic condition (a) transports marine DOC and particulate carbon (POC) (i), which can become entrapped along the flowpath as it moves through the sediments (i to ii). POC actively leaches DOC (iii). Porewater POC is sampled with porewater, representing mobile POC and/or some component of immobile POC mobilized by sampling (iv). Entrapped POC from a previous hydrologic condition (b) can appear as a hotspot (v) under current conditions.	77
Figure 3.10	Nutrient release over time during Sand Column C-2 sample incubation. Oxygen and nitrate decrease over time, while ammonium increases after ~70 h. While for other more reactive samples, changes in nutrients occurred around hour 24 or 48, more refractory samples such as above did not show changes until hour 70.	81

Figure 3.11	Cross-sectional distributions of porewater POC, DOC, PP, phosphate, and PN from July 2015. DOC is presented in % DOC of surface water concentrations, and the ‘supersaturated’ areas are spatially correlated to elevated areas of porewater POC. PP, phosphate, and PN also follow this pattern, indicating active leaching dynamics within the aquifer. Salinity contours are shown in porewater POC panel for reference.	83
Figure 4.1	Schematic diagram of particulate organic carbon contributions to biogeochemical reactions within intertidal zone of aquifers. Panel A: Marine POC is delivered to the aquifer through seawater infiltration during wave and tide activity (solid lines). Transient hydrology moves the salinity distribution (red arrows to dotted lines), but the pool of POC is retarded relative to groundwater advection. Panel B: Retarded POC is able to support reactions, such as denitrification, outside the saline groundwater flowpath. Panel C: As hydrologic conditions change to have saline water encompass the pool of POC, denitrification is heightened towards the end of the flowpath where conditions are anoxic, and the hotspot of N ₂ gas production is moved to the back of the circulation cell.	94
Figure 4.2	Numerical model schematic showing boundaries and fluxes.	98
Figure 4.3	Solute distributions for base case scenario at day 130. Black dotted line indicates location of POC, white solid line indicates salinity 10. Top four panels shown are when POC was the sole source of carbon to the aquifer. The last panel shows N ₂ gas production from NO ₃ ⁻ via denitrification when both POC and DOC are present as carbon sources.	105
Figure 4.4	Distribution of POC with different $K_d (R)$ values and resulting NO ₃ ⁻ removal for day 130. The total mass of POC is constant across model cases. Greater retardation (higher K_d) and consequently higher R results in a more elongate POC distribution. Areal extent [m ²] and total NO ₃ ⁻ removal [μM] increased with increasing K_d	106

Figure 4.5	POC distribution from different tidal amplitudes. Total POC mass for all cases was held constant (10 mg). With increasing tide amplitudes of deposition, POC was more expansively distributed. Area above 0.01 μM is calculated and indicated [m^2]. Dotted line indicates sea-level at the time of distribution. Because the distribution is the result of previous infiltration, advection, and retardation, the sea-level does not exactly correlate with shown distributions. NO_3^- removal for day 130, increasing with increasing tidal amplitude of POC deposition, is shown in the right panels.	108
Figure 4.6	Temporal variations in POC contributions to denitrification. White text (upper panels) and solid red circles (lower panel) indicates days shown, yellow dashed line the extent of the circulation cell at salinity 25, green dashed line the extent of POC. Lower panel shows simulated tidal signal with the amplitude of the principle lunar tidal constituent at 0.6 m (black line) and % of freshwater-saltwater mixing zone area that has conditions favorable for denitrification (overlaps POC and has less than the threshold concentration for oxygen (31.2 μM)).	110
Figure 4.7	Damköhler number over time for a range of carbon reactivity values. Due to the changing saltwater volume in the system over time, model case with reactivity of $7.0 \times e-7$ (blue) swings between advection-limited ($\text{Da} > 1$) and rate-limited ($\text{Da} < 1$).	111
Figure 4.8	50% NO_3^- contour for day 170 (spring tide, black dashed lines) and 190 (neap tide, red dashed lines) for $K = 5, 10, \text{ and } 15 \text{ m/d}$. POC is indicated in green. The difference in exposure area between the two days are shown. NO_3^- removal for day 190 during neap tide is shown in lower panels D-F.	113
Figure 4.9	Effects of tidal amplitude ($\text{TA} = 0.3, 0.4, 0.5, 0.6, 0.7, 0.8 \text{ m}$) on nitrate removal within the intertidal zone. A-F: POC is indicated in green. 50% NO_3^- contour during maximum nitrate removal is shown (day 200, black dashed line), and exposure area is presented. G: Nitrate removal over time by tidal amplitude.	115
Figure B-1.	Salinity vs. Dissolved Silica for September 2014. Silica production via dissolution occurs over a range of higher salinities.	147
Figure D-1.	Copyright license.....	153

ABSTRACT

The intertidal zone of coastal aquifers hosts biogeochemical reactions that alter the form and concentration of land-derived nutrients prior to their coastal discharge. The location and rate of reactions within the beach aquifer are dependent on groundwater flow patterns for the delivery and transport of reactants, which are highly dynamic due to transient hydrologic conditions. This dissertation focuses on spatially characterizing the relationship between groundwater flow and biogeochemical activity within the intertidal beach aquifer over various timescales.

A field, laboratory, and numerical modeling study investigated the spatial relationship between flow paths and chemical reactions over one sampling event. Aerobic respiration was primarily controlled by the infiltration and flow of oxic seawater, with high oxygen consumption rates near the seawater infiltration point and along the landward freshwater-saline water flowpath. Denitrification, on the other hand, progressively increased along the flowpath and to the discharge zone.

A two-year field and laboratory study of porewater revealed the transient and spatially-variable distribution of marine particulate organic carbon in the beach aquifer. Differential mobility of particulate and dissolved components led to a variable distribution of particulate carbon across the aquifer that diverged from salinity-indicated flow paths. This created reaction dynamics that deviated from salinity patterns, showing that reaction characteristics within the beach aquifer are not completely predictable based on groundwater advection alone.

A variable-density groundwater flow and a reactive solute transport model were linked to quantify the effects of retarded particulate carbon transport on the biogeochemical reactions of the aquifer. The pool of marine particulate carbon resulting from its retarded mobility intermittently supported denitrification when transient hydrologic conditions allowed for anoxic groundwater to move over its location. The study demonstrated that sediment-entrapped particulate organic carbon contributes to beach reactivity patterns and increases the denitrification potential of the aquifer beyond that previously considered.

These investigations collectively show that biogeochemical processes within beach intertidal zones are highly dynamic in time and space, influenced by, but often independent from physical hydrologic changes. These findings have noteworthy implications for quantification of chemical reactivity within beach systems over various timescales, and ultimately for the management of coastal chemical fluxes and budgets.

Chapter 1

INTRODUCTION

1.1 Hydrogeochemical Dynamics of Coastal Aquifer Intertidal Zones

Fresh groundwater discharge to coastal areas is an important transport pathway of terrestrial nutrients and solutes to the adjacent marine system. Concentrations of dissolved nutrients tend to be much higher in fresh groundwater compared to their riverine counterpart, making fresh groundwater an important and direct influence on marine ecosystem quality [Johannes, 1980; Moore, 1999; Moore, 2010; Simmons, 1992; Slomp and Van Cappellen, 2004; Valiela et al., 1990]. Changing land use and intensified anthropogenic activity in coastal areas have also increased terrestrial nutrient fluxes to nearshore environments, causing eutrophication, fish kills, and harmful algal blooms [Andersen et al., 2007; Ibánhez et al., 2013; Reay et al., 1992; Valiela et al., 1990; Vitousek et al., 1997]. Coastal water quality degradation further induces detrimental consequences on multiple fronts, including tourism, human health, and economy [Burak et al., 2004; Cloern, 2001; Diaz and Solow, 1999; Doney, 2010; Martínez et al., 2007; Smith et al., 1999; Viviani, 1992]. Therefore, understanding solute dynamics in coastal budgets and fluxes is critical for the management and preservation of fragile marine ecosystems.

Coastal fluxes of solutes and nutrients are influenced by biogeochemical reactions within the aquifer prior to coastal discharge. The intertidal zone of coastal aquifers has been shown to be particularly active in biogeochemical reactions due to freshwater (FW) and saline seawater (SW) mixing. Seawater is driven up on the

intertidal zone by waves and tides, infiltrating into the aquifer and onto the seaward-discharging freshwater. The seawater infiltration creates and sustains a distinct “intertidal circulation cell”, defined by the contrasting salinities of the two waterbodies [Heiss and Michael, 2014; Michael et al., 2005; Robinson et al., 1998; Robinson et al. 2006 & 2007]. Fresh groundwater and saline seawater respectively deliver different reactants to the intertidal circulation cell, supporting a range of biogeochemical reactions. These reactions have been observed along the land-ocean salinity gradient, and include 1) aerobic respiration [Anschutz et al., 2009; Charbonnier et al., 2013; Seidel et al., 2015], 2) nitrogen and phosphorus transformations [Hays and Ullman 2007; Kroeger et al., 2006; Kroeger and Charette, 2008; Loveless and Oldham, 2010; Santoro, 2010; Slomp and Van Cappellen, 2004; Ullman et al., 2003], 3) sulfate reduction [McAllister et al., 2015], and 4) other metal or contaminant reactions [Bone et al., 2006; Charette and Sholkovitz, 2002; Jung et al., 2009; Roy et al., 2013].

The intertidal circulation cell responds sensitively to various hydrologic forcing mechanisms, including freshwater flux [Heiss and Michael, 2014; Liu et al., 2016], tides [Abarca et al., 2013; Ataie-Ashtiani et al., 2001; Li et al., 1999; Michael et al., 2005; Robinson et al., 2006], waves [Bakhtyar et al., 2012; Boufadel et al., 2007; Xin et al., 2010; Xin et al., 2014], and precipitation [Yu et al., 2017]. These hydrologic conditions alter groundwater flow paths and mixing patterns within the circulation cell, altering its shape, location, and salinity distributions [Abarca et al., 2013; Heiss and Michael, 2014; Robinson et al., 2007; Santos et al., 2008]. However, while physical changes to groundwater flow patterns have been well-documented over various timescales (waves, tides, seasons), how these alterations to physical flow

conditions subsequently impact biogeochemical reactivity of the system and ultimately solute fluxes to coastal systems are unclear. Physical changes to groundwater flow influence the delivery and transport of reactants across the beach, which would in turn alter the location and magnitude of biogeochemical reactions within the intertidal zone. Therefore, it is critical to understand dynamic hydrology relates to changes in chemical reactions to better quantify solute fluxes to marine ecosystems.

1.2 Spatiotemporal Characteristics of Intertidal Biogeochemical Reactions

The spatial distributions and patterns of reactions depend in part on reactant delivery to a given location within the beach aquifer system. Due to its longer residence times, terrestrial fresh groundwater is often depleted in oxygen and labile organic carbon [Kim et al., 2017; Seidel et al., 2015]. Oxygen is the most thermodynamically favorable electron acceptor for redox reactions, therefore the influx of oxygen from oxic seawater is critical to aerobic respiration in beach aquifers. In organic-poor beach sands, reactive marine organic carbon is another key reactant that fuels biogeochemical reactions [Anschutz et al., 2009; Boudreau et al., 2001]. Therefore, the distribution patterns of these two reactants influence the spatial patterns of aerobic heterotrophic respiration, and indirectly other reactions down the redox gradient (i.e., denitrification, iron reduction, sulfate reduction).

Previous studies have determined spatial patterns of net reactions in the beach system by collecting surficial or cross-sectional porewater measurements across the beach and comparing concentrations of reduced reactants [Beck et al., 2017; Reckhardt et al., 2015; Seidel et al., 2015]. However, independent measurements of reaction rates have not been studied in relation to groundwater flow paths, which

would spatially elucidate the relationship between reactant delivery and reaction magnitudes across the beach system.

Carbon is a major driver of heterotrophic reactions and the associated consumption of available electron acceptors. Carbon distributions across the beach have also been studied to a limited extent. Though reactive marine carbon occurs in both dissolved and particulate forms, most previous work has solely focused on dissolved organic carbon, a mostly mobile form of labile carbon [Bardini et al., 2012; Heiss et al., 2017; Robinson et al., 2007; Seidel et al., 2015; Spiteri et al., 2008]. Particulate organic carbon, though molecularly more complex than dissolved organic carbon [Seidel et al., 2015], is still reactive and able to support biogeochemical reactions in these systems. Therefore, understanding the transport and distribution dynamic of particulate organic carbon is also a critical factor in exploring the spatiotemporal dynamic of biogeochemical reactions in beach systems.

In this dissertation, the spatial characteristics of reaction rates and reactive carbon are delineated across tidal, spring-neap, and seasonal timescales. Field investigations were used to understand reaction characteristics over tidal and seasonal timescales, while numerical models were employed to understand the effect of carbon distributions over spring-neap biogeochemical reactions.

Chapter 2 presents results from a field, laboratory, and numerical modeling study that maps rates of aerobic respiration and denitrification over one sampling event and relates these reactions to the groundwater flow paths for the concurrent hydrologic regime. Results show heightened aerobic respiration near the saline water infiltration point and along the flow path, with increasing denitrification towards the discharge point. Model results support the field and laboratory results.

Chapter 3 expands upon Chapter 2 and investigates the spatial distribution of reaction rates and reactive carbon over seasonal timescales using field and laboratory methods. The results display transport dynamics of particulate organic carbon that are retarded from the advective transport of fully mobile solutes (i.e., salt and nitrate), creating pools of reactive carbon interspersed within the aquifer. The results of Chapter 3 emphasize the importance of understanding the delivery and transport of various carbon forms in relation to groundwater flow and other reaction characteristics.

Chapter 4 employs a numerical model to quantify the biogeochemical effects of retarded particulate organic carbon on nitrate removal via denitrification. Results show that transient hydrologic conditions support transient hotspots of denitrification, as nitrate-rich fresh groundwater moves over the pool of particulate carbon. This further emphasizes that particulate carbon, previously largely disregarded in field and modeling studies, is an important carbon source to the beach system.

Chapter 5 synthesizes the results of Chapter 2-4, contextualizes the findings in a broader scope, and provides insight and recommendations for future research pursuits.

1.3 Broader Significance

Coastal areas are critical zones of economic and environmental activity [Carter, 1988; Costanza et al., 1997; Martínez et al., 2007; van der Meulen et al., 2004]. More than 40 % of the global population live on coastal areas, with 21 out of the 33 world's megacities situated on the coast [Burke et al., 2001; Martínez et al., 2007]. In coastal countries, 80 to 100 % of the population reside within 100 km of the coast line [Martínez et al., 2007]. Globally, the world benefits from the economic,

recreational, and environmental services of coasts, which collectively represent 77% of the global ecosystem services and natural capital [Costanza et al., 1997; Martínez et al., 2007]. Therefore, understanding the linkages between groundwater flow, reactant transport, and chemical reactions within beach aquifers hold important implications for the health and management of coastal systems worldwide.

REFERENCES

- Abarca, E., H. Karam, H. F. Hemond, and C. F. Harvey (2013), Transient groundwater dynamics in a coastal aquifer: The effects of tides, the lunar cycle, and the beach profile, *Water Resources Research*, 49, 1–16, <https://doi.org/10.1002/wrcr.20075>.
- Andersen, M. S., L. Baron, J. Gudbjerg, J. Gregersen, D. Chapellier, R. Jakobsen, and D. Postma (2007), Discharge of nitrate-containing groundwater into a coastal marine environment, *Journal of Hydrology*, 336 (1-2), 98-114, <https://doi.org/10.1016/j.jhydrol.2006.12.023>.
- Anschutz, P., T. Smith, A. Mouret, J. Deborde, S. Bujan, D. Poirer, and P. Lecroart (2009), Tidal sands as biogeochemical reactors, *Estuarine, Coastal, and Shelf Science*, 84, 84-90, doi:10.1016/j.ecss.2009.06.015.
- Ataie-Ashtiani, B., R. E. Volker, and D. A. Lockington (2001), Tidal effects on groundwater dynamics in unconfined aquifers, *Hydrol. Processes*, 15(4), 655-669, <https://doi.org/10.1002/hyp.183>.
- Bakhtyar, R., D. A. Barry, and A. Brovelli (2012), Numerical experiments on interactions between wave motion and variable-density coastal aquifers, *Coastal Engineering*, 60, 95–108, <http://doi.org/10.1016/j.coastaleng.2011.09.001>.
- Bardini, L., F. Boano, M. B. Cardenas, R. Revelli, and L. Ridolfi (2012), Nutrient cycling in bedform induced hyporheic zones, *Geochimica et Cosmochimica Acta*, 84, 47–61. <http://doi.org/10.1016/j.gca.2012.01.025>.
- Beck, M., A. Reckhardt, J. Amelsberg, A. Bartholomä, H. Brumsack, H. Cypionka, T. Dittmar, B. Engelen, J. Greskowiak, H. Hillebrand, M. Holtappels, R. Neuholz, J. Köster, M. Kuypers, G. Massmann, D. Meier, J. Niggemann, R. Paffrath, K. Pahnke, S. Rovo, M. Striebel, V. Vandieken, A. Wehrmann, and O. Zielinski (2017), The drivers of biogeochemistry in beach ecosystems: A cross-shore transect from the dunes to the low water line, *Marine Chemistry*, 190, 35-50, <http://dx.doi.org/10.1016/j.marchem.2017.01.001>.

- Bone, S. E., M. E. Gonneea, and M. A. Charette (2006), Geochemical cycling of arsenic in a coastal aquifer, *Environmental science & technology*, 40(10), 3273-3278, 10.1021/es052352h.
- Boudreau, B. P., M. Huettel, S. Forster, R. A. Jahnke, A. McLachlan, J. J. Middelburg, P. Nielsen, F. Sansone, G. Taghon, W. Van Raaphorst, I. Webster, J. M. Weslawski, P. Wilberg, and B. Sundby (2001), Permeable marine sediments: overturning an old paradigm, *EOS Transactions American Geophysical Union*, 82(11) 133-136, doi:10.1029/EO082i011p00133-01.
- Boufadel, M. C., H. Li, M. T. Suidan, and A. D. Venosa (2007), Tracer Studies in a Laboratory Beach Subjected to Waves. *Journal of Environmental Engineering*, 133, 722–732. [https://doi.org/10.1061/\(ASCE\)0733-9372\(2007\)133:7\(722\)](https://doi.org/10.1061/(ASCE)0733-9372(2007)133:7(722)).
- Burak, S. A., E. Dogan, and C. Gazioglu (2004), Impact of urbanization and tourism on coastal environment, *Ocean & Coastal Management*, 47 (9-10), 515-527, <https://doi.org/10.1016/j.ocecoaman.2004.07.007>.
- Burke, L., Y. Kura, K. Kassem, C. Revenga, M. Spalding, D. McAllister, and J. Caddy (2001), *Coastal ecosystems*, Washington, DC: World Resources Institute.
- Carter, R.W.G. (1988), *Coastal environments: an introduction to the physical, ecological, and cultural systems of coastlines*. London: Academic Press Limited.
- Charbonnier, C., P. Anschutz, D. Poirier, S. Bujan, and P. Lecroart (2013), Aerobic respiration in a high-energy sandy beach, *Marine Chemistry*, 155, 10-21, <http://dx.doi.org/10.1016/j.marchem.2013.05.003>.
- Charette, M. A., and E. R. Sholkovitz (2002), Oxidative precipitation of groundwater-derived ferrous iron in the subterranean estuary of a coastal bay, *Geophysical research letters*, 29(10), 85-1–85-4, doi:10.1029/2001GL014512.
- Cloern, J. E. (2001), Our evolving conceptual model of the coastal eutrophication problem, *Marine Ecology Progress Series*, 210: 223-253, doi:10.3354/meps210223.
- Costanza, R., R. d'Arge, R., De Groot, S. Farber, M. Grasso, B. Hannon, K. Limburg, S. Naeem, R. V. O'Neill, J. Paruelo, and R. G. Raskin (1997), The value of the world's ecosystem services and natural capital, *Nature*, 387 (6630), 253-260.
- Diaz, R. J. and A. Solow (1999), *Ecological and economic consequences of hypoxia*, Silver Spring, Maryland: NOAA Coastal Ocean Program.

- Doney, S. C. (2010), The growing human footprint on coastal and open-ocean biogeochemistry, *Science*, 328(5985), 1512-1516, doi: 10.1126/science.1185198.
- Hays, R. L., and W. J. Ullman (2007), Direct determination of total and fresh groundwater discharge and nutrient loads from a sandy beachface at low tide (Cape Henlopen, Delaware), *Limnology and oceanography*, 52(1), 240-247, doi:10.4319/lo.2007.52.1.0240.
- Heiss, J. W., and H. A. Michael (2014), Saltwater-freshwater mixing dynamics in a sandy beach aquifer over tidal, spring-neap, and seasonal cycles, *Water Resour. Res.*, 50, 6747–6766, doi:10.1002/2014WR015574.
- Heiss, J. W., V. E. Post, T. Laattoe, C. J. Russoniello, and H. A. Michael (2017), Physical controls on biogeochemical processes in intertidal zones of beach aquifers, *Water Resources Research*, 53(11), 9225-9244, <https://doi.org/10.1002/2017WR021110>.
- Ibáñez, J., P. Severino, C. Leote, and C. Rocha (2013), Seasonal enhancement of submarine groundwater discharge (SGD)-derived nitrate loading into the Ria Formosa coastal lagoon assessed by 1-D modeling of benthic NO_3^- profiles, *Estuarine, Coastal and Shelf Science*, 132, 56-64, <https://doi.org/10.1016/j.ecss.2012.04.015>.
- Johannes, R. E. (1980). Ecological significance of the submarine discharge of groundwater, *Marine ecol. prog. ser.*, 3(4), 365-373.
- Jung, H. B., M. A. Charette, and Y. Zheng (2009), Field, laboratory, and modeling study of reactive transport of groundwater arsenic in a coastal aquifer, *Environmental science & technology*, 43(14), 5333-5338, 10.1021/es900080q.
- Kim, K. H., J. W. Heiss, H. A. Michael, W. J. Cai, T. Laattoe, V. E. Post, and W. J. Ullman (2017), Spatial patterns of groundwater biogeochemical reactivity in an intertidal beach aquifer, *Journal of Geophysical Research: Biogeosciences*, 122(10), 2548-2562, <https://doi.org/10.1002/2017JG003943>.
- Kroeger, K. D., M. L. Cole, and I. Valiela, (2006), Groundwater-transported dissolved organic nitrogen exports from coastal watersheds, *Limnology and Oceanography*, 51(5), 2248-2261, <https://doi.org/10.4319/lo.2006.51.5.2248>.
- Kroeger, K. D., and M. A. Charette (2008), Nitrogen biogeochemistry of submarine groundwater discharge, *Limnology Oceanography*, 53(3), 1025–1039, doi:10.4319/lo.2008.53.3.1025.

- Li, L., D. A. Barry, F. Stagnitti, and J. Y. Parlange (1999), Submarine groundwater discharge and associated chemical input to the coastal sea, *Water Resources Research*, (35)11, 3253-3259, <https://doi.org/10.1029/1999WR900189>.
- Liu, Y., J. J. Jiao, and X. Luo (2016), Effects of inland water level oscillation on groundwater dynamics and land-sourced solute transport in a coastal aquifer, *Coastal Engineering*, 114, 347-360, <https://doi.org/10.1016/j.coastaleng.2016.04.021>.
- Loveless, A.M., and C.E. Oldham (2010), Natural attenuation of nitrogen in groundwater discharging through a sandy beach, *Biogeochemistry*, 98(1-3), 75–87, doi:10.1007/s10533-009-9377-x.
- Martínez, M. L., A. Intralawan, G. Vázquez, O. Pérez-Maqueo, P. Sutton, and R. Landgrave (2007), The coasts of our world: Ecological, economic and social importance, *Ecological Economics*, 63(2-3), 254-272, <https://doi.org/10.1016/j.ecolecon.2006.10.022>.
- McAllister, S.M., J.M. Barnett, J.W. Heiss, A.J. Findlay, D.J. MacDonald, C. L. Dow, G.W. Luther, H. A. Michael, and C.S Chan (2015), Dynamic hydrologic and biogeochemical processes drive microbially enhanced iron and sulfur cycling within the intertidal mixing zone of a beach aquifer, *Limnology and Oceanography*, 60, 329-345, doi: 10.1111/lno.10029.
- Michael, H. A., A. E. Mulligan, and C. F. Harvey (2005), Seasonal oscillations in water exchange between aquifers and the coastal ocean, *Nature*, 436(7054), 1145-1148, doi:10.1038/nature03935.
- Moore, W. S. (1999), The subterranean estuary: a reaction zone of ground water and sea water. *Marine Chemistry*, 65(1), 111-125, [http://dx.doi.org/10.1016/S0304-4203\(99\)00014-6](http://dx.doi.org/10.1016/S0304-4203(99)00014-6).
- Moore, W.S. (2010), The effect of submarine groundwater discharge on the ocean, *Annual review of marine science*, 2, 59-88, <https://doi.org/10.1146/annurev-marine-120308-081019>.
- Reay, W. G., D. L. Gallagher, and G. M. Simmons Jr. (1992), Groundwater discharge and its impact on surface water quality in a Chesapeake Bay Inlet, *Journal of the American Water Resources Association*, 28(6), 1121-1134, <https://doi.org/10.1111/j.1752-1688.1992.tb04023.x>.

- Reckhardt, A., M. Beck, M. Seidel, T. Riedel, A. Wehrmann, A. Bartholomä and H. J. Brumsack (2015), Carbon, nutrient and trace metal cycling in sandy sediments: A comparison of high-energy beaches and backbarrier tidal flats, *Estuarine, Coastal and Shelf Science*, 159, 1-14, <http://dx.doi.org/10.1016/j.ecss.2015.03.025>.
- Robinson, M., D. Gallagher, and W. Reay (1998), Field observations of tidal and seasonal variations in ground water discharge to tidal estuarine surface water, *Groundwater Monitoring & Remediation*, 18(1), 83-92, doi:10.1111/j.1745-6592.1998.tb00605.x.
- Robinson, C., B. Gibbes, and L. Li (2006), Driving mechanisms for groundwater flow and salt transport in a subterranean estuary, *Geophysical Research Letter*, 33, L03402, doi:10.1029/2005GL025247.
- Robinson, C., B. Gibbes, H. Carey, and L. Li (2007), Salt-freshwater dynamics in a subterranean estuary over a spring-neap tidal cycle, *J. Geophys. Res.*, 112, C09007, doi:10.1029/2006JC003888.
- Roy, M., J. B. Martin, J. E. Cable, and C. G. Smith (2013), Variations of iron flux and organic carbon remineralization in a subterranean estuary caused by interannual variations in recharge, *Geochim. Cosmochim. Acta*, 103, 301–315, doi:10.1016/j.gca.2012.10.055.
- Santoro, A. E. (2010), Microbial nitrogen cycling at the saltwater–freshwater interface, *Hydrogeol. J.*, 18(1), 187–202, doi:10.1007/s10040-009-0526-z.
- Santos, I. R., W. C. Burnett, J. Chanton, B. Mwashote, I G. N. A. Suryaputra, and T. Dittmar (2008), Nutrient biogeochemistry in a Gulf of Mexico subterranean estuary and groundwater-derived fluxes to the coastal ocean, *Limnology and Oceanography*, 53, 705-718, doi:10.4319/lo.2008.53.2.0705.
- Seidel, M., M. Beck, J. Greskowiak, T. Riedel, H. Waska, I. G. N. A. Suryaputra, B. Schnetger, J. Niggemann, M. Simon, and T. Dittmar (2015), Benthic-pelagic coupling of nutrients and dissolved organic matter composition in an intertidal sandy beach, *Marine Chemistry*, 176, 150-163, <http://dx.doi.org/10.1016/j.marchem.2015.08.011>.
- Simmons, G. M. (1992), Importance of submarine groundwater discharge (SGWD) and seawater cycling to material flux across the sediment/water interfaces in marine environments, *Mar. Ecol. Prog. Ser.*, 84, 173–184.

- Slomp, C. P., and P. Van Cappellen (2004), Nutrient inputs to the coastal ocean through submarine groundwater discharge: controls and potential impact. *Journal of Hydrology*, 295(1), 64-86, <http://dx.doi.org/10.1016/j.jhydrol.2004.02.018>.
- Smith, V. H., G. D. Tilman, and J. C. Nekola (1999), Eutrophication: impacts of excess nutrient inputs on freshwater, marine, and terrestrial ecosystems, *Environmental Pollution*, 100(1-3), 179-196, [https://doi.org/10.1016/S0269-7491\(99\)00091-3](https://doi.org/10.1016/S0269-7491(99)00091-3).
- Spiteri, C., C. P. Slomp., K. Tuncay, C. Meile (2008), Modeling biogeochemical processes in subterranean estuaries: Effect of flow dynamics and redox conditions on submarine groundwater discharge of nutrients. *Water Resources Research*, 44(2), doi:10.1029/2007WR006071.
- Ullman, W. J., B. Chang, D. C. Miller, and J. A. Madsen (2003), Groundwater mixing, nutrient diagenesis, and discharges across a sandy beachface, Cape Henlopen, Delaware (USA), *Estuarine, Coastal and Shelf Science*, 57(3), 539-552, [http://dx.doi.org/10.1016/S0272-7714\(02\)00398-0](http://dx.doi.org/10.1016/S0272-7714(02)00398-0).
- Valiela, I., J. Costa, K. Foreman, J. M. Teal, B. Howes, and D. Aubrey (1990), Transport of groundwater-borne nutrients from watersheds and their effects on coastal waters, *Biogeochemistry*, 10(3), 177-197.
- van der Meulen, F., T. W. M. Bakker, and J. A. Houston (2004), The costs of our coasts: examples of dynamic dune management from Western Europe, In *Coastal Dunes: Ecology and Conservation* (259-278), Berlin: Springer-Verlag.
- Vitousek, P.M., J. D., Aber, R. W. Howarth, G. E. Likens, P. A. Matson, D. W. Schindler, W. H. Schlesinger, and D. G. Tilman (1997), Human alteration of the global nitrogen cycle: sources and consequences, *Ecological applications*, 7(3), 737-750, [https://doi.org/10.1890/1051-0761\(1997\)007\[0737:HAOTGN\]2.0.CO;2](https://doi.org/10.1890/1051-0761(1997)007[0737:HAOTGN]2.0.CO;2).
- Viviani, R (1992), Eutrophication, marine biotoxins, human health, In *Marine coastal eutrophication* (631-662), Bologna, Italy: Elsevier Science, <https://doi.org/10.1016/B978-0-444-89990-3.50056-0>.
- Xin, P., C. Robinson, L. Li, D. A. Barry, and R. Bakhtyar (2010), Effects of wave forcing on a subterranean estuary. *Water Resources Research*, 46(12), <https://doi.org/10.1029/2010WR009632>.

- Xin, P., S. S. J. Wang, C. Robinson, L. Li, Y.-G. Wang, and D. A. Barry (2014), Memory of past random wave conditions in submarine groundwater discharge, *Geophysical Research Letters*, 41(7), 2401-2410 doi:10.1002/2014GL059617.
- Yu, X., P. Xin, C. Lu, C. Robinson, L. Li, and D. A. Barry (2017), Effects of episodic rainfall on a subterranean estuary, *Water Resources Research*, 53(7), 5774-5787, <https://doi.org/10.1002/2017WR020809>.

Chapter 2

SPATIAL PATTERNS OF GROUNDWATER BIOGEOCHEMICAL REACTIVITY IN AN INTERTIDAL BEACH AQUIFER

This work has been published as Kim, K. H., J. W. Heiss, H. A. Michael, W. Cai, T. Laattoe, V. E. A. Post, and W. J. Ullman (2017), Spatial patterns of groundwater biogeochemical reactivity in an intertidal beach aquifer, *Journal of Geophysical Research: Biogeosciences*, 122, 2548-2562, doi: 10.1002/2017JG003943.

Abstract

Beach aquifers host a dynamic and reactive mixing zone between fresh and saline groundwater of contrasting origin and composition. Seawater, driven up the beachface by waves and tides, infiltrates into the aquifer and meets the seaward-discharging fresh groundwater, creating and maintaining a reactive intertidal circulation cell. Within the cell, land-derived nutrients delivered by fresh groundwater are transformed or attenuated. We investigated this process by collecting pore water samples from multilevel wells along a shore-perpendicular transect on a beach near Cape Henlopen, Delaware, and analyzing solute and particulate concentrations. Pore water incubation experiments were conducted to determine rates of oxygen consumption and nitrogen gas production. A numerical model was employed to support field and laboratory interpretations. Results showed that chemically sensitive parameters such as pH and ORP diverged from salinity distribution patterns, indicating biogeochemical reactivity within the circulation cell. The highest respiration rates were found in the landward freshwater-saltwater mixing zone,

supported by high concentrations dissolved inorganic carbon found at this location. Chlorophyll *a*, a proxy for phytoplankton, and particulate carbon did not co-occur with the highest respiration rates but were heterogeneously distributed in deeper and hypoxic areas of the cell. The highest rates of N₂ production were also found in the mixing zone coinciding with elevated O₂ consumption rates but closer to the lower discharge point. Model results were consistent with these observations, showing heightened denitrification in the mixing zone. The results of this work emphasize the relationship between the physical flow processes of the circulation cell and its biogeochemical reactivity and highlight the environmental significance of sandy beaches.

2.1 Introduction

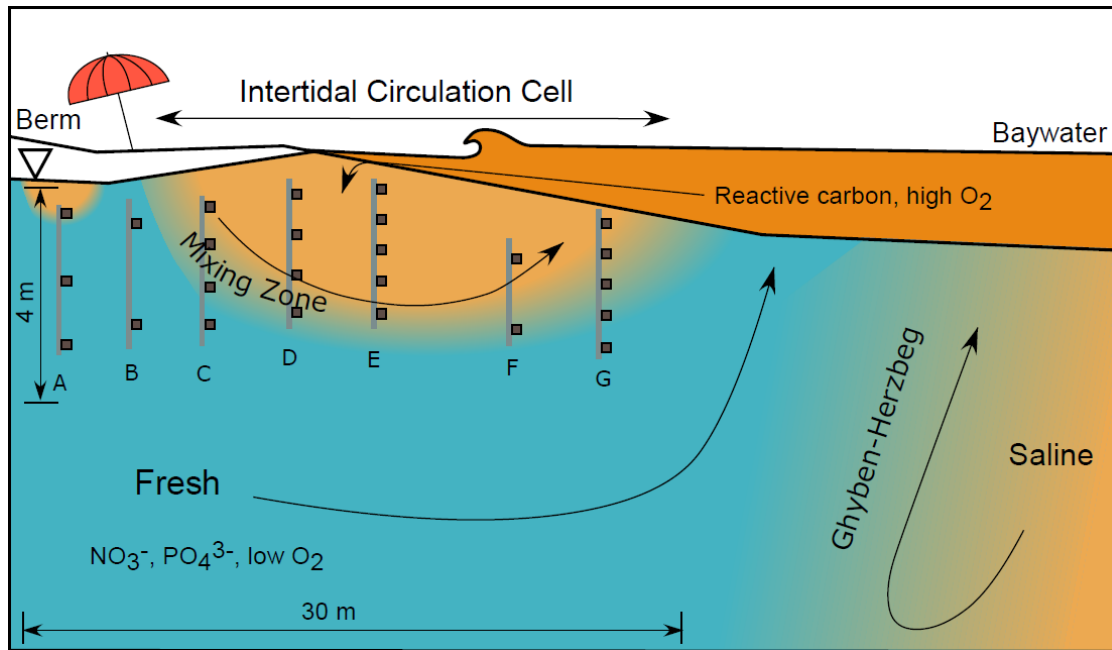


Figure 2.1 Schematic diagram of the intertidal circulation cell and the positions of multilevel pore water samplers (A–G) at Cape Shores. Each gray line indicates location of sampler and dark gray boxes indicate the approximate position and spacing of water sampling ports. Infiltration of saline seawater into the fresh groundwater creates a reactive intertidal circulation cell. Biogeochemical activity within this cell is supported by reactive organic carbon and oxygen originating from the infiltrating seawater.

Submarine groundwater discharge (SGD) is the flow of fresh or saline groundwater from the coastal aquifer to the adjacent marine surface water. SGD is an important pathway for the delivery of terrestrial solutes to coastal waters and can significantly impact marine ecosystems, as it generally contains higher concentrations of nutrients and other land-derived contaminants than surface water discharge [Johannes, 1980; Moore, 1999; Slomp & Van Cappellen, 2004].

Fresh coastal groundwater is driven seaward by an inland hydraulic gradient, while density gradients along the lower Ghyben-Herzberg interface create convective seawater circulation that contributes a portion of saline SGD (Figure 2.1) [Cooper, 1959; Kohout, 1960]. In some beaches, a smaller, but chemically significant, intertidal cell of rapidly circulating saline water occurs landward of the zone of fresh SGD [Beck et al., 2017; Heiss & Michael, 2014; Michael et al., 2005; M. Robinson et al., 1998; C. Robinson et al., 2007; Seidel et al., 2015]. Through tide and wave action, seawater moves up the beachface and infiltrates into the sand, where it circulates and mixes with the seaward moving fresh groundwater. Although the transition zone below this circulation cell is smaller than the Ghyben-Herzberg transition zone at depth, it can alter the distribution of solutes and solute fluxes.

Traditionally, quartz-rich beach sediments have been thought to be mostly unreactive due to their low organic matter content [Anschutz et al., 2009; Boudreau et al., 2001]. However, the intertidal circulation cell has been shown to host various biogeochemical reactions that transform and attenuate land-derived nutrients prior to discharge, including oxic respiration of carbon [Beck et al., 2017; Charbonnier et al., 2013; Reckhardt et al., 2015; Seidel et al., 2015], nitrogen transformations [Hays & Ullman, 2007a, 2007b; Ullman et al., 2003], Fe oxidation and reduction [Charette & Sholkovitz, 2002; McAllister et al., 2015], other metal cycling processes [Reckhardt et al., 2015], and sorption. It is hypothesized that introduction of reactive organic matter and oxygen with infiltrating seawater into the intertidal circulation cell supports biogeochemical reactions with a variety of environmentally available redox active elements [Charbonnier et al., 2013; Reckhardt et al., 2015; Seidel et al., 2015]. This has substantial implications for coastal systems, as reactions hosted in the cell can

alter the chemical characteristics of discharging waters, impacting coastal organisms and ecology [Anschutz et al., 2009; Burnett et al., 2003].

The intertidal circulation cell is highly dynamic and has been shown to respond to hydrologic, geologic, and topographic changes over various time scales (waves, tides, and seasons) [Bakhtyar et al., 2013; Heiss & Michael, 2014; M. Robinson et al., 1998; C. Robinson et al., 2006, 2007]. Therefore, the flow paths that control the delivery and availability of reactive particles and solutes into the circulation cell are also both spatially and temporally variable. As the driving forces and physical characteristics of the cell change, the extent and patterns of chemical reactions within and around the cell are expected to respond in concert. While the dynamic nature of the physical properties of the cell has been described in detail [Heiss & Michael, 2014; Michael et al., 2005; M. Robinson et al., 1998; C. Robinson et al., 2007], there are fewer observations concerning the location and relative rates of chemical reactivity within the cell and their relations to the patterns of mixing.

Previous field studies have established the reactive nature of the intertidal circulation cell based on the surficial or cross-sectional distribution of solutes. Charbonnier et al. [2013] monitored solute concentrations across the water table at Truc Vert, France, and demonstrated enhanced, but seasonally variable, aerobic respiration in the lower beach. Reckhardt et al. [2015] observed the circulation cell across different hydrodynamic forcing regimes and found lower concentrations of dissolved organic matter in beaches of higher energy. Seidel et al. [2015] conducted an in-depth study on the molecular signatures organic matter that percolated into the beach and proposed that bioavailable carbon compounds of both terrestrial and marine sources stimulated biogeochemical processes, including aerobic respiration, within the

cell. More recently, Beck et al. [2017] observed the spatial distribution of solutes, rare earth elements, and genetic material to determine different zones of biogeochemical processes, redox states, and microbial communities within the intertidal circulation cell. Oxygen consumption rates over 1 h for two surficial sediment sampling points were also determined using flow-through columns and air-saturated surface water [Beck et al., 2017]. While these studies demonstrate reactivity and reactive potential within the circulation cell, as well as their inferred locations, the depletion of oxygen, the employed proxy for aerobic respiration, is assumed to occur at a constant rate across the beach. A complete spatial distribution of reaction rates that lead to observed solute distributions within the intertidal circulation cell, relative to its salinity distribution, has not been observed.

The present work therefore aims to provide insight into the distribution and magnitudes of aerobic respiration and denitrification rates within the intertidal circulation cell, and their relationship to the salinity distributions and flow regime. We investigated the spatial distribution of reactivity by determining reaction rates using pore water incubation experiments and observing in situ solute concentrations taken from a shore-perpendicular cross section in a tide-dominated sandy beach.

Additionally, a numerical variable-density reactive transport model was employed to support the interpretation of field measurements and to provide additional insight into the spatial distribution of reactants and products in the beach aquifer under idealized conditions. The combined results highlight the link between physical processes of flow and the biogeochemical activity within sandy beaches. As sea level rise, beach erosion, or beach remediation efforts alter the slope, width, and hydrogeologic

properties of beaches, understanding how the physical flow processes and salinity patterns relate to beach reactivity will become increasingly important.

2.2 Study Area Description and Methodology

2.2.1 Study Area

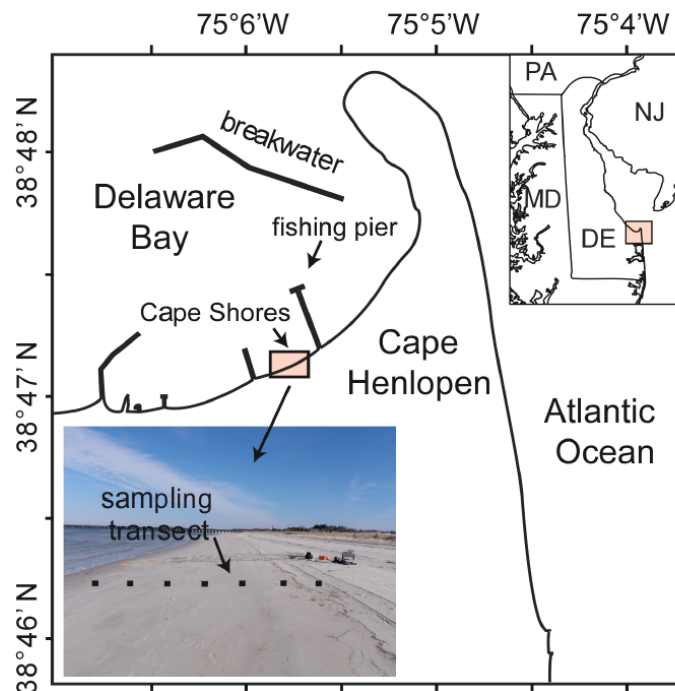


Figure 2.2 Map of the field site and sampling transect, Cape Shores, Lewes, Delaware, USA.

This study was conducted in the intertidal zone of the tide-dominated Cape Shores beach adjacent to Delaware Bay, near Cape Henlopen, Delaware, USA (Figure 2.2). Wave action at the Cape Shores site is restricted due to the offshore breakwaters that protect the Lewes Harbor of Refuge. Tides are semidiurnal with an average range

of 1.42 m. The beach aquifer is predominantly composed of coarse sand (540–668 μm grain size) and has a hydraulic conductivity of 27.6–30.2 m/d [Heiss et al., 2014].

The biology, chemistry, and hydrology of the intertidal circulation cell at Cape Shores were well characterized in a number of previous studies. Dale and Miller [2007] identified groundwater discharge zones utilizing sediment temperature and pore water salinity distributions along the Cape Shores beach. Active remineralization of organic matter, cycling of N, P, Si, Fe, and S, and seasonal shifts in local microbial communities have also been documented [Dale & Miller, 2008; Hays & Ullman, 2007a, 2007b; McAllister et al., 2015; Miller & Ullman, 2004; Ullman et al., 2003]. More recently, Heiss and Michael [2014] investigated the dynamic seasonal movements of the circulation cell in response to changing hydrologic conditions. This makes Cape Shores an ideal site to conduct further research on beach biogeochemistry, as mixing of water masses, active diagenetic cycling of nutrients, and “pulsing” of the cell due to physical forcing have been well documented in the Cape Shores intertidal circulation cell.

2.2.2 Pore water and Particulate Analysis

Pore water was collected from seven multilevel samplers along a 30 m beach-perpendicular transect. Each sampler was constructed with multiple polyethylene tubes (7 mm outer diameter) arrayed at 0.5–0.8 m vertical intervals along a PVC support pipe (13 mm outer diameter) extending up to 3 m [Heiss & Michael, 2014]. Each polyethylene tube was screened with nylon mesh to prevent clogging. At each location, the sampler was hand augered vertically into the sand (Samplers A–G, Figure 2.1). A total of 26 sampling ports were distributed within the sampled cross section. Pore water was sampled from the beach during low tide using a peristaltic GeoTech

pump, after pumping at least 100 mL to flush out each tube. A YSI Professional Plus meter (Yellow Spring, Ohio) with a flow-through cell was used to measure salinity (practical salinity units), temperature, pH, and redox potential (ORP). An OptiOx Probe (Mettler Toledo, Columbus, Ohio) was used to measure dissolved oxygen (DO) in the field. Particles in pore water were collected on three precombusted 0.7 μm glass fiber filters, one each for chlorophyll *a*, particulate carbon and nitrogen (PC/PN), and particulate phosphorus (PP), by filtering 1 L of pore water per filter. The filtrate was retained for analysis of dissolved solutes.

Chlorophyll was extracted from filters with acetone and quantified using a Turner fluorometer (10 AU; Turner Designs, San Jose California). Pure acetone and standards in acetone provided by Turner were used to calibrate the instrument. The lower detection limit of the fluorometer is 0.025 $\mu\text{g/L}$. PC/PN was measured by combustion with a Costech CHN Elemental Analyzer with a lower detection limit of 0.005 mg/L. PP was determined spectrometrically, following combustion and acidification using with the molybdenum blue method [Murphy & Riley, 1962].

The 250 mL of the filtrate was preserved in a borosilicate bottle with a greased glass stopper for dissolved inorganic carbon (DIC) and total alkalinity (TA) analysis. These samples were immediately fixed with 80 μl of saturated HgCl_2 to prevent further reactions and then stored in the dark at 4°C until analysis. DIC was determined by acidifying the samples and measuring the evolved CO_2 gas using a Model AS-C3 DIC Analyzer (Apollo SciTech, Newark, Delaware). TA was determined by Gran titration [Gran, 1952] using a Model AS-ALK2 Alkalinity Titrator (Apollo SciTech, Newark, Delaware). Both DIC and TA measurements were calibrated using the certified reference materials from Scripps Institute of Oceanography (San Diego, California).

Some samples with high sulfide could not be accurately analyzed for TA due to precipitation of HgS during its fixation with HgCl₂. For these samples, DIC and pH measurements were coupled to calculate TA using the Excel macro CO2SYS [Pierrot et al., 2006], with inorganic carbon dissociation constants from Millero et al. [2006]. Excess partial pressure of CO₂ (excess $p\text{CO}_2$) was also calculated to observe the effects of aerobic respiration. This was calculated as the difference between in situ DIC and the theoretical DIC value at atmospheric equilibrium [Abril et al., 2000], computed using TA values and atmospheric $p\text{CO}_2$ of 395 μatm (7 September 2014, Mauna Loa Observatory). All measurements of TA, DIC, and $p\text{CO}_2$ were temperature normalized to 15°C to remove thermal effects, leaving only biological and mixing processes. Approximately 100 mL from the remaining filtrate was collected in a Nalgene bottle to measure dissolved nutrients ($\text{NO}_2^- + \text{NO}_3^-$, NH_4^+ , PO_4^{3-} , Si) using standard methods on a SEAL AA3 Autoanalyzer (Mequon, Wisconsin).

Because of sampling limitations due to tide levels, daylight, and sample processing, sampling of all ports could not be completed in 1 day. Preliminary field sampling of a subset of ports, sampled over three consecutive days, found little change in the concentrations and distribution patterns of salinity, temperature, DO, chlorophyll *a*, and PC. This is consistent with prior measurements showing little change in salinity over multiple tidal cycles [Heiss & Michael, 2014]. The samples described in this paper were collected on 8 and 10 September 2014.

2.2.3 Spatial Characterization of Pore water Reactivity

Unfiltered pore water samples were collected in the field and incubated in the laboratory to determine the spatial patterns of reactivity. Initial O₂ deficit and initial N₂ excess were determined as deviations from the normal atmospheric equilibrium

concentrations (NAEC) as a function of salinity and temperature [Garcia & Gordon, 1992; Hamme & Emerson, 2004]. O₂ consumption rates and N₂ production rates were determined by incubation. All four parameters were used as indicators of pore water reactivity.

The incubation experiments were similar to those of Kana et al. [1994, 2006]. Five unfiltered replicate samples were collected in 12 mL Exetainers with gas-tight caps (Labco, Lampeter Ceredigion, UK) from each sampling port by flooding the test tubes from the bottom end and ensuring no air contamination. The first sample was fixed with 20 µL of saturated HgCl₂ at the time of collection in the field to preserve initial in situ measurements of O₂, N₂, and Ar. Initial O₂ deficit and initial N₂ excess was determined from this first aliquot. Some of the first aliquot samples were slightly enriched in O₂ compared to the OptiOx O₂ measurements taken at the time of sampling, most likely due to the short time of exposure to air while the sample was being fixed. However, the difference between the two measurements was on average less than 0.5 mg/L, which is similar to the expected uncertainty under flow-through conditions, compounded by instrumentation error (0.5%).

The remaining four aliquoted samples were fixed consecutively over 15 days while being incubated in the dark at 25°C underwater (to minimize gas exchange). No significant amount of additional O₂ was introduced into the samples. Concentrations of O₂ and N₂ relative to the concentration of Ar gas were then measured with high-precision Membrane Inlet Mass Spectrometry (MIMS, PrismaPlus Model; Bay Instruments, Easton, Maryland). The linear regression of O₂ decrease over the first 5 to 7 days of the incubation period was taken as an estimate of the “apparent oxygen consumption rate,” related to the oxidation of organic matter at the location of the

respective sampling port. Beyond 7 days most samples were anoxic, displayed an air contamination problem, or had a significant change in the rate of apparent O₂ consumption, possibly due to cell growth or exhaustion of more reactive carbon or nutrients. The measured reaction rate was then converted to an “environmental reaction rate” using the Arrhenius equation with an activation energy of 21.5 kcal/mol obtained from the incubation of one Cape Shores sample at three different temperatures [Westrich & Berner, 1988]. This activation energy of reaction is similar to those measured in other environmental studies [Aller & Yingst, 1980; Thamdrup et al., 1998]. N₂ production rates were determined in a similar manner to O₂ consumption. However, because the MIMS instrument utilized the slope change of O₂/Ar ratios as an indicator of sampling time, it was increasingly difficult to stabilize the instrument for an accurate measurement as samples approached anoxia. For this reason, the interpretation of N₂ increase was approached conservatively. Only increases in N₂ above the N₂/Ar ratio at NAEC were taken to be N₂ production.

2.2.4 Groundwater Flow and Reactive Transport Model

A numerical variable-density groundwater flow and solute transport model was combined with a reactive transport model to simulate tidally driven mixing and biogeochemistry in the beach aquifer. Groundwater flow and conservative salt transport were simulated for a 2-D cross section along the shore-perpendicular transect of multilevel sampling wells using the finite difference code SEAWAT [Langevin et al., 2008]. Dissolved organic carbon (DOC) degradation, aerobic respiration, and denitrification along groundwater flow paths was modeled using PHT3D v2.13 [Prommer & Post, 2002]. These redox processes were modeled according to the reaction kinetics of DOC, O₂, NO₃⁻, N₂ as shown in Table 2.1 and using the reaction

parameter values shown in Table 2.2. The reactive species were superimposed onto the groundwater flow field simulated using SEAWAT. Thus, the flow and reactive transport simulations were decoupled [Anwar et al. 2014; Bardini et al., 2012; Spiteri et al., 2008].

The model represented an unconfined sandy beach aquifer influenced by tidal and terrestrial freshwater forcing. To avoid boundary effects, the model domain extended 50 m seaward of the mean sea level (MSL)-beachface intersection, 150 m landward, and 30 m below MSL. The beach profile measured prior to the sampling event was set as the top active layer in the model. A nonuniform grid was used to discretize the domain to satisfy Peclet ($Pe < 2$) and Courant ($Cr < 0.75$) criteria. Grid cells were $dx = 0.31$ m by $dy = 0.06$ m in the intertidal zone where rapid flow rates and strong redox gradients occurred. The model was homogenous and isotropic with hydraulic conductivity = 25 m/d, porosity = 0.3, longitudinal dispersivity = 0.15 m, and transverse dispersivity = 0.015. These parameter values were adopted from the calibrated model in Heiss and Michael [2014] for the same sampling transect.

The flow and transport boundary conditions were assigned based on hydrologic forcing and solute concentrations in the fresh and saline groundwater end-members. A constant freshwater flux of $1.01 \text{ m}^3/\text{d}$ was set along the up-gradient vertical boundary. This flux corresponded to the flux simulated in Heiss and Michael [2014] for the hydraulic head measured at the dune on the 8 September 2014 sampling event at the Cape Shores sampling transect. The influence of tides on flow and transport was simulated with the Periodic Boundary Condition (PBC) Package [Post, 2011]. A semidiurnal (period = 0.5 d) sinusoidal tide was assigned using the time-varying head boundary in the PBC package at the shoreface nodes. The tidal

amplitude was set to 0.71 m based on the tidal range between mean lower low water (MLLW) and mean higher high water (MHHW) according to the Lewes, DE tide gauge (NOAA tidal station 8557830, Lewes, Delaware) 1 km from the field site. The tidal range between MLLW and MHHW was chosen because it integrates the aquifer conditions over many tidal cycles leading up to the sampling event. Once hydraulic heads and salt concentrations reached dynamic steady state, the tidally averaged fluid fluxes across the shoreface were used to simulate steady state (with respect to boundary conditions) flow and salt transport. The tidally averaged flow field was used to drive the transport of the reactive solutes. The top, bottom, and right boundaries were set as no flow boundaries.

The part of the shoreface where seawater was flowing into the model domain was assigned a source salinity concentration of 28, representing tidally driven seawater infiltration. A zero-concentration gradient for the outflowing portion of the shoreface was set for all species. The end-member concentrations used in the model for DOC, NO_3^- , and O_2 were assigned according to the highest measured values in the end-member source. The end-member concentration for the reactive solutes considered was 66.6 μM for DOC and 177 μM for O_2 in seawater, and 179 μM for NO_3^- in freshwater. These end-member concentrations were measured during the sampling event with the exception of DOC, which was measured on 6 November 2014. Seawater flowing into the model domain across the shoreface served as a source of DOC and O_2 , and the left vertical boundary served as a source of NO_3^- , representing high-nitrate fresh groundwater flowing into the model domain. DOC and O_2 concentrations in the inflowing fresh groundwater were set to zero, consistent with O_2

measurements and because any reactive DOC in the anoxic environment would have already denitrified a portion of the NO_3^- .

2.3 Results

2.3.1 In Situ Pore Water Measurements

Salinity, a nonreactive tracer, outlined the physical location and geometry of the intertidal circulation cell (Figure 2.3a). Landward of the intertidal zone, a berm was present during sampling period similar to the one observed and described by Heiss and Michael [2014], resulting in some pooling of water as seawater rose above the high tide mark. As a result, a smaller brackish zone was present underneath the depression landward of the berm (Sampler A).

Other chemical parameters showed more spatial variability. pH measurements were circumneutral and ranged from 6.7 to 8.4 (Figure 2.3b). The most alkaline pH values occurred within the freshwater zones high on the beach. ORP measurements ranged from -77 to +104 mV, with the most oxidizing waters near the fresher zones of Samplers A and B, and intermediate salinity water at Sampler D (Figure 2.3c). The most reducing conditions were found at the base of the beach near Samplers F and G, where iron and sulfate reduction had been previously observed [McAllister et al., 2015]. Overall, ORP patterns did not spatially correlate with salinity. The divergence of chemically sensitive parameters such as pH and ORP from nonreactive parameters like salinity is direct and strong evidence of biogeochemical reactions.

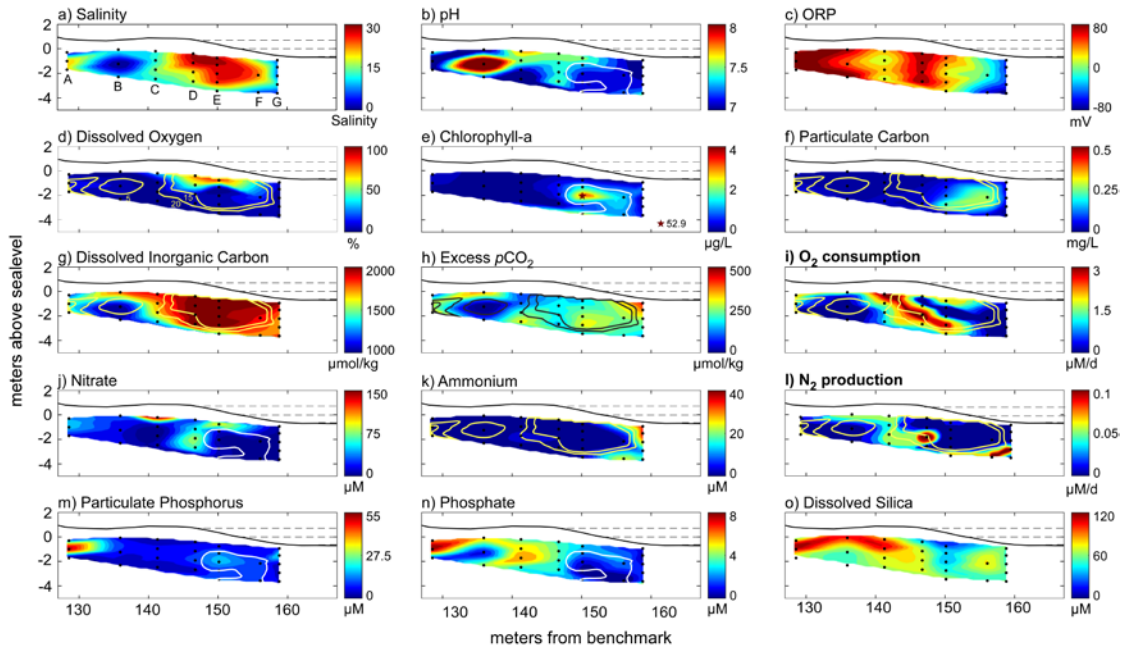


Figure 2.3 Cross-sectional distributions of measured constituents. Black solid lines delineate surface topography. Dashed lines indicate mean high water, mean sea level, and mean low water (flush with topography). Multilevel pore water samplers are labeled in Figure 2.3a, with black dots indicating sampling locations. Yellow contours in Figures 3d, 3f–3i, 3k, and 3l (black in Figure 2.3h) are salinity (5, 15, and 20, labeled in Figure 2.3d), while white contours (Figures 2.3b, 2.3j, 2.3m, and 2.3n) show chlorophyll a (Figure 3e). Hot spot of chlorophyll is indicated with a star. Figures 2.3i and 2.3l (in bold) are from incubation results, while Figures 2.3a–2.3h, 2.3j, 2.3k, and 2.3m–2.3o are in situ measurements or calculations.

Dissolved oxygen was an important indicator of both water source and beach reactivity. Fresh groundwater in the coastal aquifer below the water table was mostly anoxic, whereas infiltrating saline water was fully oxygenated due to equilibration with the atmosphere. There was a significant decrease in DO (to less than 25% saturation) within the top 2 m of the saline circulation cell, although elevated salinity levels extended to depths of 3 m (Figure 2.3d). All sampling locations within the

beach were undersaturated with respect to atmospheric O₂ (Figure 2.4) and fell below a salinity-based conservative mixing line between the highest and lowest DO samples (dotted gray line, Figure 2.4), with the largest deviations at the highest salinities. The observed dilution curve to the lowest salinity sample (solid black line, Figure 2.4) suggests rapid utilization of oxygen once infiltrated, followed by advective dilution. One exception was the data point on the conservative mixing curve, from the shallowest port on Sampler C where oxygen was still high near the water table at the landward edge of the circulation cell.

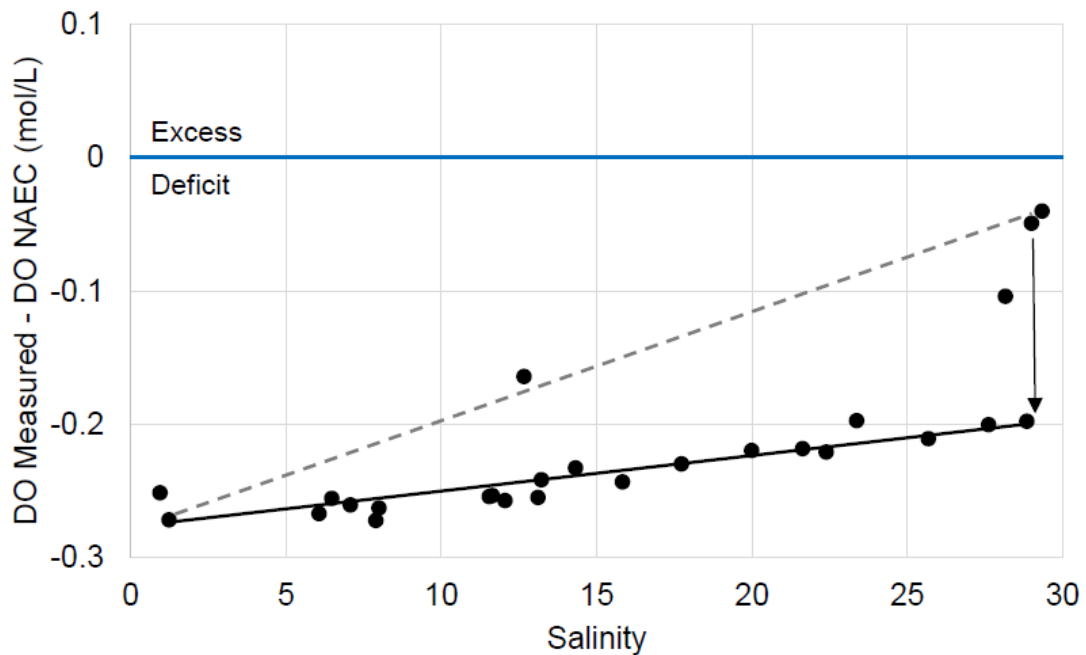


Figure 2.4 Dissolved oxygen deficit from in situ measurements. All measured DO values are less than the normal atmospheric equilibrium concentration (NAEC) values of DO at its respective salinity and temperature and fall below the zero line (blue solid line). Measurements also all fall below the conservative mixing curve (gray dotted line), except for one sample that was taken from the most landward edge of the intertidal circulation cell at Sampler C. Black vertical arrow highlights rapid depletion of oxygen at high salinities.

Chlorophyll a, a proxy for phytoplankton carbon, and particulate carbon (PC) were elevated in the deeper, hypoxic zones of the circulation cell (Figures 2.3e and 2.3f). Overall, chlorophyll a fluorescence in the subsurface waters of the beach was severely depleted relative to the baywater (~22 $\mu\text{g/L}$), with 20 ports showing values ranging from 0.0 to 0.9 $\mu\text{g/L}$. Other than the one hot spot that had 52.9 $\mu\text{g/L}$ (star, Figure 2.3e), the other five ports had concentrations ranging from 1 to 3 $\mu\text{g/L}$. PC had a range of 0.01–0.3 mg/L, and the higher values of PC co-occurred with higher

chlorophyll concentrations. The filter collected at the high-chlorophyll location was darkly colored with a substantial amount of fine-grained material, suggesting that hydrogeologic conditions at the sampling time allowed for the trapping of finer material in the sampling port. Due to light limitations at this depth (2.3 m), we do not anticipate in situ phytoplankton growth.

Dissolved inorganic carbon had different spatial patterns compared to particulate organic carbon. Most samples were enriched in DIC relative to the conservative dilution curve, indicating in situ production of CO_2 due to organic carbon remineralization down the redox gradient (Figure 3.5). Within the aquifer, elevated DIC values mostly coincided with elevated salinity but extended beyond the high-salinity contours (Figure 2.3g). Because DIC and TA values for both the freshest (1065 $\mu\text{mol/kg}$, 2066 $\mu\text{mol/kg}$, respectively) and most saline (1074 $\mu\text{mol/kg}$, 2048 $\mu\text{mol/kg}$, respectively) end-member samples were very similar, a fairly conservative 1:1 relationship of TA:DIC with respect to salinity can be assumed. While anaerobic decomposition increases both TA and DIC, aerobic respiration only increases DIC [Cai et al., 2003]. Although other minor anaerobic reactions that impact TA:DIC ratios do occur within the aquifer and are important for elemental cycles, such reactions can be overlooked for the purposes of using TA and DIC distributions as evidence of aerobic respiration. Figure 2.6 shows a relative enrichment of DIC relative to TA above the 1:1 line. Because DIC can be affected by other reactions such as carbonate dissolution or anaerobic processes along the flow path [Cai et al., 2003, 2010; Chaillou et al., 2014, 2016], excess $p\text{CO}_2$ was also calculated as a more direct indicator of aerobic respiration. Save for the lowest salinity sample, all samples had an excess of $p\text{CO}_2$. Consistent with other observations discussed above, the whole

intertidal circulation cell displayed high excess $p\text{CO}_2$, with some hot spots within the landward and seaward mixing zones.

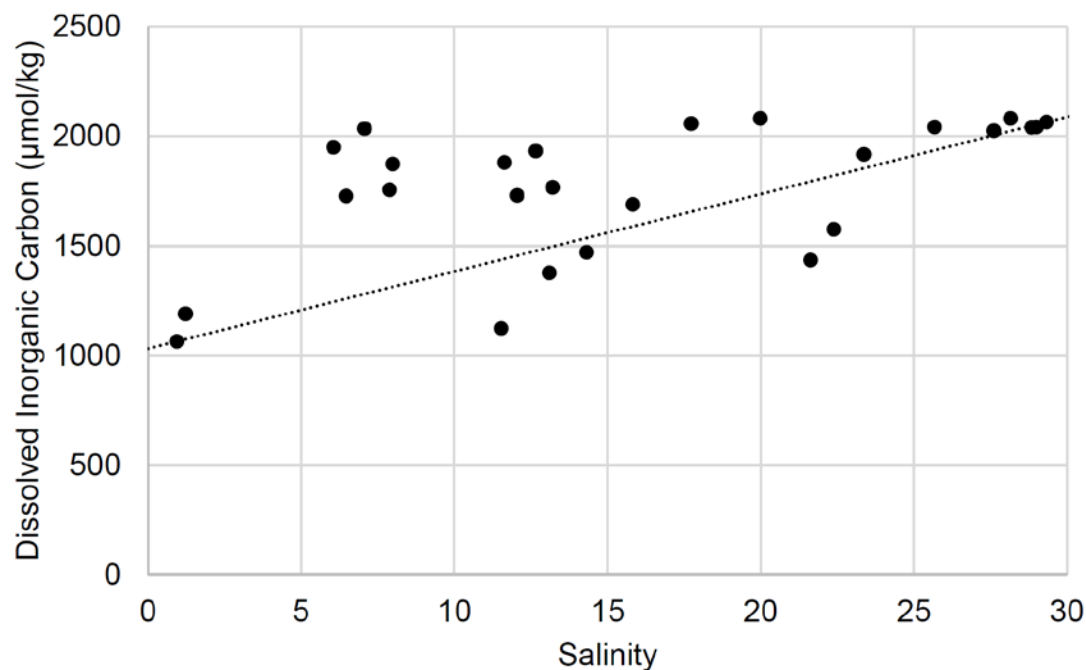


Figure 2.5 Salinity versus dissolved inorganic carbon. Dotted line indicates conservative mixing curve.

Ammonium and nitrate were spatially separated within the aquifer.

Ammonium ($\sim 37 \mu\text{M}$) was concentrated around Samplers F and G where conditions were much more reducing than the rest of the aquifer and where sulfide minerals were found by McAllister et al. [2015] (Figure 2.3k). Nitrate, highest around Samplers C and D ($\sim 177 \mu\text{M}$), was depleted in areas of high ammonium and high particulate organic carbon (Figure 2.3j). The N_2/Ar ratio measured in the first incubation aliquot at each sampling port, fixed at the time of collection, indicates in situ conditions.

N_2/Ar in water in equilibrium with air stays within a remarkably narrow range (36.3–38.5) over a large range of salinities (0–35) and temperatures (5–25) [Weiss, 1970]. Yet all samples had a N_2/Ar ratio over 38.5 at intermediate salinities, consistent with microbial N_2 production (not shown).

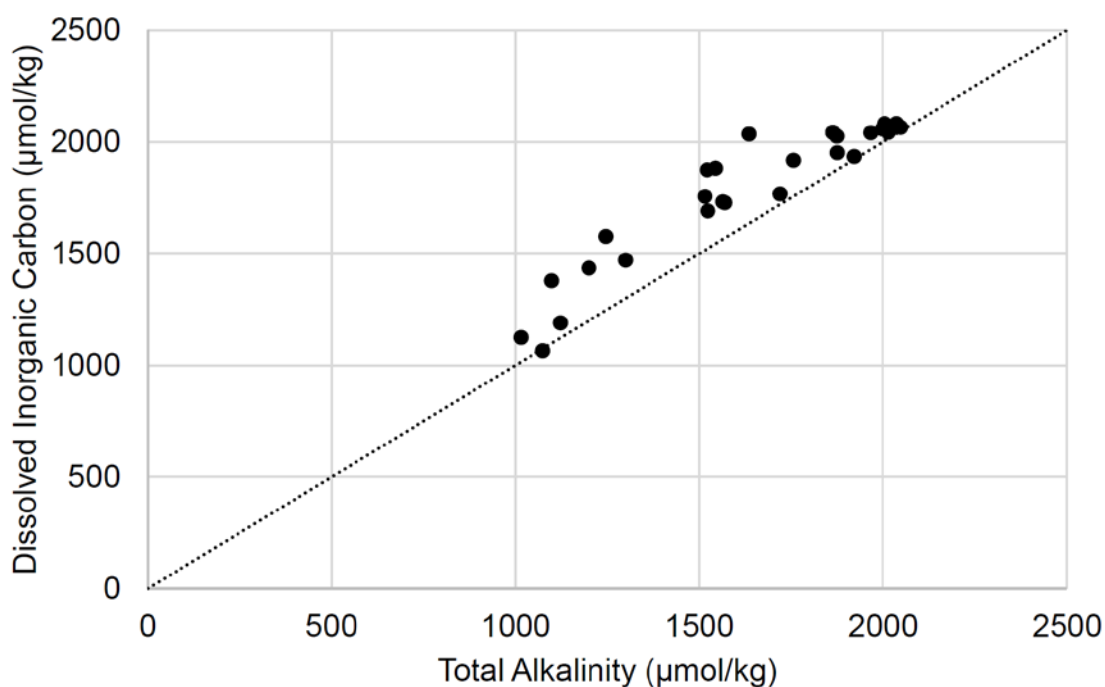


Figure 2.6 Total alkalinity versus dissolved inorganic carbon, in $\mu\text{mol/kg}$. Dotted line indicates a 1:1 line.

Particulate phosphorus (PP, Figure 2.3m) and phosphate (PO_4^{3-} , Figure 2.3n) were both highest around Sampler A ($\sim 55 \mu\text{M}$ and $\sim 8 \mu\text{M}$, respectively) but displayed divergent patterns in other areas of the aquifer. PP concentrations were low overall in the rest of the aquifer, with some elevated concentrations in areas of elevated chlorophyll (pink contour). Phosphate, on the other hand, had a spatial dilution pattern

going down gradient from Sampler A and was depleted in the zone of elevated chlorophyll.

Similar to phosphate, dissolved silica ($\sim 123 \mu\text{M}$, Figure 2.3o) was highest at Sampler A and was negatively correlated with salinity, diluting down gradient. There was some apparent production of silica along the flow path, although the highest concentrations did not exceed saturation with respect to amorphous silica by far ($\sim 115 \mu\text{M}$ at 1 atm, 25°C) [Morey et al., 1964].

2.3.2 Incubation O₂, N₂ Measurements

Aerobic respiration rates from pore water incubations displayed spatial heterogeneity across the beach. Respiration rates ranged from virtually zero to $3 \mu\text{mol/L/day}$, with the highest rates along the landward freshwater-seawater (FW-SW) mixing zone in Samplers C and D (Figure 2.3i).

The measured N₂ gas production rates during incubation was taken as laboratory evidence of denitrification. Because obtaining an accurate gas concentration with MIMS became increasingly difficult as samples became more anoxic, results were interpreted conservatively; only incubations that showed an unequivocal N₂ increase over time were taken to be indicative of denitrification. Samples that did not show an increase in N₂ were assigned a production rate of zero. The highest values of N₂ production were found proximal to the high reactivity zone found in the O₂ incubation experiments, along the landward edges of the circulation cell mixing zone (Figure 2.3) but also farther along the flow path than hot spots of O₂ consumption in the seaward mixing zone (Figure 2.3l). This is consistent with expectations that more O₂ consumption would take place near the infiltration point in

the circulation cell, while N_2 production would increase toward the end of the flow path near the discharge point.

2.3.3 Reactive Transport Model Results

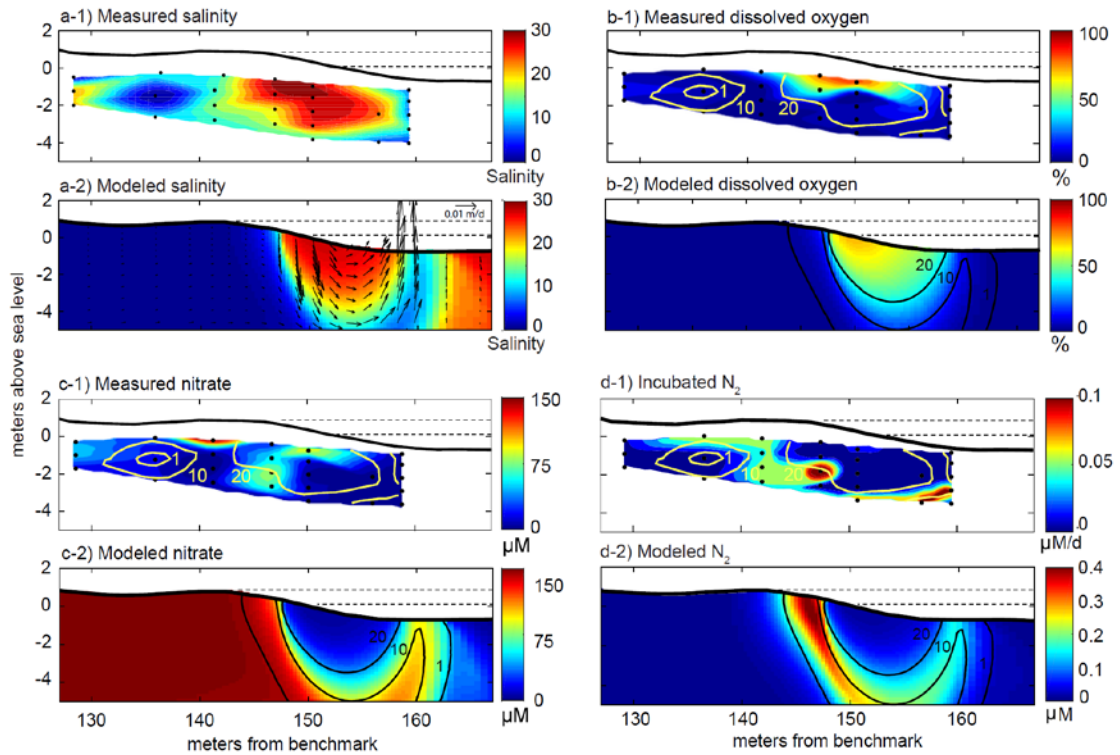


Figure 2.7 Measured (1) and modeled (2) distributions for (a) salinity, (b) dissolved oxygen, (c) nitrate, and (d) N_2 in the intertidal beach aquifer at Cape Shores, DE. The flow vectors in Figure 2.7a-2 show the tidally averaged flow direction and magnitude. The horizontal dotted lines in both panels are MHHW and MSL. MLLW is contiguous with the topography at the base of the beachface. The modeled 1, 10, and 20 salinity contours are shown in Figures 2.7b-2, 7c-2, and 7d-2.

The groundwater flow and transport model approximately reproduced the observed salinity distribution in the beach aquifer, the horizontal and vertical extent of the circulation cell, and location of the fresh discharge zone (Figures 2.7a-1 and 2.7a-2). Measured and modeled salinities were highest beneath the upper half of the beachface between the MSL-beachface intersection and the high tide mark and decreased with depth and distance seaward due to mixing with underlying fresh groundwater. The upper part of the beach where measured and modeled salinities were highest ($X = 150$ m) corresponded to the highest rates of seawater infiltration across the beachface as shown by the magnitude of the flow vectors in Figure 2.7a-2. The vectors highlight the circulating pattern of saline-brackish groundwater: seawater enters the upper part of the beachface, flows downward and seaward, and then discharges near the base of the beachface (Figure 2.7a-2). Terrestrially derived fresh groundwater flows seaward beneath the intertidal circulation cell, mixing with saline groundwater along the perimeter of the cell before upwelling at the freshwater discharge zone at the base of the beach.

Measured salinities beneath the backshore landward of the berm ($X \approx 143$ m) were higher than the simulated salinities. This is likely due to the simplifying assumptions of the model, which did not account for temporal variability of seawater input due to spring-neap cycling, seasonality in freshwater flux, storm tides, or waves, all of which can impact salinity and flow patterns in these intertidal systems [Abarca et al., 2013; Boufadel et al., 2007; Heiss & Michael, 2014; C. Robinson et al., 2007; Xin et al., 2010]. However, there was good agreement in the location of the fresh discharge zone as well as the spatial coverage of the intertidal mixing zone, key factors related to biogeochemical reactivity and fluxes to the water column.

Table 2.1 Reaction Network and Kinetic Rate Expressions (Adopted from Bardini et al. [2012])

Name	Reaction	Rate expression
DOC degradation	$\text{DOC} \rightarrow \text{CO}_2$	Rate = $k_{\text{fox}}[\text{DOC}]$;
Aerobic respiration	$\text{DOC} + \text{O}_2 \rightarrow \text{CO}_2 + \text{H}_2\text{O}$	If $[\text{O}_2] > k_{\text{mo}2}$; Rate = $k_{\text{fox}}[\text{DOC}]$; If $[\text{O}_2] < k_{\text{mo}2}$; Rate = $k_{\text{fox}}[\text{DOC}] ([\text{O}_2]/k_{\text{mo}2})$
Denitrification	$5\text{DOC} + 4\text{NO}_3^- + 4\text{H}^+ \rightarrow 5\text{CO}_2 + 2\text{N}_2 + 7\text{H}_2\text{O}$	If $[\text{O}_2] > k_{\text{mo}2}$; Rate = 0; If $[\text{O}_2] < k_{\text{mo}2}$ and $[\text{NO}_3^-] > k_{\text{mno}3}$; Rate = $k_{\text{fox}}[\text{DOC}] (1 - [\text{O}_2]/k_{\text{mo}2})$; If $[\text{O}_2] < k_{\text{mo}2}$ and $[\text{NO}_3^-] < k_{\text{mno}3}$; Rate = $k_{\text{fox}}[\text{DOC}] (1 - [\text{O}_2]/k_{\text{mo}2}) ([\text{NO}_3^-]/k_{\text{mno}3})$

Table 2.2 Reaction Parameter Values

Parameter and source	Description	Value	Units
$k_{\text{fox}}^{\text{a}}$	Rate constant for decomposition of DOC	1.5×10^{-6}	s^{-1}
$k_{\text{mo}2}^{\text{ab}}$	Limiting concentration of O_2	3.125×10^{-5}	M
$k_{\text{mno}3}^{\text{ab}}$	Limiting concentration of NO_3^-	8.065×10^{-6}	M

^avan Cappellen and Wang [1996]

^bBardini et al. [2012]

Measured and modeled dissolved oxygen were highest near the surface below the MSL-beachface intersection where salinity was highest and decreased with depth and distance seaward (Figures 7b-1 and 7b-2). The measured dissolved oxygen saturation decreased more rapidly with depth than the modeled saturation and was higher closer to the surface. The largest discrepancy between measured and modeled nitrate concentrations was in the fresh groundwater (Figures 7c-1 and 7c-2). This can be explained by the modeling choice of a specified flux of nitrate across the entire left boundary, which is consistent with conditions that were generally encountered during sampling during other months of the year, but not in September 2014, highlighting the importance of transient effects. Such transience is caused by precipitation, irregular waves [Xin et al., 2010], spring-neap cycling, seasonality [Heiss & Michael, 2014], as well as variable contaminant loading, and is not captured in the model. Other causes for the deviations between measured and modeled data include lithological and geochemical heterogeneity, or biogeochemical reactions that were not investigated in this study, including iron and sulfate reduction. The discrepancies demonstrate that the biogeochemical framework of these systems is more complex than what can be captured by the present model, even though the general spatial trends are well represented.

Despite the model simplifications, the simulated N_2 results were consistent with the spatial distribution of products and incubation-inferred reactivity in the intertidal aquifer. Modeled N_2 concentrations were elevated in the intertidal mixing zone on the perimeter of the circulation cell and highest below the high tide mark (Figure 2.7d-2). The model did not reproduce the observed N_2 hot spot 2 m deeper than the highest modeled N_2 concentrations (Figure 2.7d-1 and 2.7d-2), and the

observed pattern of N_2 is a less well-defined arc than in the model, as expected due to heterogeneity and transience discussed above. However, the patterns of high N_2 production and the high N_2 concentrations are in general agreement. Thus, the model results support the link between the physical flow system and reactivity – the occurrence of denitrification along the outer edge of the intertidal circulation cell that was inferred from the incubation experiments. This consistency supports the interpretation of reactivity derived from incubation experiments and indicates their potential utility in determining the spatial distribution of in situ reactivity in other beach aquifers.

The three independent techniques used in this study to characterize the spatial distribution of denitrification in the Cape Shores beach (N_2/Ar ratio, incubation experiments, and numerical modeling) all indicate that denitrification occurs in the mixing zone on the perimeter of the circulation cell in pore water with salinities ranging between 1 and 20. However, the actual zone of denitrification may be more restricted than the simulated or measured N_2 distribution suggests because of advective-dispersive transport of N_2 outside the active denitrification zone following production.

2.4 Discussion

It is evident from pH and ORP measurements that biogeochemical reactions are occurring throughout the intertidal circulation cell, as their cross-sectional distributions deviate substantially from the distributions of salinity. Undersaturation with respect to atmospheric O_2 clearly indicates that oxygen consumption occurs in the circulation cell, most likely through aerobic respiration (Figures 3d and 4).

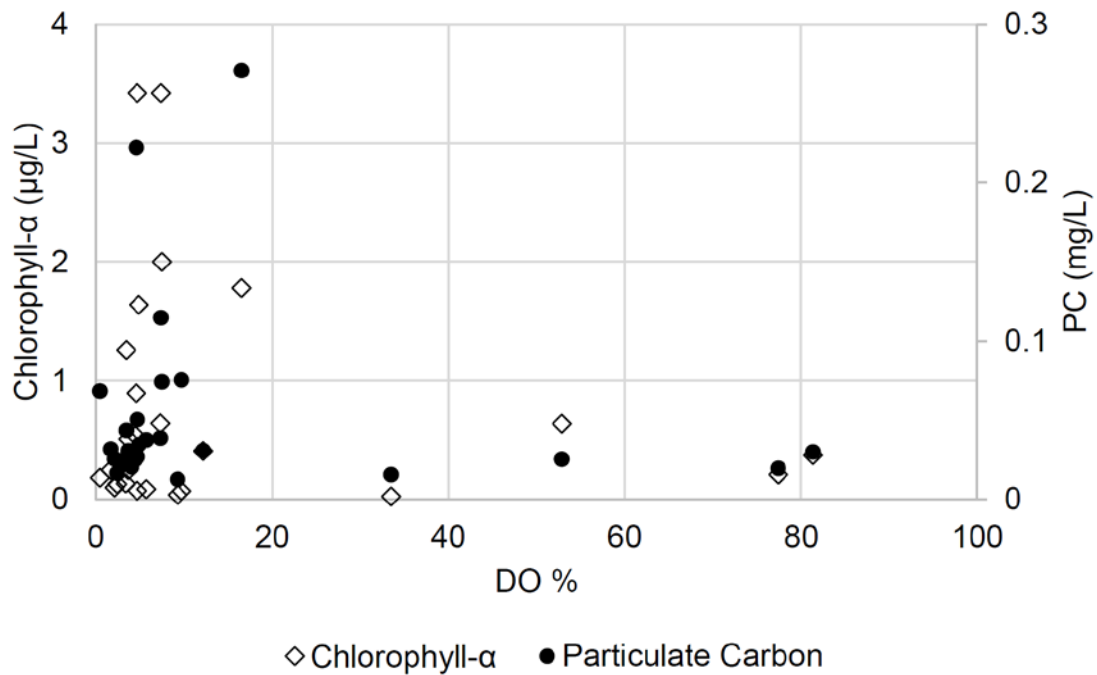


Figure 2.8 Relationship between chlorophyll and particulate carbon (PC) concentrations, and dissolved oxygen saturation.

However, measured O_2 respiration rates are heterogeneous within the system. They are highest along the landward FW-SW mixing zone where seawater infiltration occurs, supported by in situ measurements of DIC and excess pCO_2 , and consistent with CO_2 production during aerobic heterotrophic respiration (Figures 3g–3i). Contrary to our expectations, elevated O_2 consumption rates did not co-occur with higher concentrations of chlorophyll or PC in the pore water. Elevated concentrations of chlorophyll and PC in areas of low in situ DO (Figure 2.8) suggest that the transformation of these mobile forms of particulate carbon may be oxygen limited, as elevated concentrations are found in the aquifer downstream of the landward mixing zone where oxygen is depleted (Figures 2.3e, 2.3f, and 2.3i). This suggests that a more

respirable form of carbon not detected by the methods utilized above may play a larger role in intertidal aquifers than previously expected. Charbonnier et al. [2013] noted that the intertidal beach respiration was at times decoupled from the seasonal phytoplankton bloom and was, most likely, utilizing other sources of bioavailable carbon.

After the rapid consumption of oxygen in the early stages of infiltration, the resulting hypoxic water (< 20% saturation) is transported seaward. Within the seaward mixing zone, aerobic respiration occurs at suppressed rates under hypoxic conditions, utilizing less reactive forms of particulate carbon. This is supported by the observation of elevated DIC and excess $p\text{CO}_2$ that occur in cross-sectional zones proximal to elevated chlorophyll concentrations (Figures 2.3e, 2.3g, and 2.3h). In addition, Figure 2.8 shows the oxygen-limited behavior of mobile carbon: the highest concentrations of carbon were observed where DO concentrations were low. This slower respiration of carbon is not expressed in the incubation experiments, presumably because the incubation reaction rates were based on the first 7 days of incubation, when they were linear with time. After 7 days, the experimental reaction rates decreased substantially, perhaps due to a shift to a carbon source with a lower degree of reactivity or changes in the rates of cell growth. Within the beach aquifer, other sedimentary sources of carbon such as microphytobenthos, sediment-entrapped particulate organic carbon (POC), and surface-deposited POC that are not present in pore water incubations could also be supporting respiration [Beck et al., 2017; Charbonnier et al., 2013; Reckhardt et al., 2015]. Also, at Cape Shores, on some occasions, beach wrack and woody debris accumulates with the pooled water behind the berm after very high tides, which may account for the elevated respiration at Sampler A. It is possible that sediment-

entrapped particulate carbon not included in pore water incubations, with continuous replenishment of oxygen into the circulation cell during tide and wave action, would allow for respiration rates higher than observed in laboratory incubation experiments.

After aerobic respiration depletes oxygen, denitrification can occur closer to the freshwater discharge point. This is supported by the results of the incubation experiments which show the highest N_2 production rates in the mixing zone (Figure 2.3l). Reactive transport simulations were consistent with these field and laboratory results and confirm the link between the physical flow system and biogeochemical reactivity. The model demonstrated that nitrogen gas accumulates along circulating flow paths on the perimeter of the circulation cell where saltwater and freshwater mix. The model predicted the highest N_2 concentrations between the 1 and 20 salinity contours, which agrees with the distribution of high N_2 production rates obtained from the incubation experiments (Figure 2.7b). Because the whole aquifer was enriched in N_2 in situ, there is also a potential for anaerobic ammonium oxidation (anammox) in areas of elevated ammonium (Figure 2.3k, Samplers F and G). Although oxygen levels in Samplers F and G range from 1 to 13 μM O_2 , recent research conducted off the coast of Namibia and Peru by Kalvelage et al. [2011] found anammox to proceed at oxygen levels up to 20 μM , 20 times higher than oxygen levels originally proposed from laboratory cultures of anammox bacteria [Strous et al., 1997] Because the seaward boundary of the intertidal circulation cell experiences frequent shifts in oxygen regimes, it is possible that anaerobic bacteria in this region have adapted to a higher O_2 tolerance.

Other reaction dynamics, such as sorption and dissolution, further affect various solutes within the intertidal circulation cell. High amounts of particulate

phosphorus and phosphate are detected near Sampler A, presumably from degradation of the accumulated detritus on the beach surface. PO_4^{3-} then travels downgradient with a dilution pattern but disappears in the region of elevated chlorophyll (Figure 2.3n, pink contour). Instead, particulate phosphorus is detected in the same region (Figure 2.3m, pink contour). In addition to P-release during organic matter degradation, phosphate can adsorb readily to particles including the particulate organic matter in this area of the circulation cell [Benitez-Nelson, 2000]. When ORP conditions become more reducing, this PO_4^{3-} can be released back into the water and become readily available [Föllmi, 1996]. The distribution of dissolved silica is related primarily to dilution of freshwater concentrations by seawater, with evidence of production along flow paths, similar to that observed by Charbonnier et al. [2013] (Figure 2.3o). This may be related to an estuarine source of biogenic silica. Spatial and temporal correlation of dissolved N, P, and Si species are common, due to the similar sources and regeneration patterns, even when regeneration in the case of Si may be related to different processes [Ullman & Welch, 2002; Ullman et al., 2003].

The dominant mechanisms and the extent of biogeochemical reactivity can quickly change in between samplers and within a few weeks in the intertidal circulation cell. High respiration rates along the landward FW-SW mixing zone followed by suppressed rates and denitrification along the seaward FW-SW mixing zone highlight mixing, oxygen availability, and carbon lability as important controls of reactivity at a given location within the intertidal circulation cell. Because dynamic shifts in the geometric shape of the circulation cell alter flow paths, reduction potentials, oxygen and solute concentrations, the understanding of how the

biogeochemistry and reactivity relates to its location within the cell is key to the coherent study of this dynamic system.

2.5 Conclusions

To our knowledge, this work is the first to present independent concentration and reactivity data that describe the relationship between the intertidal circulation cell in beach aquifers and its biogeochemical reactivity (mainly aerobic respiration and denitrification). This complements previous work that postulates reaction locations or redox conditions utilizing solute distributions and supports the conclusion that sandy beaches are important hosts of biogeochemical activity and therefore play important roles in coastal ecology. Based on O₂ consumption and N₂ production rates from incubations, and in situ evidence of excess N₂ and DIC, the highest rates of aerobic respiration and denitrification were found along the FW-SW mixing zone of the intertidal circulation cell. Remineralization of particulate organic carbon is not responsible for the high rates of reaction in this zone but contributes to slower respiration in the seaward FW-SW mixing zone. Numerical simulations show an accumulation of N₂ gas along the 20 salinity contour, consistent with our observations, emphasizing the link between physical and chemical processes. Although the geometry of the intertidal circulation cell will vary by location according to its hydrologic, topographic, and geologic setting, the principle that organic matter consumption is enhanced at the FW-SW mixing zone is likely to endure.

REFERENCES

- Abarca, E., H. Karam, H. F. Hemond, and C. F. Harvey (2013), Transient groundwater dynamics in a coastal aquifer: The effects of tides, the lunar cycle, and the beach profile, *Water Resources Research*, 49, 1–16.
<https://doi.org/10.1002/wrcr.20075>.
- Abril, G., H. Etcheber, A. V. Borges, and M. Frankignoulle (2000), Excess atmospheric carbon dioxide transported by rivers into the Scheldt estuary, *Comptes Rendus de l'Academie des Sciences-Series IIA-Earth and Planetary Science*, 330(11), 761-768, [https://doi.org/10.1016/S1251-8050\(00\)00231-7](https://doi.org/10.1016/S1251-8050(00)00231-7).
- Aller, R. C. and J. Y. Yingst (1980), Relationships between microbial distribution and the anaerobic decomposition of organic matter in surface sediments of Long Island Sound, USA, *Marine Biology*, 56, 29-42, doi:10.1007/BF00390591.
- Anschutz, P., T. Smith, A. Mouret, J. Deborde, S. Bujan, D. Poirer, and P. Lecroart (2009), Tidal sands as biogeochemical reactors, *Estuarine, Coastal, and Shelf Science*, 84, 84-90, doi:10.1016/j.ecss.2009.06.015.
- Anwar, N., C. Robinson, and D. A. Barry (2014), Influence of tides and waves on the fate of nutrients in a nearshore aquifer: Numerical simulations. *Advances in Water Resources*, 73, 203-213,
<http://dx.doi.org/10.1016/j.advwatres.2014.08.015>.
- Bakhtyar, R., A. Brovelli, D. A. Barry, C. Robinson, and L. Li (2013), Transport of variable-density solute plumes in beach aquifers in response to oceanic forcing, *Advances in Water Resources*, 53, 208-224,
<http://dx.doi.org/10.1016/j.advwatres.2012.11.009>.
- Bardini, L., F. Boano, M. B. Cardenas, R. Revelli, and L. Ridolfi (2012), Nutrient cycling in bedform induced hyporheic zones, *Geochimica et Cosmochimica Acta*, 84, 47–61. <http://doi.org/10.1016/j.gca.2012.01.025>.

- Beck, M., A. Reckhardt, J. Amelsberg, A. Bartholomä, H. Brumsack, H. Cypionka, T. Dittmar, B. Engelen, J. Greskowiak, H. Hillebrand, M. Holtappels, R. Neuholz, J. Köster, M. Kuypers, G. Massmann, D. Meier, J. Niggemann, R. Paffrath, K. Pahnke, S. Rovo, M. Striebel, V. Vandieken, A. Wehrmann, O. Zielinski (2017), The drivers of biogeochemistry in beach ecosystems: A cross-shore transect from the dunes to the low water line, *Marine Chemistry*, 190, 35-50, <http://dx.doi.org/10.1016/j.marchem.2017.01.001>.
- Benitez-Nelson, C. (2000), The biogeochemical cycling of phosphorus in marine systems, *Earth-Science Reviews*, 51(1), 109-135, [http://dx.doi.org/10.1016/S0012-8252\(00\)00018-0](http://dx.doi.org/10.1016/S0012-8252(00)00018-0).
- Boudreau, B. P., M. Huettel, S. Forster, R. A. Jahnke, A. McLachlan, J. J. Middelburg, P. Nielsen, F. Sansone, G. Taghon, W. Van Raaphorst, I. Webster, J. M. Weslawski, P. Wilberg, B. Sundby (2001), Permeable marine sediments: overturning an old paradigm, *EOS Transactions American Geophysical Union*, 82(11) 133-136, doi:10.1029/EO082i011p00133-01.
- Boufadel, M. C., H. Li, M. T. Suidan, and A. D. Venosa (2007), Tracer Studies in a Laboratory Beach Subjected to Waves. *Journal of Environmental Engineering*, 133, 722–732. [https://doi.org/10.1061/\(ASCE\)0733-9372\(2007\)133:7\(722\)](https://doi.org/10.1061/(ASCE)0733-9372(2007)133:7(722)).
- Burnett, W. C., H. Bokuniewicz, M. Huettel, W.S. Moore, and M. Taniguchi (2003), Groundwater and pore water inputs to the coastal zone, *Biogeochemistry*, 66 (1/2), 3-33, doi: 10.1023/B:BIQG.0000006066.21240.53.
- Cai, W. J., Y. Wang, J. Krest, and W. S. Moore (2003), The geochemistry of dissolved inorganic carbon in a surficial groundwater aquifer in North Inlet, South Carolina, and the carbon fluxes to the coastal ocean, *Geochimica et Cosmochimica Acta*, 67(4), 631-639, doi: 10.1016/S0016-7037(02)01167-5.
- Cai, W. J., G. W. Luther, J. C. Cornwell, and A. E. Giblin (2010), Carbon cycling and the coupling between proton and electron transfer reactions in aquatic sediments in Lake Champlain, *Aquatic geochemistry*, 16(3), 421-446, doi: 0.1007/s10498-010-9097-9.
- Chaillou, G., M. Couturier, G. Tommi-Morin, and A. M. Rao (2014), Total alkalinity and dissolved inorganic carbon production in groundwaters discharging through a sandy beach, *Procedia Earth and Planetary Science*, 10, 88-99, <http://dx.doi.org/10.1016/j.proeps.2014.08.017>.

- Chaillou, G., F. Lemay-Borduas, and M. Couturier (2016), Transport and transformations of groundwater-borne carbon discharging through a sandy beach to a coastal ocean, *Canadian Water Resources Journal*, 41(4), 455-468, <http://dx.doi.org/10.1080/07011784.2015.1111775>.
- Charbonnier, C., P. Anschutz, D. Poirier, S. Bujan, and P. Lecroart (2013), Aerobic respiration in a high-energy sandy beach, *Marine Chemistry*, 155, 10-21, <http://dx.doi.org/10.1016/j.marchem.2013.05.003>.
- Charette, M. A., and E. R. Sholkovitz (2002), Oxidative precipitation of groundwater-derived ferrous iron in the subterranean estuary of a coastal bay, *Geophysical research letters*, 29(10), 85-1–85-4, doi:10.1029/2001GL014512.
- Cooper Jr., H. H. (1959), A hypothesis concerning the dynamic balance of fresh water and salt water in a coastal aquifer, *J. Geophys. Res.*, 64(4), 461–467, doi:10.1029/JZ064i004p00461.
- Dale, R. K., and D. C. Miller (2007), Spatial and temporal patterns of salinity and temperature at an intertidal groundwater seep, *Estuarine, Coastal and Shelf Science*, 72(1), 283-298, <http://dx.doi.org/10.1016/j.ecss.2006.10.024>.
- Dale, R. K., and D. C. Miller (2008), Hydrologic interactions of infaunal polychaetes and intertidal groundwater discharge, *Marine ecol. prog. Ser.*, 363, 205-215, <https://doi.org/10.3354/meps07455>.
- Föllmi, K. B. (1996), The phosphorus cycle, phosphogenesis and marine phosphate-rich deposits, *Earth-Science Reviews*, 40(1-2), [http://dx.doi.org/10.1016/0012-8252\(95\)00049-6](http://dx.doi.org/10.1016/0012-8252(95)00049-6).
- Garcia, H.E. and L.I. Gordon, (1992), Oxygen solubility in seawater: better fitting equations, *Limnology and Oceanography*, 37, 1307-1312 (and erratum 38, 656), doi:10.4319/lo.1992.37.6.1307.
- Gran, G. (1952), Determination of the equivalence point in potentiometric titrations, Part II, *Analyst*, 77(920), 661-671, doi: 10.1039/an9527700661.
- Hamme, R.C., and S.R. Emerson, (2004), The solubility of neon, nitrogen, and argon in distilled water and seawater, *Deep-Sea Research*, 51, 1517-1528, <http://dx.doi.org/10.1016/j.dsr.2004.06.009>.
- Hays, R. L., and W. J. Ullman (2007a), Direct determination of total and fresh groundwater discharge and nutrient loads from a sandy beachface at low tide (Cape Henlopen, Delaware), *Limnology and oceanography*, 52(1), 240-247, doi:10.4319/lo.2007.52.1.0240.

- Hays, R. L., and W. J. Ullman (2007b), Dissolved nutrient fluxes through a sandy estuarine beachface (Cape Henlopen, Delaware, USA): contributions from fresh groundwater discharge, seawater recycling, and diagenesis, *Estuaries and Coasts*, 30(4), 710-724, doi:10.1007/BF02841967.
- Heiss, J.W., W.J. Ullman, and H.A. Michael (2014), Swash zone moisture dynamics and unsaturated infiltration in two sandy beach aquifers, *Estuarine, Coastal, and Shelf Science*, 143, 20-31, doi:10.1016/j.ecss.2014.03.015.
- Heiss, J. W., and H. A. Michael (2014), Saltwater-freshwater mixing dynamics in a sandy beach aquifer over tidal, spring-neap, and seasonal cycles, *Water Resour. Res.*, 50, 6747–6766, doi:10.1002/2014WR015574.
- Johannes, R. E. (1980). Ecological significance of the submarine discharge of groundwater, *Marine ecol. prog. ser.*, 3(4), 365-373.
- Kalvelage, T., M. M. Jensen, S. Contreras, N. P. Revsbech, P. Lam, M. Günter, J. LaRoche, G. Lavik and M. M. Kuypers (2011), Oxygen sensitivity of anammox and coupled N-cycle processes in oxygen minimum zones, *PLoS One*, 6(12), e29299, doi:10.1371/journal.pone.0029299.
- Kana, T. M., C. Darkangelo, M. Duane Hunt, J. B. Oldham, G. E. Bennett, and J. C. Cornwell (1994), Membrane inlet mass spectrometer for rapid high-precision determination of N₂, O₂, and Ar in environmental water samples, *Analytical Chemistry*, 66, 4166-4166, doi: 10.1021/ac00095a009.
- Kana, T. M., J. C. Cornwell, and L. Zhong (2006), Determination of denitrification in the Chesapeake Bay from measurements of N₂ accumulation in bottom water, *Estuaries and Coasts*, 29(2), 222-231, doi: 10.1007/BF02781991.
- Kohout, F. A. (1960), Cyclic flow of salt water in the Biscayne aquifer of southeastern Florida, *J. Geophys. Res.*, 65(7), 2133–2141, doi:10.1029/JZ065i007p02133.
- Langevin, C. D., D. T. Thorne Jr., A. M. Dausman, M. C. Sukop, and W. Guo (2008), SEAWAT version 4: A computer program for simulation of multi-species solute and heat transport, U.S. in *Geol. Surv. Tech. Methods*, Book 6, Chap. A22, pp. 39, Geological Survey, US.
- Morey, G.W., R. O. Fournier, and J. J. Rowe (1964), The solubility of amorphous silica at 25 °C, *Journal of Geophysical Research*, 69 (10), 1995-2002, doi: 10.1029/JZ069i010p01995.

- McAllister, S.M., J.M. Barnett, J.W. Heiss, A.J. Findlay, D.J. MacDonald, C. L. Dow, G.W. Luther, H. A. Michael, and C.S Chan (2015), Dynamic hydrologic and biogeochemical processes drive microbially enhanced iron and sulfur cycling within the intertidal mixing zone of a beach aquifer, *Limnology and Oceanography*, 60, 329-345, doi: 10.1111/lno.10029.
- Michael, H. A., A. E. Mulligan, and C. F. Harvey (2005), Seasonal oscillations in water exchange between aquifers and the coastal ocean, *Nature*, 436(7054), 1145-1148, doi:10.1038/nature03935.
- Miller, D. C., and W. J. Ullman (2004), Ecological consequences of ground water discharge to Delaware Bay, United States. *Ground Water*, 42(7), 959-970, doi: 10.1111/j.1745-6584.2004.tb02635.x.
- Millero, F. J., T. B. Graham, F. Huang, H. Bustos-Serrano, and D. Pierrot (2006), Dissociation constants of carbonic acid in seawater as a function of salinity and temperature, *Marine Chemistry*, 100, 80–94, <http://dx.doi.org/10.1016/j.marchem.2005.12.001>.
- Moore, W. S. (1999), The subterranean estuary: a reaction zone of ground water and sea water. *Marine Chemistry*, 65(1), 111-125, [http://dx.doi.org/10.1016/S0304-4203\(99\)00014-6](http://dx.doi.org/10.1016/S0304-4203(99)00014-6).
- Murphy, J. R. and J. P. Riley (1962), A modified single solution method for the determination of phosphate in natural waters, *Analytical Chimica Acta*, 27, 31-36, [https://doi.org/10.1016/S0003-2670\(00\)88444-5](https://doi.org/10.1016/S0003-2670(00)88444-5).
- Pierrot, D., E. Lewis, and D. W. R. Wallace (2006), CO2SYS DOS Program Developed for CO₂ System Calculations, in ORNL/CDIAC-105, Carbon Dioxide Information Analysis Center, Oak Ridge National Laboratory, US Department of Energy, Oak Ridge, TN.
- Post, V. E. A. (2011), A new package for simulating periodic boundary conditions in MODFLOW and SEAWAT, *Computers and Geosciences*, 37(11), 1843-1849, doi:10.1016/j.cageo.2011.01.012.
- Prommer, H., and V. Post (2002), A reactive multicomponent transport model for saturated porous media, *User's manual version 1*, 141.
- Reckhardt, A., M. Beck, M. Seidel, T. Riedel, A. Wehrmann, A. Bartholomä and H. J. Brumsack (2015), Carbon, nutrient and trace metal cycling in sandy sediments: A comparison of high-energy beaches and backbarrier tidal flats, *Estuarine, Coastal and Shelf Science*, 159, 1-14, <http://dx.doi.org/10.1016/j.ecss.2015.03.025>.

- Robinson, M., D. Gallagher, and W. Reay (1998), Field observations of tidal and seasonal variations in ground water discharge to tidal estuarine surface water, *Groundwater Monitoring & Remediation*, 18(1), 83-92, doi:10.1111/j.1745-6592.1998.tb00605.x.
- Robinson, C., B. Gibbes, and L. Li (2006), Driving mechanisms for groundwater flow and salt transport in a subterranean estuary, *Geophysical Research Letters*, 33(3), L03402, doi: 10.1029/2005GL025247.
- Robinson, C., B. Gibbes, H. Carey, and L. Li (2007), Salt-freshwater dynamics in a subterranean estuary over a spring-neap tidal cycle, *J. Geophys. Res.*, 112, C09007, doi:10.1029/2006JC003888.
- Seidel, M., M. Beck, J. Greskowiak, T. Riedel, H. Waska, I. G. N. A. Suryaputra, B. Schnetger, J. Niggemann, M. Simon, and T. Dittmar (2015), Benthic-pelagic coupling of nutrients and dissolved organic matter composition in an intertidal sandy beach, *Marine Chemistry*, 176, 150-163, <http://dx.doi.org/10.1016/j.marchem.2015.08.011>.
- Slomp, C. P., and P. Van Cappellen (2004), Nutrient inputs to the coastal ocean through submarine groundwater discharge: controls and potential impact. *Journal of Hydrology*, 295(1), 64-86, <http://dx.doi.org/10.1016/j.jhydrol.2004.02.018>.
- Spiteri, C., C. P. Slomp., K. Tuncay, C. Meile (2008), Modeling biogeochemical processes in subterranean estuaries: Effect of flow dynamics and redox conditions on submarine groundwater discharge of nutrients. *Water Resources Research*, 44(2), doi:10.1029/2007WR006071.
- Strous, M., E. Van Gerven, J. G. Kuenen, and M. Jetten (1997), Effects of aerobic and microaerobic conditions on anaerobic ammonium-oxidizing (anammox) sludge, *Applied and environmental microbiology*, 63(6), 2446-2448.
- Thamdrup, B., J.W. Hansen, and B.B. Jorgensen, (1998), Temperature dependence of aerobic respiration in a coastal sediment, *FEMS Microbiology Ecology*, 25(2), 189-200, <https://doi.org/10.1111/j.1574-6941.1998.tb00472.x>.
- Ullman, W. J., and S. A. Welch (2002), Organic ligands and feldspar dissolution, in *Water-rock interactions, ore deposits, and environmental geochemistry: A tribute to David Crerar.*, special publication 7, edited by R. Hellmann and S. A. Wood, pp. 3-35, The Geochemical Society, St. Louis, MO.

- Ullman, W. J., B. Chang, D. C. Miller, and J. A. Madsen (2003), Groundwater mixing, nutrient diagenesis, and discharges across a sandy beachface, Cape Henlopen, Delaware (USA), *Estuarine, Coastal and Shelf Science*, 57(3), 539-552, [http://dx.doi.org/10.1016/S0272-7714\(02\)00398-0](http://dx.doi.org/10.1016/S0272-7714(02)00398-0).
- Van Cappellen, P., and Y. Wang (1996), Cycling of iron and manganese in surface sediments: A general theory for the coupled transport and reaction of carbon, oxygen, nitrogen, sulfur, iron, and manganese, *Am. J. Sci.*, 296(3), 197–243, doi:10.2475/ajs.296.3.197.
- Weiss, R.F. (1970), The solubility of nitrogen, oxygen and argon in water and seawater, *Deep Sea Research and Oceanographic Abstracts*, 17(4), 721-735, [https://doi.org/10.1016/0011-7471\(70\)90037-9](https://doi.org/10.1016/0011-7471(70)90037-9).
- Westrich, J.T. and R.A. Berner, 1988, The effect of temperature on rates of sulfate reduction in marine sediments, *Geomicrobiology Journal*, 6, 99-117, <http://dx.doi.org/10.1080/01490458809377828>.
- Xin, P., C. Robinson, L. Li, D. A. Barry, and R. Bakhtyar (2010), Effects of wave forcing on a subterranean estuary. *Water Resources Research*, 46(12), <https://doi.org/10.1029/2010WR009632>.

Chapter 3

HYDROLOGIC SHIFTS CREATE COMPLEX TRANSIENT DISTRIBUTIONS OF PARTICULATE ORGANIC CARBON AND BIOGEOCHEMICAL RESPONSES IN BEACH AQUIFERS

This work has been submitted to *Journal of Geophysical Research: Biogeosciences* as Kim, K. H., H. A. Michael, E. K. Field, and W. J. Ullman (2019), Hydrologic shifts create complex transient distributions of particulate organic carbon and biogeochemical responses in beach aquifers.

Abstract

Biogeochemical reactions within intertidal zones of coastal aquifers have been shown to alter the concentrations of terrestrial solutes prior to discharge to surface waters. In organic-poor sandy aquifers, the input of marine organic matter from infiltrating seawater supports active biogeochemical reactions within the sediments. However, while the seasonality of surface water organic carbon concentrations (primary production) and groundwater mixing have been documented, there is limited understanding of the transience of various organic carbon pools (porewater particulate, dissolved, sedimentary) within the aquifer and how these relate to the location and magnitudes of biogeochemical reactions over time. To understand the relationship between changes in groundwater flow and the seasonal migration of geochemical patterns, beach porewater and sediment samples were collected and analyzed from six field sampling events spanning two years. While the seasonally-dynamic patterns of aerobic respiration closely followed those of salinity, redox conditions and nutrient

characteristics (distributions of N and P, denitrification rates) were unrelated to contemporaneous salinity patterns. This divergence was attributed to the spatial variations of reactive particulate organic carbon distributions, unrelated to salinity patterns, likely due to filtration, retardation, and immobilization dynamics during transport within the sediments. Results support a “carbon memory” effect within the beach, with the evolution and migration of reaction patterns relating to the distribution of these scattered carbon pools as more mobile solutes move over less mobile pools during changes in hydrologic conditions. This holds important implications for the prediction and quantification of biogeochemical reactions within beach systems.

3.1 Introduction

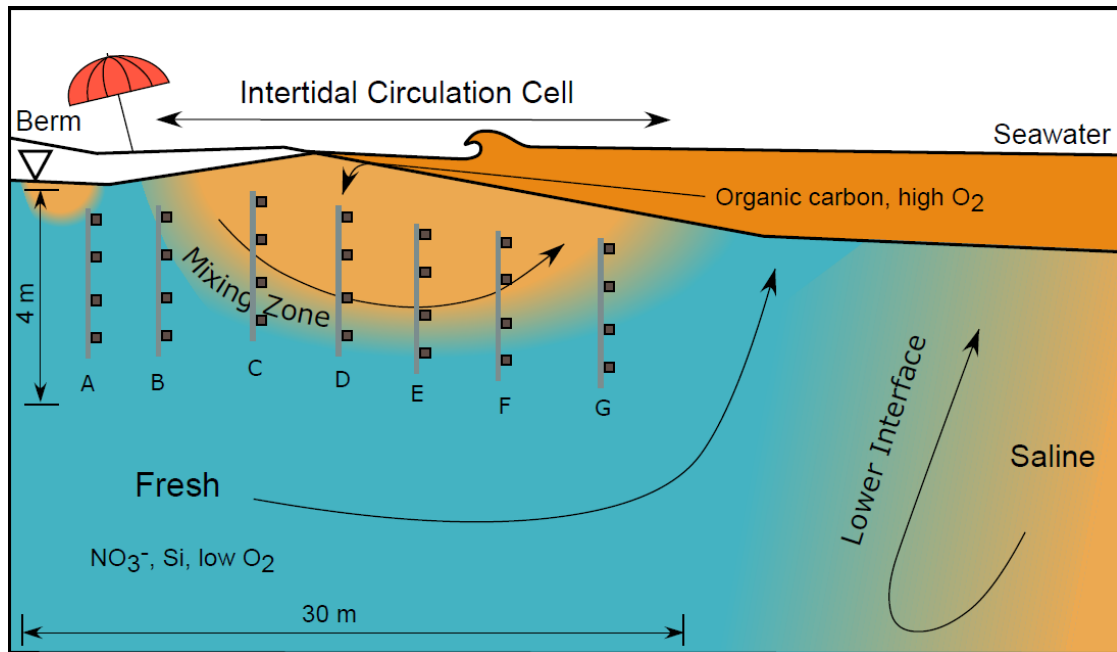


Figure 3.1 Cross-sectional schematic of a coastal beach aquifer. Fresh groundwater discharges seaward, meeting the convectively-circulating seawater at the lower interface. Wave and tide action deliver seawater to the beachface, which then infiltrates into the aquifer creating and sustaining the intertidal circulation cell. Porewater sampling ports are indicated in black squares on the multi-level samplers (A-G). Fresh groundwater transports terrestrial nutrients (NO_3^- , PO_4^{3-} , and Si) while seawater delivers reactive organic carbon and oxygen. Modified from Kim et al. [2017].

Fresh groundwater in coastal aquifers mixes with saline seawater prior to its discharge to the ocean as submarine groundwater discharge (SGD) [Li et al., 2008; Michael et al., 2005; Robinson (M) et al., 1998; Robinson (C) et al., 2007]. SGD includes the discharge of fresh groundwater (blue, Figure 3.1), convectively-recirculated seawater at the base of the beach (lower interface, Figure 3.1), and circulating brackish water due to tide and wave activity on the beach (intertidal

circulation cell, Figure 3.1). The influx of oxygen and reactive marine organic carbon from saline seawater into hypoxic to anoxic fresh groundwater creates strong geochemical gradients along freshwater-seawater (FW-SW) mixing zones, promoting biogeochemical reactions within the intertidal circulation cell. The chemical reactivity within the cell and of coastal aquifers has been the subject of a number of field [M. Beck et al., 2017; Charbonnier et al., 2013; Reckhardt et al., 2015; Seidel et al., 2015] and numerical modeling studies [Abarca et al., 2013; Anwar et al., 2014; Heiss et al., 2017; C. Robinson et al., 2007], due to its ability to transform and mitigate inputs of nutrients [Hays and Ullman, 2007a&b; Kim et al., 2017; Slomp and Van Cappellen, 2004; Ullman et al., 2003], metals and trace elements [Bone et al., 2006; Charette and Sholkovitz, 2002, 2006; Charette et al., 2005; Jung et al., 2009; McAllister et al., 2015], and contaminants [Geng et al., 2015; Robinson et al., 2009] to coastal systems.

Seasonal sea-level and groundwater table fluctuations, climate-driven sea-level anomalies, wave conditions, storms, and precipitation patterns create variability in SGD flux [Gonneea et al., 2013; Heiss and Michael, 2014; Michael et al., 2005; Moore and Wilson, 2005; Wilson et al. 2011; Xin et al., 2014; Yu et al., 2017], and consequently, the fluxes of nutrients, trace elements, and radioactive tracers to the adjacent ocean [Beck (A) et al., 2007; Gonneea et al., 2013(b); Jeong et al., 2012; Kelly and Moran 2002; Roy et al., 2013; Seidel et al., 2015; Santos et al., 2009; Waska and Kim, 2011]. The circulation cell is spatiotemporally dynamic, responding primarily to seasonal freshwater gradient fluctuations, and also to spring-neap cycles, and tidal stage to a lesser extent [Heiss and Michael, 2014]. These physical shifts alter groundwater flowpaths within the beach aquifer and consequently change the delivery of gases, solutes, and particles necessary to support biogeochemical reactions at a

given location. It has been shown that the locations and rates of solute-dependent reactions, such as aerobic respiration and denitrification, are related to groundwater flowpaths defined by the geometry of the circulation cell [Kim et al., 2017]. Therefore, transient distribution of various reactants that result from seasonal hydrologic changes imply an equally dynamic movement of reaction centers and characteristics over the seasons.

Sandy sediments are not often associated with large reservoirs of organic matter [Anschutz et al., 2009; Boudreau et al., 2001]. Therefore, the delivery and transport of reactive carbon into the beach aquifer is a principal factor controlling the rates and distribution of biogeochemical reactions within the circulation cell. Continental shelf and intertidal sandflat sediments have been shown to entrap organic matter, bacteria, and particles which then undergo bioturbation, resuspension, and/or degradation [Bacon et al., 1994; Huettel and Rusch 2000; Pilditch and Miller 2006; Rusch and Huettel 2000; Rusch et al 2000]. Analogously, beach sediments also act like a filter, entrapping fine particles [Anschutz et al., 2009; Charbonnier et al., 2013; McLachlan et al., 1985] and bacteria [Gast et al., 2015], resulting in spatial variations in the respiration rate of sediments [A. Beck et al., 2016]. However, while the seasonality of hydrology, surface water primary production, porewater DOC concentrations, and subsequent changes to reaction rates are relatively well-documented [M. Beck et al., 2008; Charbonnier et al., 2013; Seidel et al., 2014; Seidel et al., 2015; O'Connor et al., 2018], there has been limited focus on the transport and immobilization of particulate organic matter distributions and related reaction characteristics. As the extent and geometry of the intertidal circulation cell evolve over

seasons, changing flow and transport patterns would variably distribute particulate organic carbon within the aquifer.

Charbonnier et al. [2013] explored temporal variations of solute concentrations in shallow porewater at Truc Vert, France, noting that in the summer, oxygen depletion and associated nitrate enrichment in the lower beach areas were decoupled from surface water chlorophyll concentrations, indicating an alternative organic carbon source. A. Beck et al., [2016] observed increases of ammonium within the sediments that may be related to solid-phase organic matter degradation. Similarly, O'Connor et al. [2018] observed the seasonality of redox conditions in the intertidal aquifer at Gloucester Point, VA, and documented increases in dissolved organic carbon above the conservative mixing curve in the summer that may be linked to the breakdown of particulate carbon. Detailed molecular characterization of dissolved organic matter on samples from the Northern Germany Wadden Sea suggested the release of labile marine DOC and other nutrients from buried algal and microbial biomass, which were preferentially consumed relative to DOC of terrestrial origin [Seidel et al., 2014]. Dissolved organic matter composition of intertidal sands also showed significant correlation to the supplied marine and terrestrial organic matter, while organic matter composition in tidal flats were decoupled from seasonality and more related to early diagenetic processes [M. Beck et al., 2017; Seidel et al., 2015]. These studies collectively indicate that organic matter dynamics within sediments are influenced by both hydrologic transport and diagenesis and call for further work that comprehensively integrate the roles of particulate and dissolved carbon dynamics in beach systems.

In this paper, we present a two-year porewater and sediment study to illustrate the transient behavior of reaction zones and particulate organic matter distributions within sandy beach aquifers. Our results show that while salinity and aerobic respiration rates respond and equilibrate to hydrologic changes, reaction and nutrient distributions deviate from changes in salinity patterns. We attribute this asynchronous behavior to the variable distribution of reactive organic carbon and the transport dynamics of reactants. This study demonstrates the spatiotemporal complexity of reaction characteristics with beach aquifers, caused by, but spatially and temporally decoupled from, positional shifts of the intertidal circulation cell.

3.2 Field site and Methods

3.2.1 Field Site

The research was conducted at Cape Shores, Lewes, Delaware, a public beach adjacent to Cape Henlopen State Park. The beach is tide-dominated (semi-diurnal, 1.42 m range) with limited wave activity due to offshore breakwaters. The beach aquifer is mostly coarse sand (540-668 μm), with two pebbly layers interfingering the aquifer and finer sediments (128-360 μm) in deeper locations (> 2 m).

The intertidal circulation cell at Cape Shores has been extensively characterized, with previous work confirming the remineralization of organic matter and cycling of nitrogen, phosphorus, silica, iron, and sulfur [Ullman et al., 2003; Hays and Ullman, 2007a&b; McAllister et al., 2015; Kim et al., 2017]. Heiss and Michael [2014] measured and modeled the dynamics of the cell over tidal, spring-neap, and seasonal cycles, and showed that the most prominent changes to the cell geometry occurred over seasonal cycles. The spatial distributions of reactions within the

intertidal circulation cell and their relationships to its flowfield have also been documented by Kim et al. [2017], with higher oxic respiration rates near the point of seawater infiltration at the beach surface and along the landward edge of the freshwater-seawater mixing zone at depth. Because the intertidal circulation cell at Cape Shores displays migrations seasonally, and reaction rates related to the flowfield have been well characterized, this field site is well-suited for further research on how reaction rates in the aquifer are related to the flow and sedimentary characteristics in the aquifer over seasonal timescales.

3.2.2 Porewater Sampling and Incubation Experiments

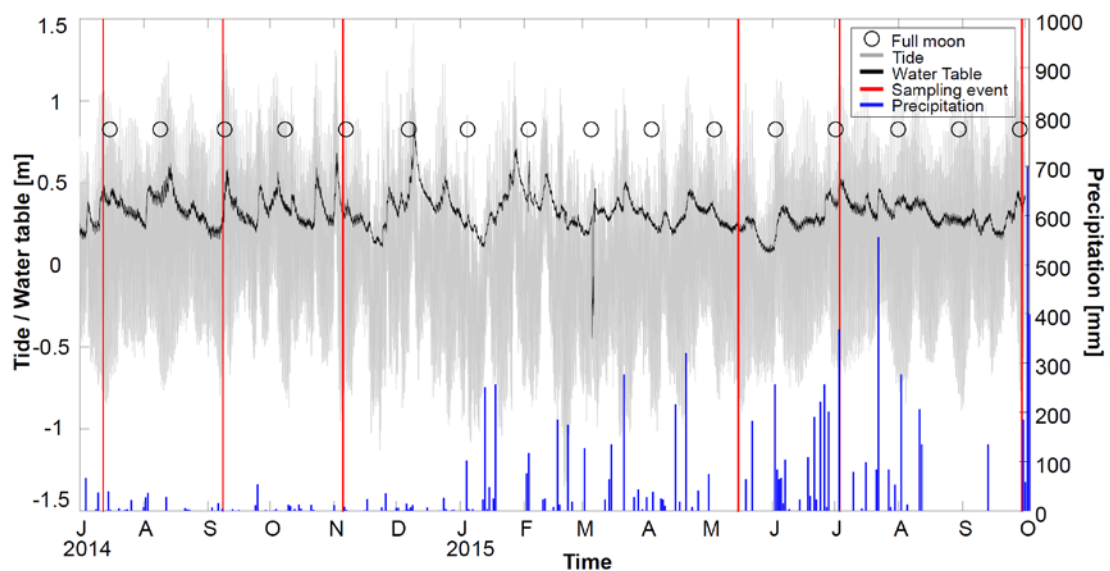


Figure 3.2 Time-series of hourly tide levels, freshwater head, and precipitation. Grey lines indicate recorded tides at the nearby NOAA tidal station 8557830, with full moon indicated by open circles. Precipitation from NOAA Georgetown Sussex County Airport Station (GHCND: USW00013764) is marked in blue bar graph, and sampling events are indicated in red.

Multi-level porewater samplers were constructed from polyethylene tubes mounted along a PVC support pipe. Porewater was collected from the samplers using a peristaltic pump (GeoTech, Denver, Colorado) along a shore-perpendicular transect over six time periods in 2014 (July, September, November) and 2015 (May, July, September). Lost or damaged samplers were replaced as close to their original locations as possible to capture the full extent of the intertidal circulation cell, and best efforts were made to sample from as close to the same locations and depths as possible. As a consequence of the beach dynamics and damage to samplers, some ports could not be used for sample collection on all sampling dates. Inland water table levels were measured every 15 minutes at a well installed at the dune landward of the intertidal circulation cell using a TD-Diver with barometric corrections (Van Essen Instruments, Delft, Netherlands).

Salinity, temperature, oxidation-reduction potential (ORP), and dissolved oxygen (DO) were measured in the field while other solutes and constituents (chlorophyll, dissolved organic carbon (DOC), particulate nitrogen, NO_3^- , NH_4^+ , particulate phosphorus, PO_4^{3-} , dissolved Si) were measured in the laboratory. Porewater particulate organic carbon (here referred to as porewater POC) was quantified by filtering 1 L of porewater through a 0.7 μm glass fiber filter, which were then combusted using the Costech CHN Elemental Analyzer to measure carbon. For May 2015, accurate ORP measurements were unavailable due to a probe malfunction. Five unfiltered replicate porewater samples were incubated in the laboratory in the dark to determine the successive decrease of oxygen and increase of nitrogen to obtain apparent oxygen consumption and denitrification rates. Additional details about the

design and construction of samplers, solute and particulate sampling and analyses, and incubation experiments can be found in Kim et al. [2017].

3.2.3 Sediment Vibracores

Two vibracores were collected in July 2015 adjacent to Sampler C (Core C, 1.1 m depth) and Sampler F (Core F, 1.9 m depth) (Figure 3.3, Figure 3.8) to characterize the sediments and potential respiration rates at the field site. Pebbly layers and finer sand at depth, as well as color variations along the core (light brown to greyish black) were visible to the naked eye. Each core was divided into four sections according to grain size and color. Then, each section was homogenized, and five replicate sediment samples were taken from the homogenized batch. The sediment samples were then incubated in borosilicate biological oxygen demand bottles with filtered, oxygenated seawater to obtain rates of oxygen consumption and nitrogen gas production at the sampling sites. Oxygen consumption rates from sediment-free control samples (filtered, oxygenated seawater with no sediment input) were subtracted from measured rates to obtain reaction rates that reflect the contributions of sedimentary organic matter to bulk reaction rates. Sediments were analyzed for carbon content (here referred to as entrapped sedimentary carbon) using the loss on ignition method. Elemental concentrations (Al, B, Ca, Cu, Fe, K, Mg, Mn, Na, P, S, Zn, As, Cd, Cr, Ni, and Pb) were also analyzed using the EPA method 3051 for digestion and Inductively Coupled Plasma Mass Spectrometry (ICP-MS).

3.2.4 Sand Column Deployments

Sand column deployments were conducted to distinguish respiration associated with porewater-delivered organic matter that had been entrapped by the sand from in-

situ organic matter deposited with sediments. Five 10 ft PVC pipes (1/2" OD) were slotted over their full length and filled with homogenized beach sand that had been pre-combusted overnight to remove all organics. Top and bottom of the columns were glue-capped, and a rope handle was attached at the top for easy retrieval. In 31 July 2015, the columns were installed by hand-augering along a transect adjacent to the porewater sampling transect, 6 ft east of each porewater sampler (Figure 3.8, Sampler B, C, E, F, and H). All columns remained 10 ft in length, save for one column next to Sampler C that had to be trimmed in half due to difficulties during its deployment. On 13 October 2015, after they had time to equilibrate with the beach aquifer system, the columns were pulled out of the beach. The retrieved columns were then divided into lower, mid, and upper sections by cutting them at their 4 and 8 ft mark from the bottom (except for the sand column next to Sampler C, which were only sectioned into two sections due to its shorter length). Lower 10 inches of sediment from each section was then divided among five borosilicate incubation bottles and were incubated following the same sediment incubation procedures outlined above. An incubation with filtered, oxygenated seawater with combusted sediment was used as a control.

3.3 Results

3.3.1 Physicochemical Parameters

Salinity, a conservative tracer, outlines the geometry and location of the intertidal circulation cell. The measured salinity confirms the observations of Heiss and Michael [2014], with the intertidal circulation cell displaying seasonal variations in its size and position in response to seasonal changes in tidal amplitude and freshwater head (Figure 3.3, left column). In both 2014 and 2015, the circulation cell

expanded horizontally, and salinity increased through summer and into the fall (Figure 3.3 Column 1, July to November in 2014; May to September in 2015), in response to the falling freshwater head after its spring (May 2014) or winter maximum (February 2015). In July 2015, intense rain prior to sampling increased the upland water table measured near the top of the beach from 37 cm to 50 cm over 3 days. This increased freshwater gradient constricted and pushed the saline circulation cell seaward, consistent with simulations of Yu et al. [2017]. Salinity sampling for a sub-set of sampling points 8 days (16 July 2015) after the July 2015 sampling event (08 July 2015) displayed higher salinities in Sampler C & D and lower salinities in Sampler F, indicating a landward progression of the intertidal circulation cell as the inland freshwater head decreased (unpublished data). These results demonstrate the dynamic response of the intertidal circulation cell to both seasonal changes and episodic hydrologic events.

The cross-sectional distributions of dissolved oxygen had higher saturation levels located on the upper part of the circulation cell, where the highest rates of infiltration occurred, as indicated by salinity (Figure 3.3, second column). Seawater infiltrates the beach aquifer at fully oxygenated conditions, so the decrease in dissolved oxygen saturation along the circulating flowpath indicates active consumption of oxygen (see also [Kim et al., 2017]). Overall, more dissolved oxygen was available within the intertidal circulation cell during colder months when O₂ is more soluble, biogeochemical reactions were slower, and less seawater carbon from primary production was available. November 2014 and September 2015 had 3 and 6 µg/L of surface water chlorophyll, respectively, compared to the 15.3 µg/L average for other months sampled.

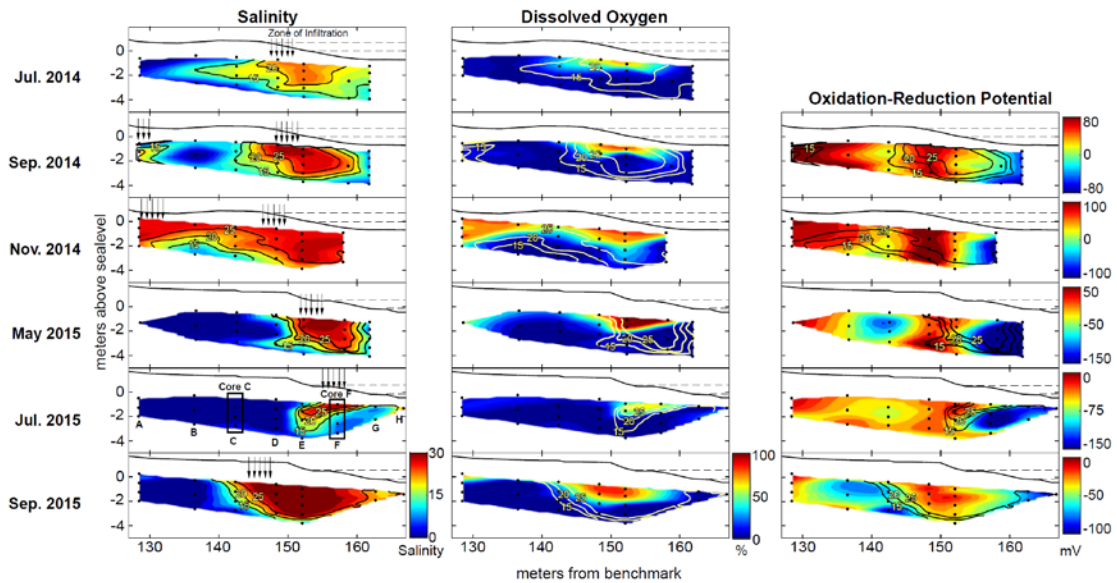


Figure 3.3 Cross-sectional interpolations of measurements of salinity, dissolved oxygen saturation (%), and oxidation-reduction potential (mV). Black dots indicate sampling locations. Salinity contours (15, 20, 25) are overlain in yellow or black to show position of the intertidal circulation cell. Zones of seawater infiltration are indicated with black arrows. Locations of vibracores (C, F) taken in July 2015 are indicated with a rectangle. Note colorbar variation for ORP.

Oxidation-reduction potential (ORP) patterns, reflecting the net effects of oxidation and reduction within the beach aquifer, did not covary with salinity, consistent with previous findings at this site (Figure 3.3, column 3; [Kim et al., 2017]). More reducing conditions were found towards the discharge zone and in some months, near the landward FW-SW mixing zone (May and September 2015). However, the seasonal patterns of ORP were largely independent of salinity shifts within the aquifer.

3.3.2 Dissolved Nutrients

Dissolved nutrients within the aquifer responded to different hydrological and geochemical conditions. While variable in concentrations and distribution over time,

NO_3^- and NH_4^+ had a distinct spatial separation from each other. Nitrate ($\sim 150 \mu\text{M}$) was elevated in the shallower, more landward parts of the aquifer, while ammonium ($\sim 8 \mu\text{M}$), was elevated in deeper parts of the aquifer and near the discharge zone. Hotspots of ammonium were often spatially correlated to elevated concentrations of POC (Figure 3.6), indicating ammonium release during the degradation of POC (Section 3.4.3). However, increased ammonium toward the discharge zone despite low POC in that region (i.e., Figure 3.4, September 2015 & Figure 3.6, September 2015) supports active nitrification within the aquifer [Kroeger and Charette, 2008; Boufadel et al., 2010]. Silica concentrations were generally high in freshwater and low in saline groundwater, likely due to differences in water residence times during which dissolved silica is produced by dissolution in freshwater aquifers [Dove, 1997; Loucaides et al., 2008]. Concentrations elevated above the mixing line in brackish zones indicate mixing-promoted silica dissolution (Appendix B, Figure B-1). Phosphate, on the other hand, was less linked to salinity and displayed more patchiness. Phosphate-rich zones were related to elevated particulate organic carbon in the porewater, supporting active leaching and release of phosphate from organic material. This behavior was also displayed by particulate N (see Section 3.4.3).

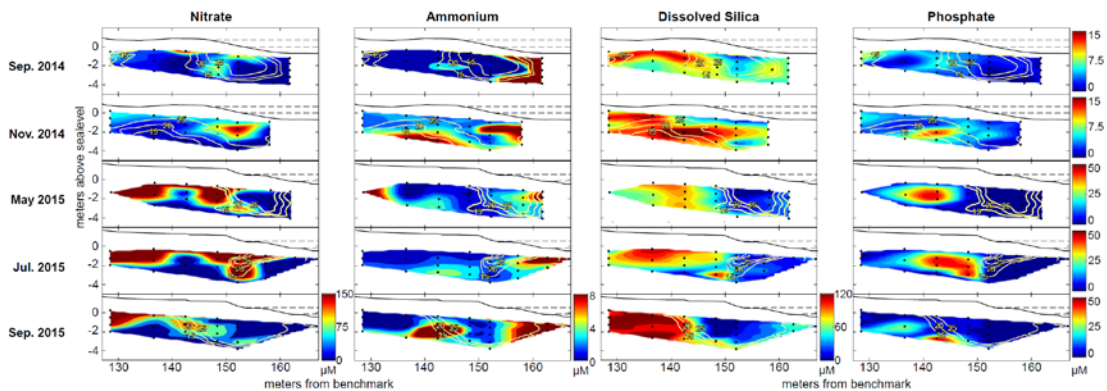


Figure 3.4 Cross-sectional distributions of dissolved nutrients. Salinity contours (15, 20, 25) are overlain in yellow for reference. Note changing colorbar for phosphate.

3.3.3 Porewater Reaction Rates

The results of four of the six sampling events for porewater reaction rates and organic carbon content are presented (September 2014, November 2014, July 2015, and September 2015; Figures 3.5 and 3.6). Incubation data from July 2014 and May 2015 were not dependable due to prolonged incubation time.

Oxygen gas consumption and nitrogen gas production rates determined by incubation reveal the spatial migration of biogeochemical hotspots within the beach aquifer (Figure 3.5). Oxygen consumption rates were the highest near the saline water infiltration point and continued along the saltwater circulation flowpath, along the landward FW-SW mixing zone. This was consistent throughout the months sampled, and high oxygen consumption rates adhered to the changes in salinity distributions. Since aerobic respiration is most dependent on oxygen supplied by saline water infiltration to the system, this observation is consistent with expectations. High respiration rates, however, did not correlate with hotspots of other solutes, or organic carbon (both particulate and dissolved, Figure 3.6), suggesting that aerobic respiration

within this beach is limited primarily by oxygen and only secondarily by carbon availability.

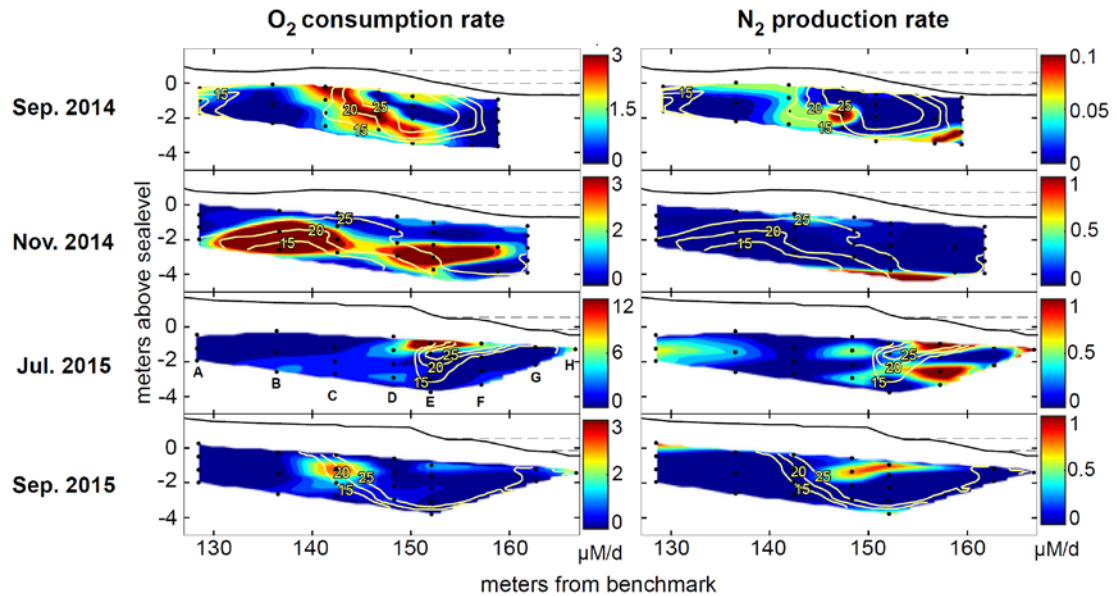


Figure 3.5 Distribution of oxygen consumption rates and denitrification rates. Note changing colorbar.

Potential denitrification rates were determined by production of nitrogen gas beyond its N_2/Ar equilibrium gas solubility ratios with respect to air [Kim et al., 2017]. Nitrogen gas production via denitrification is expected to occur in areas of low oxygen, high nitrate, and high reactive carbon concentrations, making the zones of mixing between hypoxic, nitrate-bearing freshwater and carbon-rich seawater ideal sites for this reaction, especially near the discharge zone where oxygen availability is low. However, some hotspots of denitrification were less consistent with the expected patterns. Unlike oxygen consumption rates that were almost always spatially

associated with the landward FW-SW mixing zone, hotspots of denitrification were patchier in their distributions, and were generally located further along the circulating flowpath. This may be attributed to the variability in nitrate availability and the various pools of carbon within the beach system, discussed in the following sections.

3.3.4 Spatial Distributions of Porewater POC, DOC, and Sedimentary Carbon

The distribution and concentration of porewater POC shifted over seasons (Figure 3.6), independent from the patterns of salinity. Additionally, elevated chlorophyll (not shown) did not correlate with elevated porewater POC, indicating that particulate carbon from different sources may have contrasting transport dynamics and reactivities. All months had some degree of elevated POC at the seaward discharge zone where oxygen availability was low. This was heightened during November 2014 and July 2015. While this may suggest a persistent pool of POC in the seaward parts of the aquifer, concentrations decreased during September 2015, suggesting transience of the POC pool. Although the sampler at 157 m was missing for September 2015, the two most seaward samplers at 162 and 167 m had low POC concentrations, in contrast to the elevated POC concentrations at these locations during July 2015. Notably, some hotspots of porewater POC were found more landward of the intertidal circulation cell, upland of the boundaries of the circulation cell defined by elevated salinity (July 2015).

Zones of elevated DOC coincided spatially with zones of elevated porewater POC. Both the distributions and the concentrations exceeding that of surface water indicate that DOC is produced by active leaching from POC, along with other nutrients (see Section 3.4.3).

Sedimentary carbon content in vibracore samples determined by loss on ignition method was minimal ($1.95 - 7 \text{ mg}_{\text{organic}}/\text{g}_{\text{sediment}}$), and there was no apparent relationship between depth, grain size, organic matter content, and oxygen consumption rate (Appendix B, Table B-1). However, despite the low organic matter content, vibracore samples displayed measurable oxygen consumption when incubated with oxic water ($9.3 - 77.9 \Delta\text{O}_2 \mu\text{M}/\text{d}$) (Figure 3.8-i). This demonstrates that the minor amounts of sedimentary carbon found in beach sands are nonetheless sufficiently labile to contribute to bulk respiration. Oxygen consumption rates did not increase linearly with absolute carbon content (Appendix B, Table B-1), again suggesting differences in reactivity in various carbon sources [Seidel et al., 2014]. There was insufficient nitrate present in the incubated water to determine nitrogen gas production rates in the core samples. Deeper samples at Location F with iron-oxide coatings around the sediment grains also had elevated concentrations of Al, Ca, K, P, Mg, Mn, Na, Zn, As, Cr, Pb, and S compared to other samples, indicating an active interception of elements on the iron-oxide coatings (e.g., [Charette and Sholkovitz, 2002]).

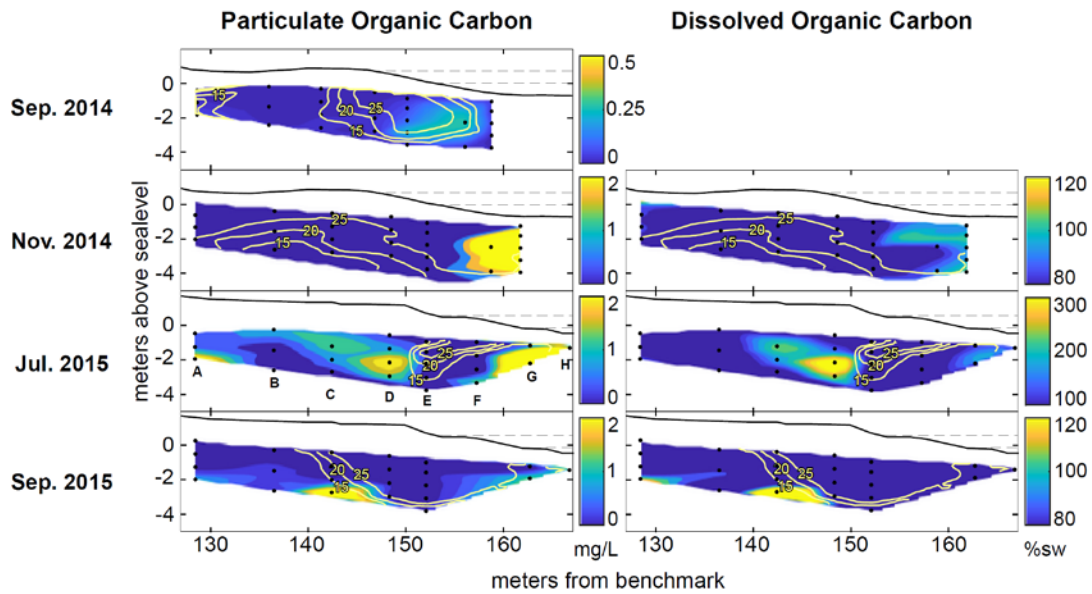


Figure 3.6 Distributions of porewater POC and DOC. Note that DOC scale is % seawater DOC and goes above 100%. DOC was not measured for September 2014.

Slotted sand column deployments demonstrated that delivery of reactive organic carbon into the sediments via porewater infiltration is a key source of organic carbon to beach systems. Retrieved sand column samples (combusted and then deployed in-situ for 75 days) had a fine layer of grey flocculated material not found in the control samples with only combusted sand (Figure 3.7). The fine particles were evaluated using microscopy and green autofluorescence (520 ~ 560 nm), common in dinoflagellates, diatoms, and microalgae [Tang and Dobbs, 2007]. Based on the autofluorescence observations, bacteria, cell fragments, and algal detritus were found within the grey material layer.

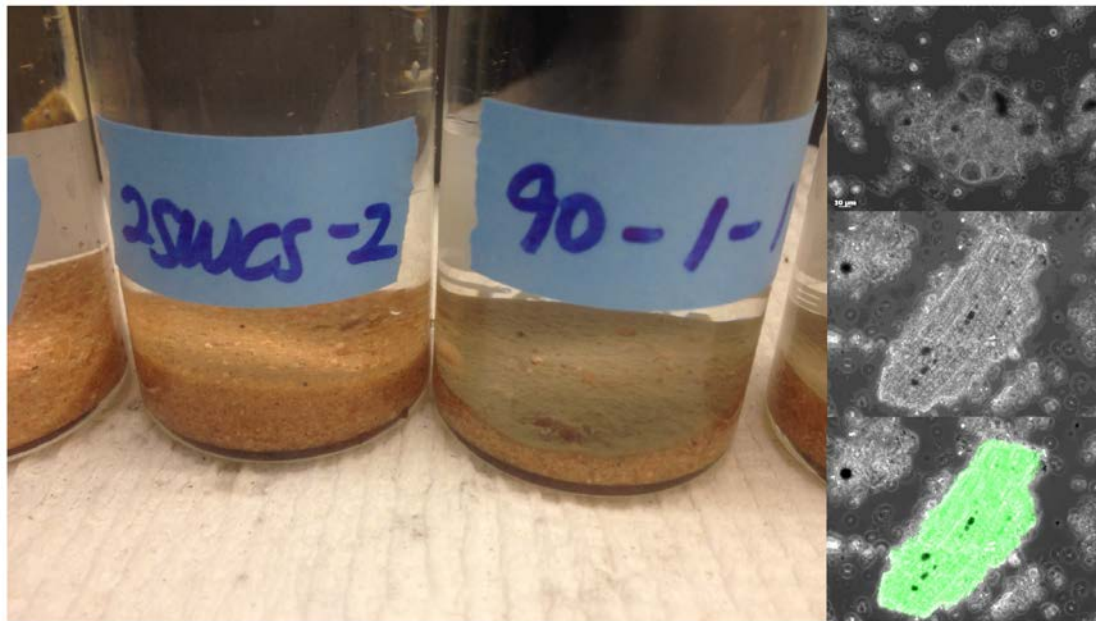


Figure 3.7 Retrieved sand column sediments with a fine layer of grey particles (left column, control on left and retrieved sample on right) and microscopic images of cells and algal fragments found (right column). Green autofluorescence (520~560 nm) was observed in the material (right column, bottom).

The retrieved sand samples were very reactive, with oxygen consumption rates up to $48 \Delta O_2 \mu\text{M/d}$, comparable to rates measured in vibracore sediment samples (Figure 3.8). Oxygen consumption rates across the beach were virtually zero at the most landward location (Figure 3.8-ii, Location B) and increased toward the ocean across the region where saline infiltration occurs (Figure 3.8-ii, Location H). While the particles were identified through microscopy as algae and bacteria, their green autofluorescence, and seaward increases of reactivity, cannot independently serve as conclusive evidence of the particles' marine origin. However, they collectively support a marine origin of at least the reactive portion of the particles. While the absolute carbon concentrations of the sand column samples were not quantified,

oxygen consumption rates presented in Figure 3.8-ii serve as a proxy of labile carbon distribution within the beach aquifer. The respiration patterns did not correspond to the salinity, depth, or POC patterns of either the deployment or the retrieval month, indicating divergent transport dynamics within the aquifer between solutes and fine particulates.

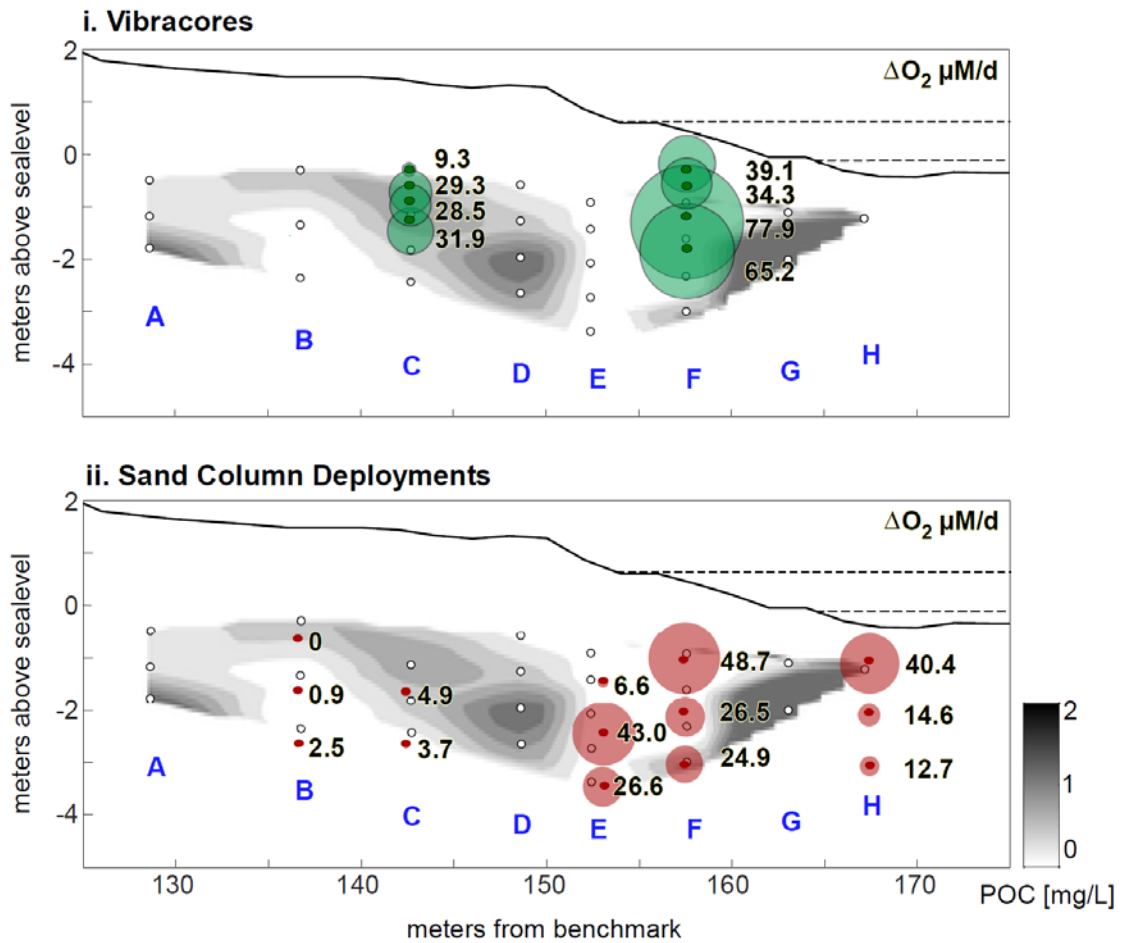


Figure 3.8 Cross-sectional distribution of oxygen consumption rates from i) vibracore sediment samples, in green circles (samples taken 16 July 2015); and ii) sand column deployment samples, in red circles (samples deployed 31 July 2015 and retrieved 13 October 2015). Circle sizes reflect the magnitude of respiration rates, indicated in numbers. Porewater POC distribution from 08 July 2015 is shown in greyscale for reference, with open circles indicating porewater sampling locations.

3.4 Discussion

3.4.1 Seasonal Dynamics of Salinity, Nutrient Distributions, and Reaction Characteristics

Solute distributions over seasons show the spatial and temporal dynamics of both conservative and reactive components of the intertidal circulation cell (Figure 3.3) resulting from porewater advection, filtration, redox reactions, and dissolution processes. Oxygen concentrations and respiration rates closely followed the anticipated patterns along advective flowpaths prescribed by the geometry and salinity of the intertidal circulation cell. This behavior is expected, as oxygen, salinity, and reactive organic carbon share a common seawater source. However, distributions of chemically reactive parameters such as ORP, dissolved inorganic nitrogen, and nitrogen gas production displayed dynamic patterns over seasonal timescales that were far less coupled with changes in salinity (Figure 3.4, 3.5, 3.6). Nitrogen gas production rates, while often elevated farther along groundwater flowpaths where oxygen availability is low, also exhibited patches of high rates in other areas. This can be attributed to the nitrate and carbon distributions that were not correlated to salinity, suggesting a divergence between reaction characteristics and groundwater flowpaths. The distributions of salinity and various solutes collectively indicate that on seasonal timescales, hydrology influences, but is not the sole driver of, shifts in the distributions of porewater constituents and reaction characteristics. The divergent migration of reaction characteristics from salinity patterns within the beach system is likely influenced by heterogeneous pools of organic matter with varying forms and degrees of reactivity resulting from hydrologic transience.

3.4.2 Carbon Pool Distributions and Dynamics

Three main types of carbon are found within the beach aquifer: 1) DOC (Figure 3.9, seawater (i) and leached (iii)), 2) entrapped sedimentary carbon (Figure 3.9, i, ii, v), and 3) porewater POC (Figure 3.9, iv). We show that 1) the three pools are distributed heterogeneously in the beach aquifer and do not correspond to salinity-indicated saltwater circulation flowpaths, 2) that carbon is mobile, reactive, and at least partially of marine origin, and 3) the distribution of porewater POC and entrapped sedimentary carbon likely represents deposition during both current and past hydrologic conditions, thus particulate carbon distributions may ‘lag’ those of fully mobile solutes.

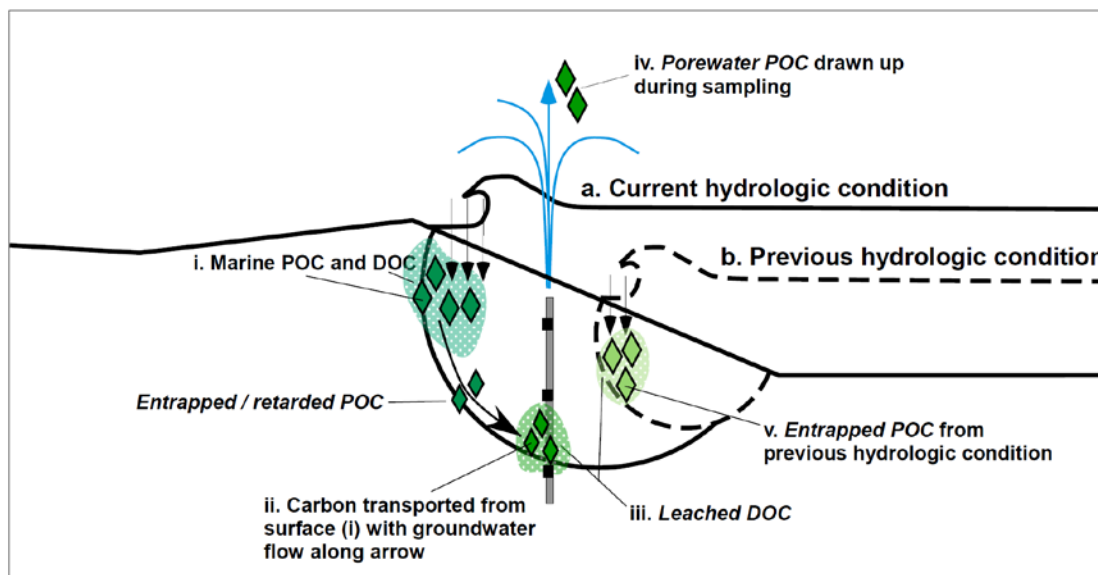


Figure 3.9 Conceptual diagram of carbon movement within the intertidal beach aquifer. Groundwater flow in the current hydrologic condition (a) transports marine DOC and particulate carbon (POC) (i), which can become entrapped along the flowpath as it moves through the sediments (i to ii). POC actively leaches DOC (iii). Porewater POC is sampled with porewater, representing mobile POC and/or some component of immobile POC mobilized by sampling (iv). Entrapped POC from a previous hydrologic condition (b) can appear as a hotspot (v) under current conditions.

The heterogeneous distributions of carbon pools indicate contrasting transport mechanisms between particulates and solutes. Hotspots of porewater POC and DOC concentrations did not correspond with inferred flowpaths, nor did the entrapped carbon content of vibracore samples. These observations might suggest that these hotspots are associated with a geologic deposit, rather than the result of seawater infiltration and circulation through the aquifer. However, we believe that is not the case for two reasons. First, both particulate and dissolved reactive carbon pools are mobile, and second, they are of marine origin. Both conclusions are supported by the

sand column deployments, as samples displayed active aerobic respiration (an indicator of labile organic matter, often associated with marine primary production) that increased seaward (Figure 3.8-ii), and green autofluorescence common in dinoflagellates, diatoms, and microalgae (Figure 3.7). Because the particulate carbon sources do not always coincide with hydrologic flow despite originating with infiltrating seawater and moving through the aquifer, we infer that transport and degradation/consumption occur more slowly than hydrologic shifts (Figure 3.9, condition b to a). While marine DOC travels within the beach aquifer synchronous with seawater, larger carbon fragments ($> 0.7\mu\text{m}$) may experience retarded movement once delivered into the sediments. As the delivered POC travels within the aquifer along groundwater flow paths, it may become entrapped and immobilized (Figure 3.9, i, ii, v), depending on particle size, grain size distributions, groundwater flow velocity, and sorption behavior. July 2015 data clearly show this lagged behavior. After the rainstorm, the intertidal circulation cell was constricted and pushed offshore (Figure 3.3). The pool of elevated porewater POC was found landward of the high salinity region of active saltwater circulation, in the zone where seawater was likely infiltrating prior to the storm. This shows the divergent movement between fully mobile solutes (i.e., salt) and particulates in beaches. The mobile nature of fine particles, immobilization, and remobilization due to physical or chemical forces in other porous settings have been well-described [El-Farhan et al., 2000; Gast et al., 2015; McDowell-Boyer et al., 1986; Pronk et al., 2009].

Comparison between oxygen consumption rates of porewater samples and vibracore sediment samples suggest that these carbon pools, while oxygen-limited under current hydrologic conditions, have the potential to react at a later time when

conditions become favorable (Figure 3.5 and 3.8). At location F, both porewater and vibracore sediment samples were incubated, but under different oxygen concentrations. Porewater incubations were conducted using in-situ oxygen concentrations ($< 15 \mu\text{M}$ except for surficial sample), with no additional introduction of oxygen, while sediment incubations were conducted with oxic water. Oxygen consumption rates for porewater samples were highest at the surficial sampling points for Location D and E, and samples at Location F had respiration rates that were far below the highest rate observed across the aquifer (mean of four depths at F: $3.5 \Delta\text{O}_2 \mu\text{M/d}$; highest rate across aquifer: $23 \Delta\text{O}_2 \mu\text{M/d}$). However, when sediments from the same location were incubated with oxic water, the oxygen consumption rate reached $77.90 \Delta\text{O}_2 \mu\text{M/d}$, displaying the full respiration potential of sedimentary carbon at this location (Figure 3.8-i and Appendix B, Table B-1). While Location F is currently limited in oxygen, given changes in the geometry of the intertidal circulation cell and its subsequent flowpath changes, oxygen or other dissolved reactants could become available in time, allowing the sedimentary carbon to respire and contribute to beach reactivity by acting as an electron donor for redox reactions. The presence of these carbon pools and potential for previously deposited carbon to react suggests that intertidal aquifers may be a more reactive system than if labile DOC is the sole carbon source, as previously assumed (e.g., [Heiss et al., 2017]). A shift in hydrologic conditions, such as rainstorms, tidal variations, and changes to freshwater flux, therefore have the potential to tap into unutilized reservoirs of carbon, promoting shifts in reactions in zones unpredicted by salinity patterns, and creating a “carbon memory” effect within the aquifer.

The timescale of this “carbon memory” effect within the circulation cell will depend on the amount of carbon delivered, its rate of movement, and its degradation/reaction rate. Hotspots of porewater POC did not appear to endure beyond the two months between successive sampling events (Figure 3.6 and unpublished data). This suggests that the memory effect in this aquifer has a lifespan shorter than two months, due to degradation and eventual transport, and is more relevant for spring-neap and shorter timescales rather than seasonal cycles. While changes to the intertidal circulation cell over spring-neap cycles are less pronounced than changes over seasonal timescales [Heiss and Michael, 2014], gradual movements over spring-neap tides and abrupt hydrologic changes (i.e., storms) have the potential to promote microbial utilization of these reactive carbon pools. On longer timescales and/or at shallow depths, the erosion and accretion of sand on beaches may be an important mechanism for POC burial. At Cape Shores, monthly surveys of topographic profiles have shown elevation differences of up to 0.5 m between seasons, and 1 m between consecutive years due to winter storms (e.g., [Quartel et al., 2008]). During excavation of porewater samplers, especially from the upland dune to the hightide mark, it was common to see decomposing layers of beach wrack that had been buried within the first 1 m of the surface. While these debris layers were within the dry, unsaturated zone and thus did not affect porewater sampling, they indicate that for such large, hardy forms of POC, the “carbon memory” effect may be much longer than mobile POC fragments primarily discussed in this work, even over seasonal morphological changes. However, further work is needed at different timescales to resolve the variable temporal relationship between groundwater flow and reactive carbon transport within the beach.

3.4.3 Nutrient Release and Leaching Dynamics

Our data provide evidence that the particulate carbon in intertidal aquifers, both immobile and mobile, is an important source of DOC and nutrients, enhancing reactivity and altering land-sea fluxes. Laboratory incubations with sand column samples show that as aerobic respiration progresses, oxygen decreases (Figure 3.10). The slope of nitrate decrease steepens after oxygen falls below a certain threshold, and ammonium increases. This indicates that as reactive carbon degrades, nutrients are consumed or released, which alters the local chemistry and redox conditions. These solutes and their reaction products may be subsequently transported with the groundwater.

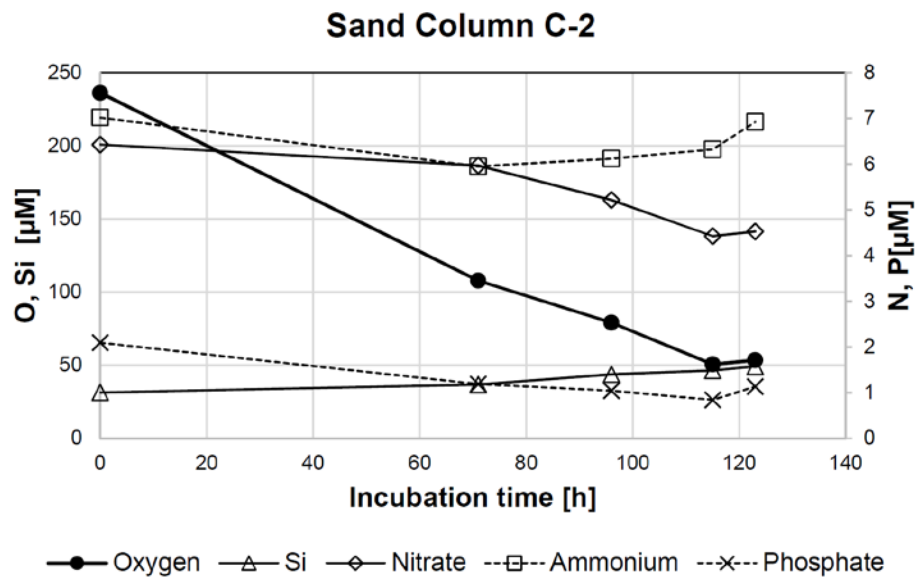


Figure 3.10 Nutrient release over time during Sand Column C-2 sample incubation. Oxygen and nitrate decrease over time, while ammonium increases after ~70 h. While for other more reactive samples, changes in nutrients occurred around hour 24 or 48, more refractory samples such as above did not show changes until hour 70.

Further, porewater POC and entrapped sedimentary carbon act as local sources of potential reactants (dissolved and particulate) such as DOC, particulate nitrogen, particulate phosphorus, and phosphate via leaching (Figure 3.11). DOC was higher than surface water concentrations in all sampled months, even up to 300% in July 2015, indicating a source other than seawater (Figure 3.6, Figure 3.11). This suggests that leaching, in addition to the seasonal changes in seawater carbon concentration and input, is another mechanism for seasonal changes in DOC concentrations. Leaf matter has the potential to increase labile DOC concentrations nearly ten-fold in nearby waters [Wetzel and Manny, 1972], suggesting that the observed porewater POC leaching in beach porewaters is analogous to processes observed in other environments. The differences in leaching efficiency among seasons, presumably contingent on the quality of infiltrated carbon, could alter the DOC concentrations within the sediments independent of surface water DOC concentrations.

While the molecular quality and reactivity of porewater POC and DOC was not considered in this study, it can be expected based on previous studies that the DOC that leaches from porewater POC of surface water origin is reactive and labile [Wetzel and Manny 1972; Seidel et al., 2014]. In beach aquifer systems, where organic carbon and nutrients are generally scarce, it can be expected that these reactive organic matter pools become important reservoirs of electron donors that fuel biogeochemical reactions outside the existent intertidal circulation cell. Biogeochemical reactions within the aquifer, therefore, are not just a function of reactant transport but rather a complex system governed by hydrologic, geochemical, and biological characteristics that are spatially and temporally transient on different timescales.

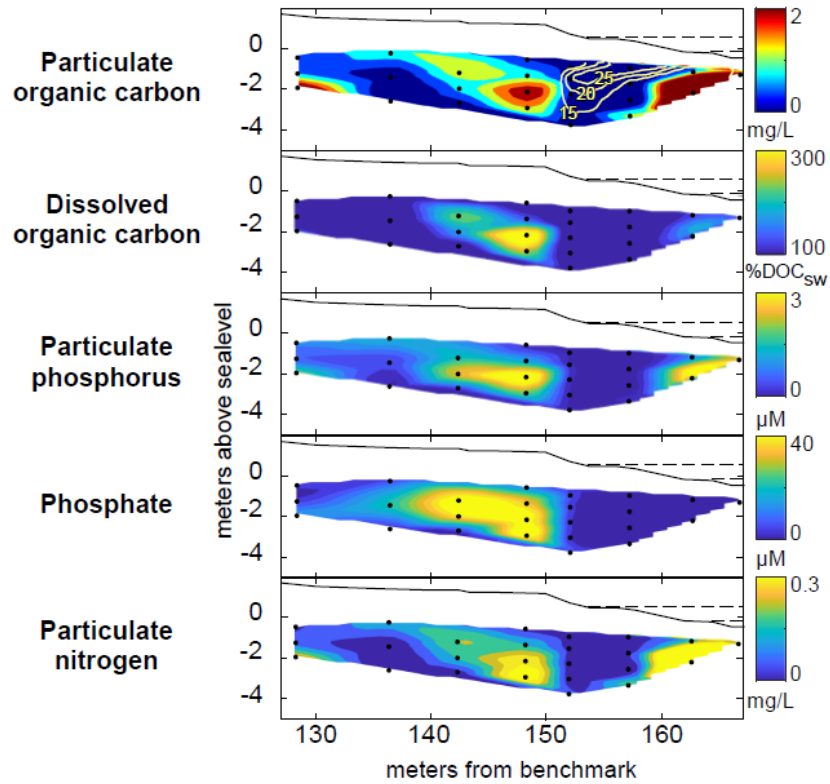


Figure 3.11 Cross-sectional distributions of porewater POC, DOC, PP, phosphate, and PN from July 2015. DOC is presented in % DOC of surface water concentrations, and the ‘supersaturated’ areas are spatially correlated to elevated areas of porewater POC. PP, phosphate, and PN also follow this pattern, indicating active leaching dynamics within the aquifer. Salinity contours are shown in porewater POC panel for reference.

3.5 Conclusions

Intertidal circulation cells of beach aquifers are complex and dynamic in their location, extent, and geometry due to seasonal hydrologic and oceanic conditions. However, the distributions of chemical constituents and reaction characteristics do not always synchronously correspond to hydrologic shifts. While salinity, dissolved oxygen, and oxic respiration rates closely followed shifts in groundwater flowpaths, the distributions of other parameters did not. The divergence of nitrogen gas

production and ORP conditions from salinity was attributed to the spatially-variable distributions of solute reactants and reactive organic carbon. Hydrologic transience and the filtration effect of sediments created heterogeneously distributed pools of organic carbon within the aquifer that did not correspond to conservative mixing patterns. These reactive carbon pools were at least in part delivered by seawater and displayed differential mobility within the sediments, creating reaction dynamics within the aquifer that deviated from salinity-defined hydrologic patterns. POC was shown to actively leach DOC and other nutrients into the beach aquifer system, acting as a local source of reactants and causing further deviation of nutrient distributions from salinity patterns. These carbon pools, though oxygen-limited, were readily reactive, indicating their potential to support reactions once conditions become favorable as hydrologic conditions change. These results together emphasize that the evolution and migration of reaction characteristics in coastal aquifers, often highly dependent on carbon, can be caused by, but decoupled from, positional changes of the circulation cell and may not be completely predictable from current hydrologic conditions due to a “carbon memory” effect.

REFERENCES

- Abarca, E., H. Karam, H. F. Hemond, and C. F. Harvey (2013), Transient groundwater dynamics in a coastal aquifer: The effects of tides, the lunar cycle, and the beach profile, *Water Resources Research*, 49, 1–16.
<https://doi.org/10.1002/wrcr.20075>.
- Anschutz, P., T. Smith, A. Mouret, J. Deborde, S. Bujan, D. Poirer, and P. Lecroart (2009), Tidal sands as biogeochemical reactors, *Estuarine, Coastal, and Shelf Science*, 84, 84-90, doi:10.1016/j.ecss.2009.06.015.
- Anwar, N., C. Robinson, and D. A. Barry (2014), Influence of tides and waves on the fate of nutrients in a nearshore aquifer: Numerical simulations, *Advances in Water Resources*, 73, 203-213,
<http://dx.doi.org/10.1016/j.advwatres.2014.08.015>.
- Bacon, M. P., R. A. Belastock, and M. H. Bothner (1994), 210Pb balance and implications for particle transport on the continental shelf, US Middle Atlantic Bight, *Deep Sea Research Part II: Topical Studies in Oceanography*, 41(2-3), 511-535, [https://doi.org/10.1016/0967-0645\(94\)90033-7](https://doi.org/10.1016/0967-0645(94)90033-7).
- Beck, A. J., Y. Tsukamoto, A. Tovar-Sanchez, M. Huerta-Diaz, H. J. Bokuniewicz, and S.A. Sanudo-Wilhelmy (2007), Importance of geochemical transformations in determining submarine groundwater discharge-derived trace metal and nutrient fluxes, *Applied Geochemistry*, 22(2), 477-490,
<https://doi.org/10.1016/j.apgeochem.2006.10.005>.
- Beck, A. J., A. A. Kellum, J. L. Luek, and M. A. Cochran (2016), Chemical flux associated with spatially and temporally variable submarine groundwater discharge, and chemical modification in the subterranean estuary at Gloucester Point, VA (USA), *Estuaries and coasts*, 39(1), 1-12,
<https://link.springer.com/article/10.1007/s12237-015-9972-0>.
- Beck, M., O. Dellwig, B. Schnetger, and H. J. Brumsack (2008), Cycling of trace metals (Mn, Fe, Mo, U, V, Cr) in deep pore waters of intertidal flat sediments, *Geochimica et Cosmochimica Acta*, 72(12), 2822-2840,
<https://doi.org/10.1016/j.gca.2008.04.013>.

- Beck, M., A. Reckhardt, J. Amelsberg, A. Bartholomä, H. Brumsack, H. Cypionka, T. Dittmar, B. Engelen, J. Greskowiak, H. Hillebrand, M. Holtappels, R. Neuholz, J. Köster, M. Kuypers, G. Massmann, D. Meier, J. Niggemann, R. Paffrath, K. Pahnke, S. Rovo, M. Striebel, V. Vandieken, A. Wehrmann, and O. Zielinski (2017), The drivers of biogeochemistry in beach ecosystems: A cross-shore transect from the dunes to the low water line, *Marine Chemistry*, 190, 35-50, <http://dx.doi.org/10.1016/j.marchem.2017.01.001>.
- Bone, S. E., M. E. Gonnee, and M. A. Charette (2006), Geochemical cycling of arsenic in a coastal aquifer, *Environmental science & technology*, 40(10), 3273-3278, [10.1021/es052352h](https://doi.org/10.1021/es052352h).
- Boudreau, B. P., M. Huettel, S. Forster, R. A. Jahnke, A. McLachlan, J. J. Middelburg, P. Nielsen, F. Sansone, G. Taghon, W. Van Raaphorst, I. Webster, J. M. Weslawski, P. Wilberg, and B. Sundby (2001), Permeable marine sediments: overturning an old paradigm, *EOS Transactions American Geophysical Union*, 82(11) 133-136, [doi:10.1029/EO082i011p00133-01](https://doi.org/10.1029/EO082i011p00133-01).
- Boufadel, M.C., Y. Sharifi, B. Van Aken, B. A. Wrenn, and K. Lee (2010), Nutrient and oxygen concentrations within the sediments of an Alaskan beach polluted with the Exxon Valdez oil spill, *Environmental Science & Technology*, 44(19),: 7418-7424, <https://doi.org/10.1021/es102046n>.
- Charbonnier, C., P. Anschutz, D. Poirier, S. Bujan, and P. Lecroart (2013), Aerobic respiration in a high-energy sandy beach, *Marine Chemistry*, 155, 10-21, <http://dx.doi.org/10.1016/j.marchem.2013.05.003>.
- Charette, M. A., and E. R. Sholkovitz (2002), Oxidative precipitation of groundwater-derived ferrous iron in the subterranean estuary of a coastal bay, *Geophysical research letters*, 29(10), 85-1–85-4, [doi:10.1029/2001GL014512](https://doi.org/10.1029/2001GL014512).
- Charette, M.A. and E. R. Sholkovitz (2006), Trace element cycling in a subterranean estuary: Part 2, Geochemistry of the pore water, *Geochimica et Cosmochimica Acta*, 70(4), 811-826, <https://doi.org/10.1016/j.gca.2005.10.019>.
- Charette, M.A., E.R. Sholkovitz, and C. M. Hansel (2005), Trace element cycling in a subterranean estuary: Part 1. Geochemistry of the permeable sediments, *Geochimica et Cosmochimica Acta*, 69(8),: 2095-2109, <https://doi.org/10.1016/j.gca.2004.10.024>.
- Dove, P.M. and C.J. Nix (1997), The influence of the alkaline earth cations, magnesium, calcium, and barium on the dissolution kinetics of quartz. *Geochimica et Cosmochimica Acta*, 61(16), 3329-3340, [https://doi.org/10.1016/S0016-7037\(99\)00218-5](https://doi.org/10.1016/S0016-7037(99)00218-5).

- El-Farhan, Y.H., N.M. DeNovio, J.S. Herman, and G.M. Hornberger (2000), Mobilization and transport of soil particles during infiltration experiments in an agricultural field, Shenandoah Valley, Virginia, *Environmental science & technology*, 34(17), 3555-3559, doi: 10.1021/es991099g.
- Gast, R.J., S. Elgar, and B. Raubenheimer (2015), Observations of transport of bacterial-like microspheres through beach sand, *Continental Shelf Research*, 97, 1-6, <https://doi.org/10.1016/j.csr.2015.01.010>.
- Geng, X., M. C. Boufadel, K. Lee, S. Abrams, and M. Suidan (2015), Biodegradation of subsurface oil in a tidally influenced sand beach: Impact of hydraulics and interaction with pore water chemistry, *Water Resources Research*, 51(5):, 3193-3218, [dx.doi.org/10.1002/2014WR016870](https://doi.org/10.1002/2014WR016870).
- Gonneea, M. E., A. E. Mulligan, and M. A. Charette (2013), Climate-driven sea level anomalies modulate coastal groundwater dynamics and discharge, *Geophysical Research Letters*, 40(11), 2701-2706, <https://doi.org/10.1002/grl.50192>.
- Gonneea, M. E., A. E. Mulligan, and M. A. Charette (2013b), Seasonal cycles in radium and barium within a subterranean estuary: Implications for groundwater derived chemical fluxes to surface waters, *Geochimica et Cosmochimica Acta*, 119, 164-177, <https://doi.org/10.1016/j.gca.2013.05.034>.
- Hays, R. L., and W. J. Ullman (2007a), Direct determination of total and fresh groundwater discharge and nutrient loads from a sandy beachface at low tide (Cape Henlopen, Delaware), *Limnology and oceanography*, 52(1), 240-247, doi:10.4319/lo.2007.52.1.0240.
- Hays, R. L., and W. J. Ullman (2007b), Dissolved nutrient fluxes through a sandy estuarine beachface (Cape Henlopen, Delaware, USA): contributions from fresh groundwater discharge, seawater recycling, and diagenesis, *Estuaries and Coasts*, 30(4), 710-724, doi:10.1007/BF02841967.
- Heiss, J. W., and H. A. Michael (2014), Saltwater-freshwater mixing dynamics in a sandy beach aquifer over tidal, spring-neap, and seasonal cycles, *Water Resour. Res.*, 50, 6747-6766, doi:10.1002/2014WR015574.
- Heiss, J. W., V. E. Post, T. Laattoe, C. J. Russoniello, and H. A. Michael (2017), Physical controls on biogeochemical processes in intertidal zones of beach aquifers, *Water Resources Research*, 53(11), 9225-9244, <https://doi.org/10.1002/2017WR021110>.

- Huettel, M., and A. Rusch (2000), Transport and degradation of phytoplankton in permeable sediment, *Limnology and Oceanography*, 45(3), 534-549, <https://doi.org/10.4319/lo.2000.45.3.0534>.
- Jeong, J., G. Kim, and S. Han (2012), Influence of trace element fluxes from submarine groundwater discharge (SGD) on their inventories in coastal waters off volcanic island, Jeju, Korea, *Applied geochemistry*, 27(1), 37-43, <https://doi.org/10.1016/j.apgeochem.2011.08.014>.
- Jung, H. B., M. A. Charette, and Y. Zheng (2009), Field, laboratory, and modeling study of reactive transport of groundwater arsenic in a coastal aquifer, *Environmental science & technology*, 43(14), 5333-5338, 10.1021/es900080q.
- Kelly, R. P. and S. B. Moran (2002), Seasonal changes in groundwater input to a well-mixed estuary estimated using radium isotopes and implications for coastal nutrient budgets, *Limnology and Oceanography*, 47(6), 1796-1807, <https://doi.org/10.4319/lo.2002.47.6.1796>.
- Kim, K. H., J. W. Heiss, H. A. Michael, W. J. Cai, T. Laattoe, V. E. Post, and W. J. Ullman (2017), Spatial patterns of groundwater biogeochemical reactivity in an intertidal beach aquifer, *Journal of Geophysical Research: Biogeosciences*, 122(10), 2548-2562, <https://doi.org/10.1002/2017JG003943>.
- Kim, K. H. (2018), Cape Shores Porewater Data Compilation 2014-2015, HydroShare, <https://doi.org/10.4211/hs.440e89b8cc8c4c43bdbc6176e8f38a70>.
- Kroeger, K. D., and M. A. Charette (2008), Nitrogen biogeochemistry of submarine groundwater discharge, *Limnology Oceanography*, 53(3), 1025-1039, doi:10.4319/lo.2008.53.3.1025. Li, H., M. C. Boufadel, and J. W. Weaver (2008), Tide-induced seawater-groundwater circulation in shallow beach aquifers, *Journal of Hydrology*, 352(1-2), 211-224, <https://doi.org/10.1016/j.jhydrol.2008.01.013>. Loucaide, S., P. Van Cappellen, and T. Behrends (2008), Dissolution of biogenic silica from land to ocean: role of salinity and pH. *Limnology and Oceanography*, 53(4), 1614-1621, <https://doi.org/10.4319/lo.2008.53.4.1614>.
- McAllister, S.M., J.M. Barnett, J.W. Heiss, A.J. Findlay, D.J. MacDonald, C. L. Dow, G.W. Luther, H. A. Michael, and C.S Chan (2015), Dynamic hydrologic and biogeochemical processes drive microbially enhanced iron and sulfur cycling within the intertidal mixing zone of a beach aquifer, *Limnology and Oceanography*, 60, 329-345, doi: 10.1111/lno.10029.

- McDowell-Boyer, L.M., J.R. Hunt, and N. Sitar, (1986), Particle transport through porous media, *Water Resources Research*, 22(13), 1901-1921, <https://doi.org/10.1029/WR022i013p01901>.
- McLachlan, A., I. G. Eliot, and D. J. Clarke (1985), Water filtration through reflective microtidal beaches and shallow sublittoral sands and its implications for an inshore ecosystem in Western Australia, *Estuarine, Coastal and Shelf Science*, 21(1), 91-104.
- Michael, H. A., A. E. Mulligan, and C. F. Harvey (2005), Seasonal oscillations in water exchange between aquifers and the coastal ocean, *Nature*, 436(7054), 1145-1148, doi:10.1038/nature03935.
- Moore, W. S. and A. M. Wilson (2005), Advective flow through the upper continental shelf driven by storms, buoyancy, and submarine groundwater discharge, *Earth and Planetary Science Letters*, 235(3-4), 564-576, <https://doi.org/10.1016/j.epsl.2005.04.043>.
- O'Connor, A. E., J. L. Krask, E. A. Canuel, and A. J. Beck (2018), Seasonality of major redox constituents in a shallow subterranean estuary, *Geochimica et Cosmochimica Acta*, 224, 344-361, <https://doi.org/10.1016/j.gca.2017.10.013>.
- Pilditch, C. A. and D. C. Miller (2006), Phytoplankton deposition to permeable sediments under oscillatory flow: Effects of ripple geometry and resuspension, *Continental Shelf Research*, 26(15), 1806-1825, <https://doi.org/10.1016/j.csr.2006.06.002>.
- Pronk, M., N. Goldscheider, J. Zopfi, and F. Zwahlen (2009), Percolation and particle transport in the unsaturated zone of a karst aquifer, *Groundwater*, 47(3), 361-369, <https://doi.org/10.1111/j.1745-6584.2008.00509.x>.
- Quartel, S., A. Kroon, and B. G. Ruessink (2008), Seasonal accretion and erosion patterns of a microtidal sandy beach, *Marine Geology*, 250(1-2), 19-33, <https://doi.org/10.1016/j.margeo.2007.11.003>.
- Reckhardt, A., M. Beck, M. Seidel, T. Riedel, A. Wehrmann, A. Bartholomä, and H. J. Brumsack (2015), Carbon, nutrient and trace metal cycling in sandy sediments: A comparison of high-energy beaches and backbarrier tidal flats, *Estuarine, Coastal and Shelf Science*, 159, 1-14, <http://dx.doi.org/10.1016/j.ecss.2015.03.025>.

- Robinson, M., D. Gallagher, and W. Reay (1998), Field observations of tidal and seasonal variations in ground water discharge to tidal estuarine surface water, *Groundwater Monitoring & Remediation*, 18(1), 83-92, doi:10.1111/j.1745-6592.1998.tb00605.x.
- Robinson, C., B. Gibbes, H. Carey, and L. Li (2007), Salt-freshwater dynamics in a subterranean estuary over a spring-neap tidal cycle, *J. Geophys. Res.*, 112, C09007, doi:10.1029/2006JC003888.
- Robinson, C., A. Brovelli, D. A. Barry, and L. Li (2009), Tidal influence on BTEX biodegradation in sandy coastal aquifers, *Advances in Water Resources*, 32(1), 16–28, doi:10.1016/j.advwatres.2008.09.008.
- Roy, M., J. B. Martin, J. E. Cable, and C. G. Smith (2013), Variations of iron flux and organic carbon remineralization in a subterranean estuary caused by inter-annual variations in recharge, *Geochimica et Cosmochimica Acta*, 103, 301-315. <https://doi.org/10.1016/j.gca.2012.10.055>.
- Rusch, A. and M. Huettel (2000), Advective particle transport into permeable sediments—evidence from experiments in an intertidal sandflat, *Limnology and Oceanography*, 45(3), 525-533, <https://doi.org/10.4319/lo.2000.45.3.0525>.
- Rusch, A., M. Huettel, and S. Forster (2000), Particulate organic matter in permeable marine sands—dynamics in time and depth, *Estuarine, Coastal and Shelf Science*, 51(4), 399-414.
- Santos, I. R., W. C. Burnett, T. Dittmar, I. G. Suryaputra, and J. Chanton (2009), Tidal pumping drives nutrient and dissolved organic matter dynamics in a Gulf of Mexico subterranean estuary, *Geochimica et Cosmochimica Acta*, 73(5), 1325-1339, <https://doi.org/10.1016/j.gca.2008.11.029>.
- Seidel, M., M. Beck, T. Riedel, H. Waska, I. G. Suryaputra, B. Schnetger, J. Niggemann, M. Simon, and T. Dittmar (2014), Biogeochemistry of dissolved organic matter in an anoxic intertidal creek bank, *Geochimica et Cosmochimica Acta*, 140, 418-434, <https://doi.org/10.1016/j.gca.2014.05.038>.
- Seidel, M., M. Beck, J. Greskowiak, T. Riedel, H. Waska, I. G. N. A. Suryaputra, B. Schnetger, J. Niggemann, M. Simon, and T. Dittmar (2015), Benthic-pelagic coupling of nutrients and dissolved organic matter composition in an intertidal sandy beach, *Marine Chemistry*, 176, 150-163, <http://dx.doi.org/10.1016/j.marchem.2015.08.011>.

- Slomp, C. P., and P. Van Cappellen (2004), Nutrient inputs to the coastal ocean through submarine groundwater discharge: controls and potential impact. *Journal of Hydrology*, 295(1), 64-86, <http://dx.doi.org/10.1016/j.jhydrol.2004.02.018>.
- Tang, Y. Z. and F. C. Dobbs (2007), Green autofluorescence in dinoflagellates, diatoms, and other microalgae and its implications for vital staining and morphological studies, *Appl. Environ. Microbiol.*, 73(7), 2306-2313, doi: 10.1128/AEM.01741-06.
- Ullman, W. J., B. Chang, D. C. Miller, and J. A. Madsen (2003), Groundwater mixing, nutrient diagenesis, and discharges across a sandy beachface, Cape Henlopen, Delaware (USA), *Estuarine, Coastal and Shelf Science*, 57(3), 539-552, [http://dx.doi.org/10.1016/S0272-7714\(02\)00398-0](http://dx.doi.org/10.1016/S0272-7714(02)00398-0).
- Waska, H. and G. Kim (2011), Submarine groundwater discharge (SGD) as a main nutrient source for benthic and water-column primary production in a large intertidal environment of the Yellow Sea, *Journal of Sea Research*, 65(1), 103-113, <https://doi.org/10.1016/j.seares.2010.08.001>.
- Wetzel, R. G. and B. A. Manny (1972), Decomposition of dissolved organic carbon and nitrogen compounds from leaves in an experimental hard-water stream, *Limnology and Oceanography*, 17(6), 927-931, <https://doi.org/10.4319/lo.1972.17.6.0927>.
- Wilson, A. M., W. S. Moore, S. B. Joye, J. L. Anderson, and C. A. Schutte (2011), Storm-driven groundwater flow in a salt marsh, *Water Resour. Res.*, 47, W02535, doi:10.1029/2010WR009496.
- Xin, P., S. S. J. Wang, C. Robinson, L. Li, Y.-G. Wang, and D. A. Barry (2014), Memory of past random wave conditions in submarine groundwater discharge, *Geophys. Res. Lett.*, 41, 2401–2410, doi:10.1002/2014GL059617.
- Yu, X., P. Xin, C. Lu, C. Robinson, L. Li, and D. A. Barry (2017), Effects of episodic rainfall on a subterranean estuary, *Water Resources Research*, 53(7), 5774-5787, <https://doi.org/10.1002/2017WR020809>.

Chapter 4

TRANSIENT CONTRIBUTIONS OF RETARDED PARTICULATE ORGANIC CARBON TO NITRATE REMOVAL IN BEACH AQUIFERS

Abstract

The intertidal zone of beach aquifers carries out biogeochemical transformations of terrestrial nutrients, mediated by the reactive organic carbon from seawater infiltration. While dissolved organic carbon is often assumed the sole reactive component, both advected and entrapped particulate organic carbon (POC) is also capable of supporting chemical reactions. Retarded advection of POC relative to groundwater flow forms pools of reactive carbon within beach sediments, which support biogeochemical reactions as dissolved solutes move across it due to transient hydrology. In this work, we investigate the contributions of POC to beach reactions and identify parameters that control its relative contribution using a groundwater flow and reactive transport model. Results show intermittent contributions of POC to denitrification, as the extent of the saline circulation cell varies over time due to changing hydrologic factors. Increased retardation factor and tidal amplitude of POC deposition was shown to increase the relative contributions of POC to beach reactions. Conversely, increased hydraulic conductivity and tidal amplitude decreased the utilization of POC by allowing the oxic, saline water to completely encompass the pool of POC. Results highlight that POC is a transient, spatially variable source of carbon that displays complex relationships with groundwater flow conditions and overall beach biogeochemistry. This demonstrates that POC may be a sporadically

important, but overlooked contributor to biogeochemical reactions in carbon-poor beach aquifers.

4.1 Introduction

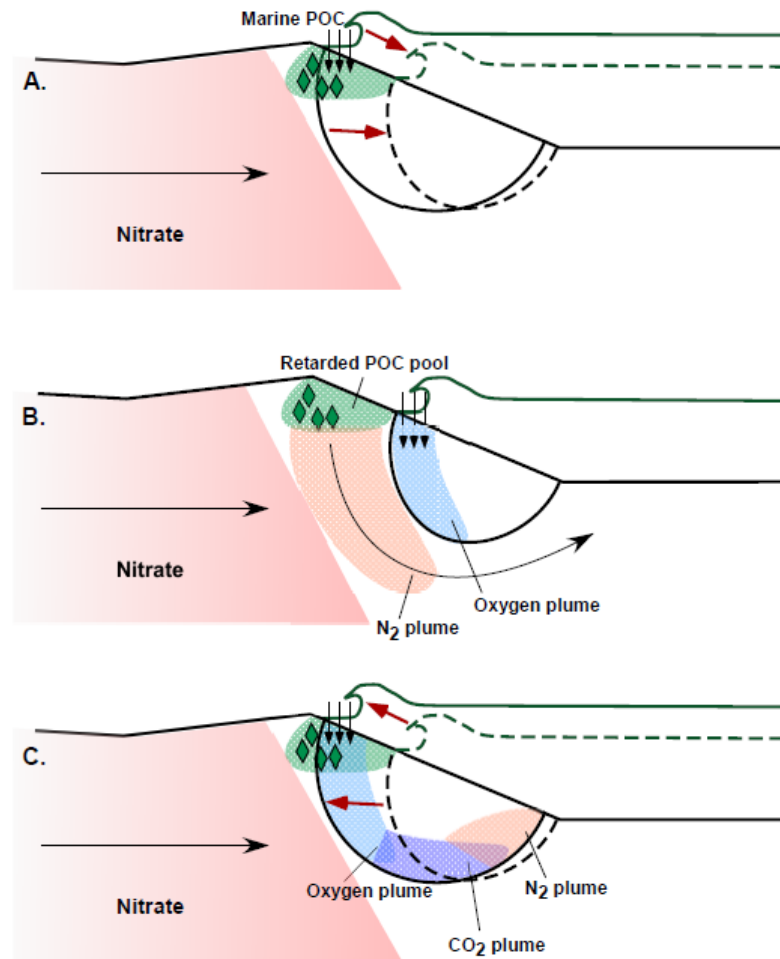


Figure 4.1 Schematic diagram of particulate organic carbon contributions to biogeochemical reactions within intertidal zone of aquifers. Panel A: Marine POC is delivered to the aquifer through seawater infiltration during wave and tide activity (solid lines). Transient hydrology moves the salinity distribution (red arrows to dotted lines), but the pool of POC is retarded relative to groundwater advection. Panel B: Retarded POC is able to support reactions, such as denitrification, outside the saline groundwater flowpath. Panel C: As hydrologic conditions change to have saline water encompass the pool of POC, denitrification is heightened towards the end of the flowpath where conditions are anoxic, and the hotspot of N₂ gas production is moved to the back of the circulation cell.

Coastal environments are ecologically, commercially, and recreationally valuable areas, supporting marine organisms, local fisheries, and tourism industries [Carter, 1988; Martínez et al., 2007]. However, due to changes in land-use and increased human activities in coastal areas, these systems are under immediate threat [Burak et al., 2004; Doney, 2010; Valiela et al., 1990]. Increased fluxes of terrestrial nutrients to the ocean have caused detrimental consequences in coastal areas, including eutrophication, harmful algal blooms, and habitat losses [Andersen et al., 2007; Cloern, 2001; Diaz and Solow, 1999; Valiela et al., 1990; Vitousek et al., 1997]. Ecosystem degradation further induces economic damage, by influencing human health, tourism, and the fishing industry [Carter, 1988; Costanza et al., 1997; Martínez et al., 2007; van der Muelen et al., 2004]. Therefore, managing terrestrial nutrient fluxes to marine systems is a critical aspect in the preservation of coastal environments.

Biogeochemical activity in coastal aquifers is an important regulator of solute and nutrient fluxes to the adjacent marine system [Heiss et al., 2017; Kim et al., 2017 & 2019 (submitted); Slomp and Van Cappellen, 2004; Valiela et al., 1990]. Terrestrial nutrients are delivered to beach sediments and ultimately to adjacent marine systems by fresh submarine groundwater discharge (SGD) [Johannes, 1980; Moore, 1999; Slomp and Van Cappellen, 2004; Valiela et al., 1990]. During wave and tide activity, seawater travels up the beachface and infiltrates into the aquifer, overtopping seaward-discharging fresh SGD [Abarca et al., 2013; Michael et al., 2005; Robinson et al., 2006]. The mixing between fresh groundwater and saline seawater creates a saline circulation cell in the intertidal zone [Michael et al., 2005; Heiss and Michael, 2014; Robinson et al., 2006; Vandenbohede and Lebbe, 2006], which hosts dynamic

biogeochemical reactions [Hays and Ullman, 2007; Kim et al., 2017 & 2019; Slomp and Van Cappellen, 2004; Spiteri et al., 2008; Ullman et al., 2003]. Fresh groundwater delivers terrestrial nutrients such as nitrate and iron, which can be utilized as alternative electron acceptors after oxygen depletion. Seawater, on the other hand, delivers oxygen and reactive organic carbon. Various reactions including active aerobic respiration [Anschutz et al., 2009; Charbonnier et al., 2013; Seidel et al., 2015], denitrification [Jiao et al., 2018; Kroeger et al., 2006; Kroeger and Charette, 2008; Lamontagne et al., 2018], and metal transformations [Charette and Sholkovitz, 2002; McAllister et al., 2015; Roy et al., 2010] have been observed in the intertidal zone system, impacting discharging concentrations of solutes.

In carbon-poor beach aquifer systems, the influx of reactive organic carbon from seawater is a key supply of electron donors supporting redox reactions down gradient [Anschutz et al., 2009; Charbonnier et al., 2013; Heiss et al., 2017]. However, much of this previous work has been focused on dissolved organic carbon (DOC) as the dominant form of carbon within beach sediments. Field studies often measure surface water or porewater DOC to quantify and characterize organic carbon supply into the system [A. Beck et al., 2007; Charbonnier et al., 2013; O'Connor et al., 2018; Reckhardt et al., 2015; Seidel et al., 2014 & 2015; Chaillou et al., 2016; Oh et al., 2017; Kim et al., 2012 & 2013], while numerical modeling studies use DOC associated with seawater infiltration to support reactions [Anwar et al., 2014; Spiteri et al., 2008a & 2008b; Bardini et al., 2012 ; Heiss et al., 2017]. While particulate organic carbon has not been completely disregarded in field settings [Beck et al., 2017; Charbonnier et al., 2013; Kim et al., 2017 & 2019; Reckhardt et al., 2015], especially in its association with metal oxides [Roy et al., 2010 & 2013; Charette et al., 2005], to

date, most of the focus has been on the distribution, supply, and molecular quality of DOC and how they relate to biogeochemical reactions within beach sediments.

However, fine carbon particles suspended in seawater have been shown to enter permeable coastal shelf sediments [Bacon et al., 1994; Huettel and Rusch 2000; Pilditch and Miller 2006; Rusch and Huettel 2000; Rusch et al 2000; McLachlan et al., 1985] and contribute to biogeochemical reactions [Huettel and Rusch 2000; Kim et al., 2019; Huettel et al., 2014; Rusch et al 2000]. Analogously, particulate organic carbon (POC) in seawater enters the beach aquifer with DOC during seawater infiltration. Unlike DOC that is completely mobile, transport of particulate organic carbon suspended in porewater is subject to dynamic transport mechanisms including retardation relative to groundwater advection, entrapment, immobilization, and remobilization [McDowell-Boyer et al., 1986; El-Farhan et al., 2000; Pronk et al., 2009]. In beach aquifers, such particulate transport dynamics and frequent shifts in hydrologic conditions result in a spatially variable distribution of POC across the beach aquifer (Figure 4.1, A). Recent field investigations at Cape Shores, Lewes, DE showed that these pools of reactive POC, retarded in their movement relative to groundwater flow, are important sources of nutrients and biogeochemical reactivity to the adjacent porewater [Kim et al., 2019]. As hydrological conditions (freshwater flux, tidal amplitude, storms) change and mobile reactants move across the pool of POC, favorability of biogeochemical redox reactions may result in close proximity to these carbon pools, contributing to the spatial heterogeneity of reaction zones and overall reactivity of beach aquifers. Further, overall reactivity of beach aquifers may have an “ebb and flow”, congruous with a transient hydrologic framework moving across a heterogeneous patchwork of POC pools.

In this work, we show how the retarded movement and resulting heterogeneous distribution of POC, traditionally disregarded in beach-hosted biogeochemical reactions, contribute to the magnitude and distribution of reaction zones within beach aquifers. A groundwater flow and reactive transport model was employed to understand how POC, retarded from groundwater advection, alters the biogeochemical efficiency of beach aquifer systems during hydrologic transience. Results demonstrate the intermittent biogeochemical contributions of POC dependent redox reactions on deposition conditions and transient hydrology, thereby highlighting the amplified reactive potential of beach sediments beyond that previously conceptualized.

4.2 Numerical Simulations

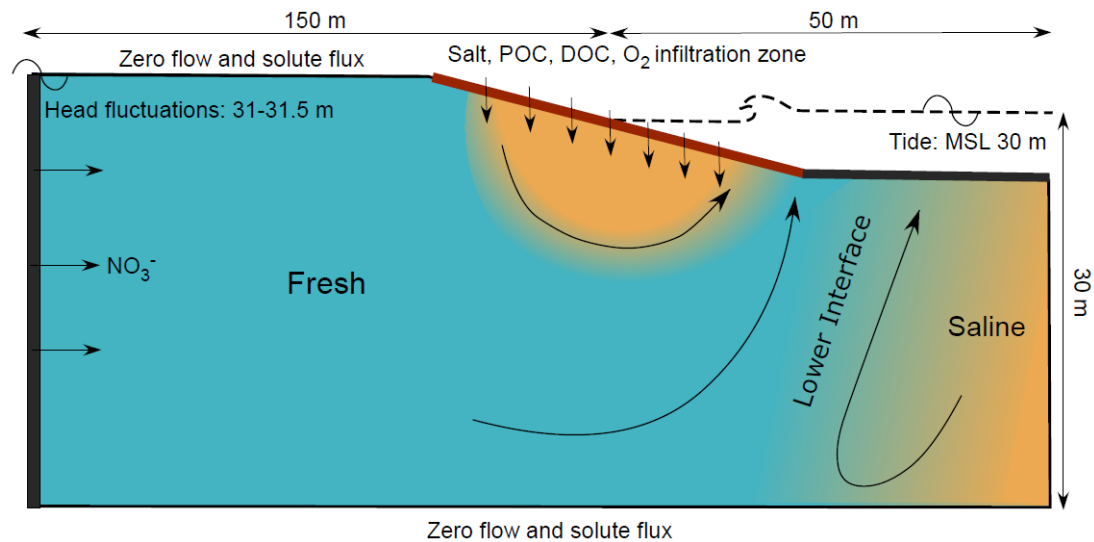


Figure 4.2 Numerical model schematic showing boundaries and fluxes.

Modeling was done in two stages. Groundwater flow, salt transport, and retarded POC transport with variable density was first simulated using a transient SEAWAT v4.0 [Langevin et al., 2007] model (Phase I). The distribution of POC and groundwater flow from SEAWAT was then linked to a transient reactive transport model PHT3D v2.13 [Prommer & Post, 2002] to simulate aerobic respiration and denitrification (Phase II).

4.2.1 Phase I: Groundwater Flow, Salt Transport, and Retarded POC Transport Model

A homogeneous, unconfined coastal aquifer was represented in the model domain, with seaward freshwater discharge and intertidal circulation of saline seawater. From the beachface-MSL intersection, the domain extended 150 m landward, 50 m seaward, and 30 m vertically. The grid had 125 layers and 184 columns, with higher discretization ($dx = 0.31$ m, $dy = 0.06$ m) in the intertidal zone [Heiss et al., 2017] (Figure 4.2).

The left vertical boundary was set as a constant-head Dirichlet boundary with a constant salinity of 0. The Periodic Boundary Condition (PBC) package [Post, 2011] was used to represent sinusoidal tidal fluctuations along the beachface and the offshore boundary, with time-varying head calculated as:

$$h_t = h_0 + A \cos(xt - h)$$

where h_t (m rel. MSL) is the tide elevation at time t , h_0 is MSL (0 m), A (0.6 m) is tidal amplitude, x (12.5 rad d^{-1}) is the frequency. Phase shift h (rad) was set as 0, save for one model case that used five tidal constituents to better simulate circulation cell movements on spring-neap timescales (Section 4.2.4; Appendix C, Table C-1).

Infiltrating seawater along the aquifer-ocean boundary was assigned a salinity of 35,

while a zero-concentration gradient was set for outward flow. Zero flow and solute flux were assigned to the bottom, the right boundary, and the top of the model domain landward of the shoreface.

Linear isotherm sorption with a retardation factor was used to simulate the retarded flow of particulate organic carbon. The retardation factor was calculated using the equation:

$$R = 1 + \frac{\rho_b}{\theta} K_d$$

where R is the retardation factor, ρ_b is the bulk density in g/cm^3 , θ is porosity, and K_d is the distribution coefficient. R for the base case was calculated using average for ρ_b , θ , and K_d values based on Cape Shores, Lewes, DE to yield a retardation factor of 1.416 [Davis, 2000; Krupka, 1999] (Appendix C, Table C-2). A range of K_d (R) values were tested in the sensitivity analysis.

A constant concentration ($C = 1$) of a retarded solute infiltrated across the shoreface boundary with seawater infiltration. After the salinity distribution reached steady-state, the diurnal average of the solute distribution was taken to be representative of POC distribution within the aquifer. The distribution was then scaled in its concentration to have a total of 10 mg within the distribution pattern. Conditions during this retarded solute infiltration were varied in Phase I to get differential distribution patterns of POC, with varying geometry and extent. This POC distribution pattern was assigned as the initial condition within the aquifer and linked to the reactive transport model in Phase II.

4.2.2 Phase II: Reactive Transport Model

DOC degradation, aerobic respiration and nitrate removal via denitrification were run to determine the contributions of POC to beach reactivity. Constant concentrations of O₂ (313 μM) and DOC (60 μM) were assigned across the shoreface to represent tidal infiltration. NO₃⁻ (179 μM) was assigned to fresh groundwater inflow from the left side of the model domain. The ranges and initial concentrations of species were based on previous literature [Heiss et al., 2017] or field values from Cape Shores, Lewes, DE [Kim et al., 2017 & 2019]. CO₂ and N₂ were assigned as mobile kinetic species produced as a byproduct of aerobic respiration and denitrification. POC was assigned as an immobile kinetic species within the aquifer, with its location and geometry prescribed from Phase I. The reaction network and the kinetic rate expressions (Table 4.1) were adapted from previous work [Bardini et al. 2012; Heiss et al. 2019; Kim et al. 2017].

Table 4.1 Reaction network and kinetic rate expressions (adopted from Bardini et al., 2012 & Heiss et al., 2019).

Name	Reaction	Rate expression
DOC degradation	DOC → CO ₂	Rate = k _{fox} [DOC];
Aerobic respiration	DOC + O ₂ → CO ₂ + H ₂ O	If [O ₂] > k _{mO2} ; Rate = k _{fox} [DOC] + k _{fox} [POC]; If [O ₂] < k _{mO2} ; Rate = (k _{fox} [DOC] + k _{fox} [POC]) × ([O ₂]/k _{mO2})
Denitrification	5DOC + 4NO ₃ ⁻ + 4H ⁺ → 5CO ₂ + 2N ₂ + 7H ₂ O	If [O ₂] > k _{mO2} ; Rate = 0; If [O ₂] < k _{mO2} and [NO ₃ ⁻] > k _{mNO3} ; Rate = (k _{fox} [DOC] + k _{fox} [POC]) × (1 - [O ₂]/k _{mO2}); If [O ₂] < k _{mO2} and NO ₃ ⁻ < k _{mNO3} ; Rate = (k _{fox} [DOC] + k _{fox} [POC]) × (1 - [O ₂]/k _{mO2}) × ([NO ₃ ⁻]/k _{mNO3})

4.2.3 Sensitivity Analysis

Various physical and chemical parameters were varied to identify the factors that control biogeochemical reactions with POC. The relative importance of POC was quantified using total nitrate removal, moles of NO_3^- converted to N_2 gas, within the intertidal circulation zone at a given time. A base case model was developed after Heiss et al. [2019] with parameters listed below (Table 4.2).

Table 4.2 Parameter values used for the Base Case model and range of parameter values used for sensitivity analyses.

Parameter	Range	Base Case Value
Phase I – POC deposition		
K_d [R]	0.1, 1, 2 (1.416, 3.08, 5.16)	0.1 [1.416]
Tidal amplitude for initial POC deposition	0.3, 0.5, 0.6, 0.9 m	0.6
Phase II – Dissolved Solute Movement		
Hydraulic conductivity	5, 10, 15 m/d	10
Tidal amplitude for reactive transport modeling	0.3, 0.4, 0.5, 0.6, 0.7, 0.8 m	0.6
Total POC mass	83, 249, 1248, 2081 μmol (1, 3, 15, 25 mg)	832
DOC concentration	5, 10, 30, 60, 120 μM	60
Carbon reactivity (k_{fox}^a)	1.5×10^{-7} , 7.0×10^{-7} , 1.5×10^{-6} , 7.0×10^{-6} , $1.5 \times 10^{-5} \text{ s}^{-1}$	1.5×10^{-6}
Phase II Unvaried		
kmo_2^{ab}	-	$3.125 \times 10^{-5} \text{ M}$
$\text{kmno}_3^{\text{ab}}$	-	$8.065 \times 10^{-6} \text{ M}$

^avan Cappellen and Wang [1996] ^bBardini et al. [2012].

The importance of the spatial distribution of POC was tested by varying the retardation factor and tidal condition during POC deposition (Phase I variables). Retardation factor controlled the subsurface expansion and geometry of the POC pool. The impacts of POC deposition location on beach reactivity were tested by using diurnal average POC distributions from various tidal amplitudes. For each parameter varied, four different POC distributions were generated. All cases had a total POC mass of 10 mg. Hydrologic conditions during the Phase II reactive transport simulation were held constant at base case conditions, and thus the set of simulations demonstrates the effect of antecedent hydrologic conditions on beach reactivity.

Conversely, carbon concentrations and hydrologic conditions that control the mobility of dissolved reactants were varied in Phase II. Simulations with the base case POC distribution were set with varying hydraulic conductivity and tidal amplitudes of reactive solute movement, to understand how aquifer properties that affect patterns of reactants relate to POC utilization. To understand how nitrogen removal depends on chemical conditions, total POC mass, infiltrating DOC concentration, and carbon reactivity were varied while holding other parameters at base case values. The dimensionless Damköhler (Da) number was also calculated to compare different model cases [Briggs et al., 2015; Gu et al., 2007; Heiss et al., 2017; Ocampo et al., 2006; Zarnetske et al., 2012]. Da is defined as:

$$Da = k_{fox} \times \frac{v_s}{Q}$$

where k_{fox} is carbon reactivity [T^{-1}] and $\frac{v_s}{Q}$ the residence time of saltwater within the saline circulation cell [T]. The residence time was calculated as the ratio between v_s [L^3], the volume of saltwater at a given time in the saline circulation cell, and the influx of saltwater per unit length of shoreline [L^3/T]. In cases where the reaction rate

is balanced by the advective delivery of mobile reactants, $Da = 1$. With higher reaction rates or lower advective rates, $Da > 1$ and the reactivity of the system is limited by the delivery of reactants. Conversely, $Da < 1$ implies that the system is reaction rate-limited.

4.2.4 Spring-Neap Transience Model

To see the impacts of transient circulation cell movements on the temporal aspects of POC utilization, a special model case was developed (Section 4.3.3). The model utilized five tidal constituents rather than just one (Appendix C, Table C-1), effectively simulating the movement of the intertidal circulation cell over spring-neap timescales. This allowed the POC pool, static within the beach aquifer, to be utilized at different times in response to the movement of the circulation cell.

4.3 Results

4.3.1 POC and Reactivity Distribution – Base Case

Tidal infiltration of seawater across the beachface created an intertidal circulation cell, consistent with previous field and modeling studies of the intertidal zone [Michael et al., 2005; Heiss and Michael, 2014; Kim et al., 2017]. Retarded advection of POC relative to groundwater created a pool of POC across the infiltration zone, smaller in its overall shape compared to the salt distribution. Figure 4.3 shows conditions at day 130, just after the salinity distribution reached dynamic steady-state.

Consistent with previous field and modeling findings [Heiss and Michael, 2014; Kim et al., 2017], NO_3^- removal via denitrification occurred along the freshwater-seawater mixing zone as nitrate-rich freshwater came in contact with POC (Figure 4.3). This produced N_2 gas, which moved along the groundwater flowpath and

was transported toward the discharge zone [Kim et al., 2017]. When DOC was added to the system with seawater infiltration, denitrification increased and the arc of N_2 gas along the mixing zone became more defined.

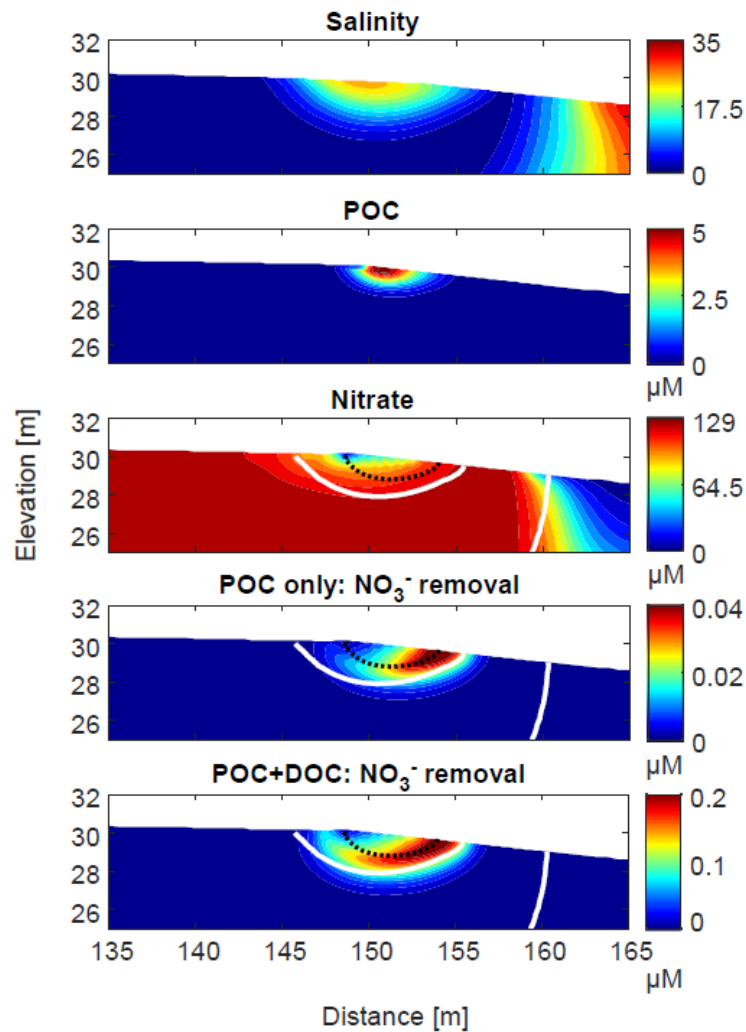


Figure 4.3 Solute distributions for base case scenario at day 130. Black dotted line indicates location of POC, white solid line indicates salinity 10. Top four panels shown are when POC was the sole source of carbon to the aquifer. The last panel shows N_2 gas production from NO_3^- via denitrification when both POC and DOC are present as carbon sources.

4.3.2 Phase I: Spatial Distributions of POC and Nitrate Removal

The effect of the spatial distribution of POC (or antecedent hydrologic conditions) on denitrification was explored by varying the retardation factor (varying K_d) and the tidal amplitude during the deposition phase (Phase I). All cases were scaled to introduce the same total mass of POC.

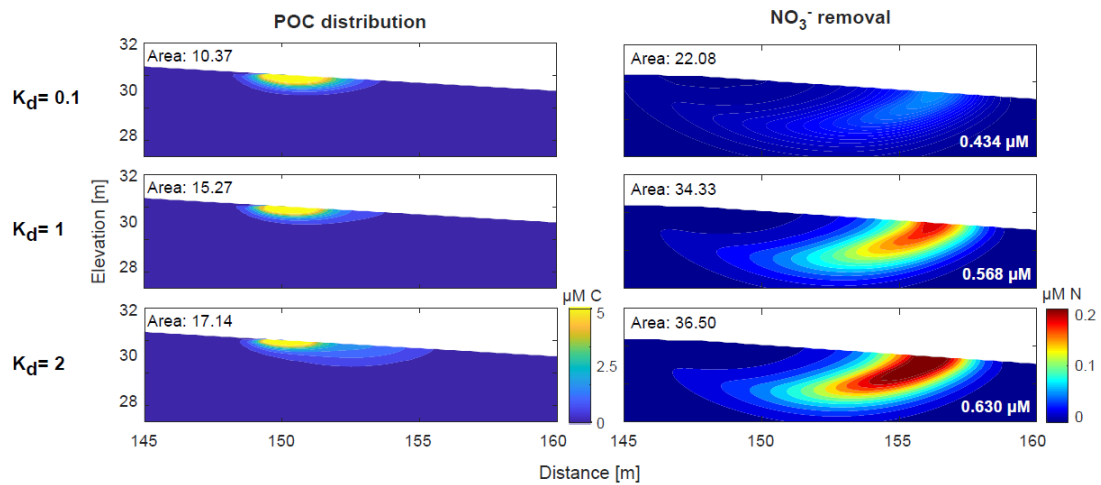


Figure 4.4 Distribution of POC with different K_d (R) values and resulting NO_3^- removal for day 130. The total mass of POC is constant across model cases. Greater retardation (higher K_d) and consequently higher R results in a more elongate POC distribution. Areal extent [m^2] and total NO_3^- removal [μM] increased with increasing K_d .

The changing spatial distribution of POC from varying retardation factors altered NO_3^- removal rates and patterns. With a higher retardation factor, the POC distribution greatly increased in its horizontal extent, and developed an elongated tail seaward. The magnitude and areal extent of denitrification increased with increasing retardation (Figure 4.4). This indicates that a large, dispersed POC pool may be more effective at supporting denitrification than a concentrated, smaller POC pool with the

same total carbon mass. POC in beach aquifers has been found in both well-defined and elongate pools of elevated concentrations [Kim et al., 2017 & 2019], which suggests that the retardation factor is dynamic along its flowpath.

POC distributions expanded greatly with increasing tidal amplitude of deposition (Phase I) (Figure 4.5). This in turn increased nitrate removal despite the same amount of carbon across cases, with the model case having a 0.9 m deposition tide removing 12.3 % more NO_3^- relative to the case having a 0.3 m tide over 100 days of model time. Therefore, wide POC deposition due to previously high tidal conditions and storm surge may serve to increase the magnitude and area of nitrate removal within the beach aquifer.

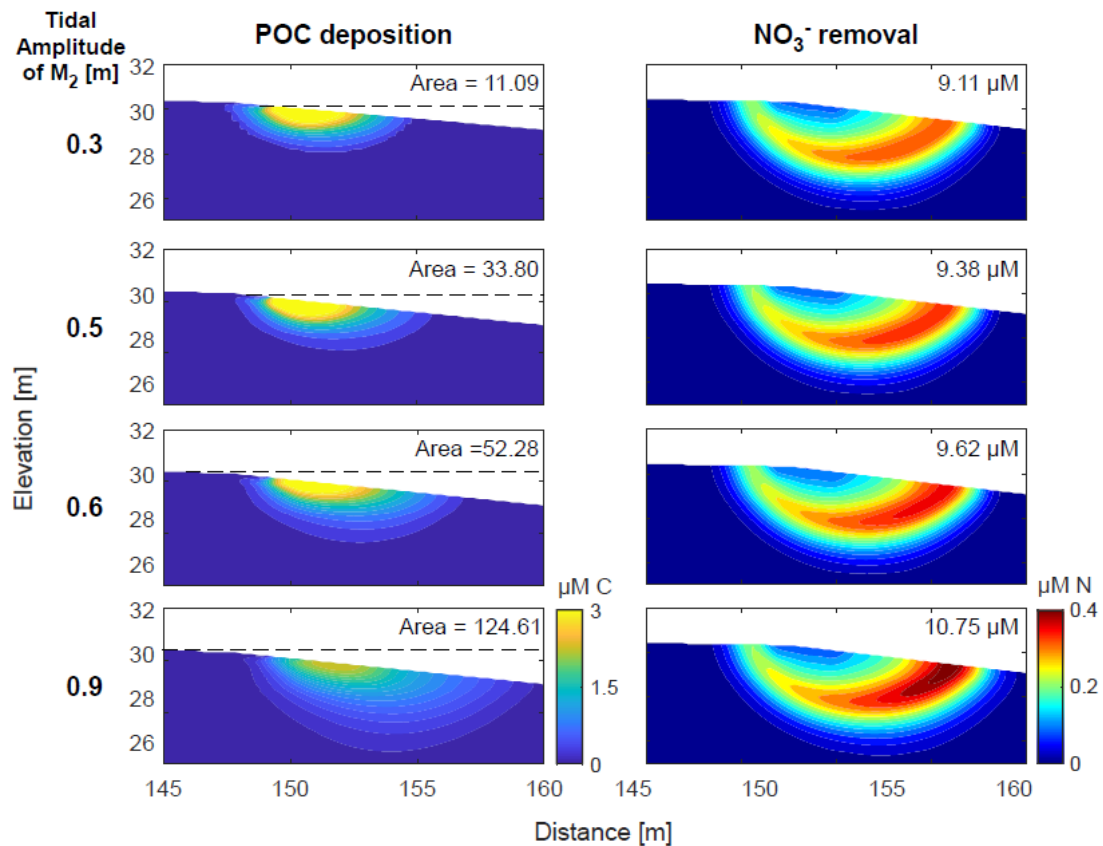


Figure 4.5 POC distribution from different tidal amplitudes. Total POC mass for all cases was held constant (10 mg). With increasing tide amplitudes of deposition, POC was more expansively distributed. Area above $0.01 \mu M$ is calculated and indicated [m^2]. Dotted line indicates sea-level at the time of distribution. Because the distribution is the result of previous infiltration, advection, and retardation, the sea-level does not exactly correlate with shown distributions. NO_3^- removal for day 130, increasing with increasing tidal amplitude of POC deposition, is shown in the right panels.

4.3.3 Temporal Variations in POC Contributions

The model case developed with five tidal constituents to show spring-neap transience in the geometry of the circulation cell displayed the transient nature of POC utilization. The pool of POC intermittently contributed to denitrification, removing

NO_3^- and producing N_2 as the seaward movement of the saline circulation cell caused it to overlap with anoxic fresh groundwater. This behavior was heightened when repeated with higher retardation factors, with a highly concentrated pool of POC near head of the saline water infiltration zone and a long, elongate POC tail seaward. As the saline circulation cell moved seaward, the nitrate-rich freshwater moved over the POC, increasing the “POC exposure area”, or the area where NO_3^- -rich ($\sim 129 \mu\text{M}$) water overlaps POC and has oxygen concentrations lower than the threshold concentration ($31.2 \mu\text{M}$). This in turn strengthened nitrate removal near the landward edge of the circulation cell (Figure 4.6, A: 19.48 %). With increasing tidal amplitudes (B to C), the circulation cell was pushed higher up the beach, and the infiltrating oxygen decreased the areal extent where POC was within anoxic waters (Figure 4.6, C: 11.72 %). This in turn decreased denitrification (Figure 4.6, B to C). As tidal amplitudes fell, both POC exposure area (18.9 %) and denitrification increased (Figure 4.6, D). This shows that POC supports denitrification intermittently at its location, allowing denitrification to occur outside its expected location near the discharge zone of groundwater circulation. Hotspots of denitrification may therefore migrate within the beach, sporadically supported by upland POC.

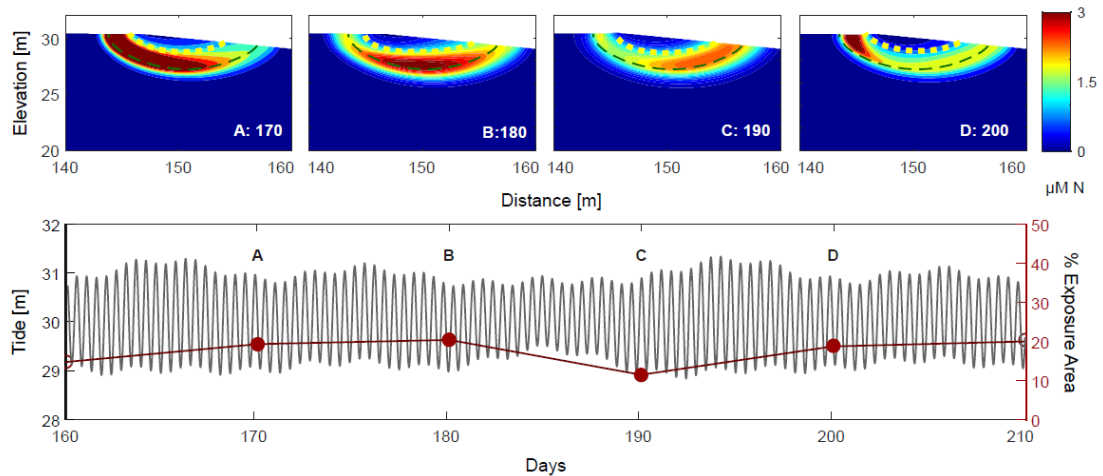


Figure 4.6 Temporal variations in POC contributions to denitrification. White text (upper panels) and solid red circles (lower panel) indicates days shown, yellow dashed line the extent of the circulation cell at salinity 25, green dashed line the extent of POC. Lower panel shows simulated tidal signal with the amplitude of the principle lunar tidal constituent at 0.6 m (black line) and % of freshwater-saltwater mixing zone area that has conditions favorable for denitrification (overlaps POC and has less than the threshold concentration for oxygen ($31.2 \mu\text{M}$)).

4.3.4 Phase II: Carbon Characteristics and their Impacts on Nitrate Removal

Parameters related to carbon were varied and cases were compared for denitrification efficiency. Increasing POC concentrations did not affect denitrification within the intertidal zone, because no zero-order degradation was set up for POC for model stability. Even with the lowest POC concentration of 1 mg, the system was effectively unlimited in carbon, and hence nitrate removal and was more controlled by hydrologic transience, intermittent POC utilization, and transient DOC delivery (Section 3.3).

However, when DOC was added as an additional carbon source, there was a linear increase of nitrate removal with increasing DOC concentrations in the infiltrating seawater. With higher DOC concentrations, oxic seawater was able to

consume oxygen faster, allowing denitrification to occur earlier in the flowpath. The case with an infiltrating DOC concentration of 120 μM allowed for an additional 10-42 μM of NO_3^- removed per day compared to the case with a DOC concentration of 5 μM .

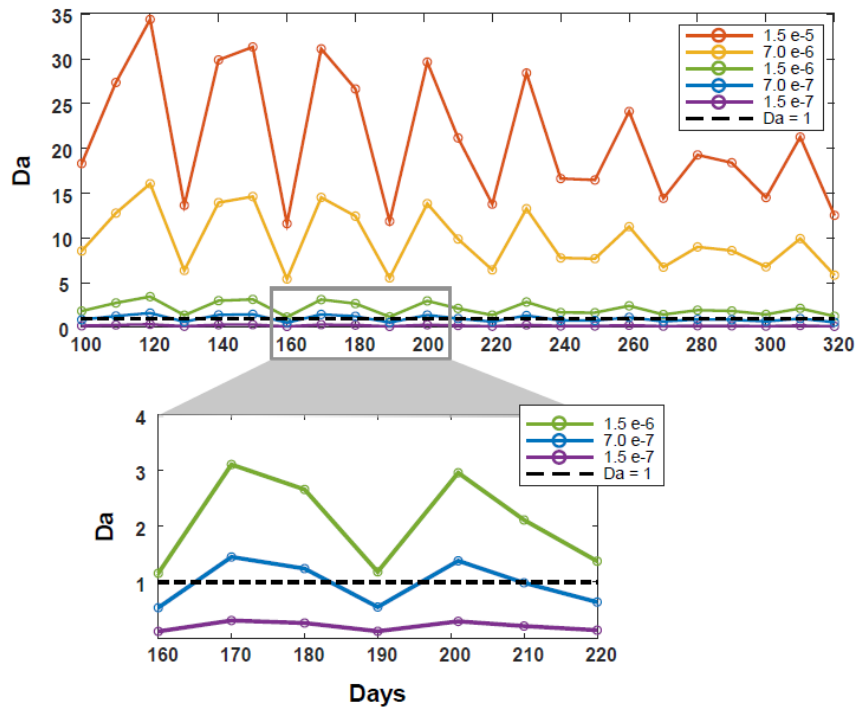


Figure 4.7 Damköhler number over time for a range of carbon reactivity values. Due to the changing saltwater volume in the system over time, model case with reactivity of $7.0 \times e-7$ (blue) swings between advection-limited ($\text{Da} > 1$) and rate-limited ($\text{Da} < 1$).

Altering the reactivity rate changed the Damköhler number between cases, which fluctuated over time as the extent of the saline circulation cell changed (Figure 4.7). Low reactivity rates decreased the Damköhler number below 1, making the

system rate-limited, and higher reactivity rates increased Da and the system became advection-limited. The advection-limited behavior was apparent in the case with the largest carbon reactivity rate. While there was a slight successive increase of NO_3^- removal by 4-8 μM per day as reactivity increased, at the highest reactivity rate, nitrate removal decreased as the system became DOC supply-limited. At certain reaction rates, the Damköhler number fluctuated between $Da > 1$ and $Da < 1$ as the extent of the saline circulation cell changed over time, shifting between advection- and rate-limited (Figure 4.7, lower panel). This displays an added aspect of transience in beach biogeochemical reactions in addition to the intermittent utilization of POC due to changing hydrologic conditions, as the relative importance of POC may be increased when systems are DOC supply-limited ($Da > 1$). Overall, results show that higher DOC concentrations and higher carbon reactivity rates increase denitrification within the intertidal zone. In field settings, with increased variability in saline circulation cell extent, POC/DOC availability, and reactivity rates due to seasonal biological cycles, further complexity in beach reactions is expected.

4.3.5 Phase II: Hydraulic Conductivity and Tidal Amplitude on POC Utilization

Hydraulic conductivity affected the denitrification potential of the intertidal beach system by altering the areal extent of the saline circulation cell and freshwater nitrate. With increasing hydraulic conductivity, the depth of the circulation cell was responsive, resulting in a larger range in the area with less than 50% nitrate (Figure 4.8, A-C, black and red dashed lines). While during spring tide conditions (Figure 4.8, A-C, black dash), the saline circulation cell often almost completely engulfed the POC, during neap tide (Figure 4.8, A-C, red dash), higher hydraulic conductivity

scenarios increased the exposure area of POC to high nitrate groundwater, increasing NO_3^- removal (Figure 4.8, D-F). While only POC was introduced as a carbon source in the cases presented in Figure 9, all cases had $\text{Da} > 1$, indicating that the systems were DOC-limited thus would become more reactive with POC within the aquifer.

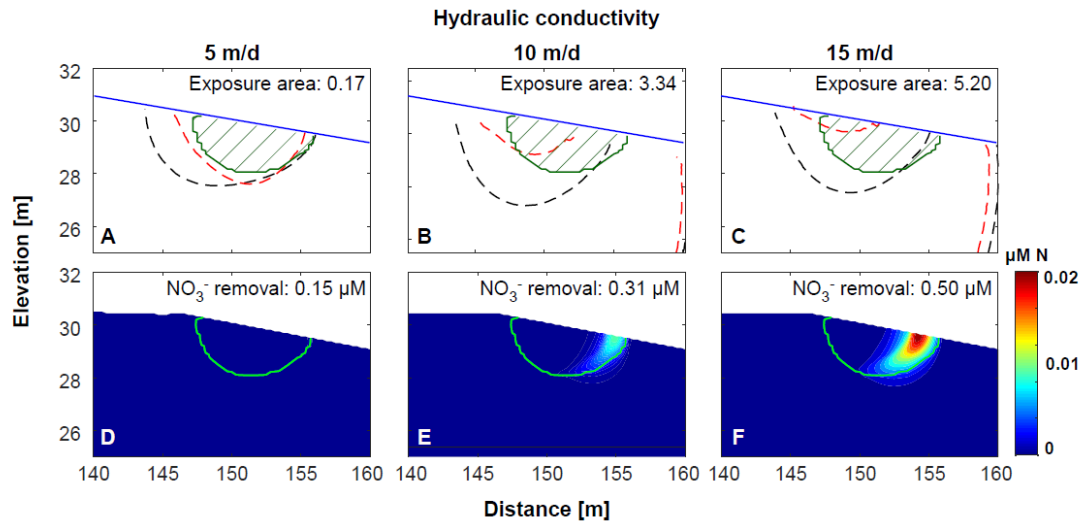


Figure 4.8 50% NO_3^- contour for day 170 (spring tide, black dashed lines) and 190 (neap tide, red dashed lines) for $K = 5, 10,$ and 15 m/d. POC is indicated in green. The difference in exposure area between the two days are shown. NO_3^- removal for day 190 during neap tide is shown in lower panels D-F.

Increasing tidal amplitude had a similar effect on the denitrification efficiency of the saline circulation cell. With increasing tidal amplitude, the extent of the saline circulation cell increased and decreased the exposure area of POC (Figure 4.9, A-F), which counteracted POC utilization for nitrate removal (Figure 4.9, G). POC was deposited during Phase I using an tidal amplitude of 0.6 m. When the tidal amplitude for Phase II became greater than the depositional amplitude (Figure 4.9, E-F), the POC

was completely engulfed by the saline circulation cell and no area of POC was exposed to high- NO_3^- , low- O_2 groundwater. This indicates that POC utilization is increased for systems that follow a large-tidal amplitude deposition event (Phase I) followed by smaller tidal amplitude of reactive transport and saline circulation cell development (Phase II). While Da numbers for lower tidal amplitudes (0.3~0.6 m) ranged between $0.7 < \text{Da} < 2$, switching between rate- and supply-limited systems, Da for the higher amplitudes (0.7~0.8 m) ranged between $5 < \text{Da} < 7$ due to the large circulation cell area. A high-Da system resulting from high carbon respiration rates still had spatial configurations of the circulation cell and POC that fostered POC-supported denitrification. In contrast, a high-Da system from high tidal amplitudes controlling the extent of the circulation cell limited any contribution of POC to denitrification. This emphasizes that the spatial relationship between deposited POC and the saline circulation cell is important in establishing the relative contributions of POC to beach biogeochemical reactions.

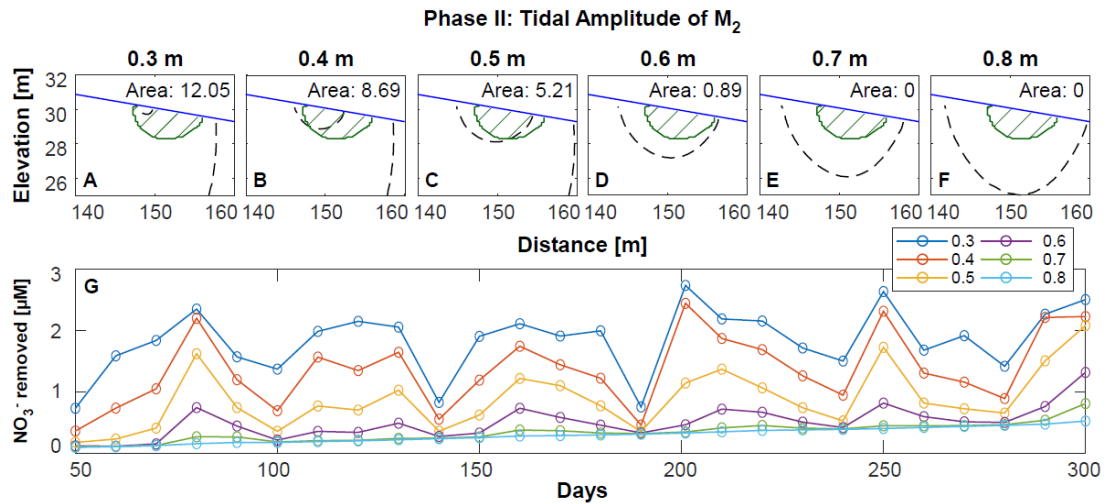


Figure 4.9 Effects of tidal amplitude (TA = 0.3, 0.4, 0.5, 0.6, 0.7, 0.8 m) on nitrate removal within the intertidal zone. A-F: POC is indicated in green. 50% NO_3^- contour during maximum nitrate removal is shown (day 200, black dashed line), and exposure area is presented. G: Nitrate removal over time by tidal amplitude.

4.4 Discussion

4.4.1 Contributions of POC in a Dynamic Beach Environment

POC was shown to increase the reactive potential of an intertidal circulation cell system by serving as an additional source of carbon with a distribution that is spatially decoupled from that of DOC. While various parameters were adjusted to identify conditions that allow for increased utilization of POC in beach reactions, more complex dynamics of POC utilization are expected in field settings.

The geometry, extent, and transience of both the POC pool and the saline circulation cell create variability in POC utilization and reactivity of beach aquifers. POC supported reactions intermittently, during times when the saline circulation cell decreased in its spatial extent or moved seaward to allow greater contact between POC and fresh groundwater (Figure 4.6). However, due to the necessary spatial overlap

between POC and nitrate for POC-supported denitrification, there was a spatial dynamic between POC expansion and the areal extent of the circulation cell. When hydraulic conductivity allowed the areal extent of the saline circulation cell to vary considerably from the deposition of POC, smaller circulation cells developed from higher hydraulic conductivity increased POC exposure to nitrate-rich groundwater (Figure 4.8). However, circulation cells that were developed with higher tidal amplitudes than the conditions used during POC deposition completely engulfed the POC (Figure 4.9) and nitrate removal was dampened from limited contact with POC.

Transient hydrologic conditions not only control the mobility of dissolved reactants across the previously-deposited POC, but also continuously deliver more POC to the beach system. Therefore, previous hydrologic conditions are as pertinent to beach reactivity as much as the present. Even with the same hydrologic conditions and circulation cell extent, the circulation cell following a spring-tide deposition (Phase I) of POC rather than the one recovering from neap-tide would have increased biogeochemical activity, dominated by POC rather than DOC (Figure 4.5). Conversely, as tides rise (Phase II), increase the extent of the circulation cell and engulf the POC deposited during smaller tidal amplitudes, POC may be utilized for aerobic respiration within the circulation cell rather than denitrification outside of the cell. When the POC is deposited higher on the beach, from an anomalously high tide or storm event, denitrification in circulation cells developed with larger tidal amplitudes may be able to utilize this carbon source, while smaller cells further seaward cannot. This indicates that the location of POC deposition and its overlap with nitrate-rich fresh groundwater, and ultimately transient hydrologic conditions, are

important controls on the spatial patterns of denitrification and other beach biogeochemical reactions [Kim et al. 2019].

In natural environmental settings, continuous changes to hydrologic conditions, transport of POC along groundwater flow, and POC degradation would result in a more transient, heterogeneous distribution of POC than the static, idealized pool presented in this work [Kim et al., 2019]. This implies that contributions of POC to beach reactions would be spatiotemporally patchier, notwithstanding the temporal variations in seawater concentrations and infiltration rates of POC and DOC. With POC variably scattered across the aquifer, biogeochemical reactions would similarly be supported in a patchy manner, further deviating from locations expected according to oxygen concentrations along groundwater flowpaths. This suggests that denitrification, previously suggested as a mixing-dependent reaction, is able to occur in areas outside the bounds of seawater circulation [Kim et al., 2019]. While denitrification was used as a proxy reaction to identify factors relevant for POC utilization, POC within beach sediments can support other biogeochemical transformations that require a carbon source. While POC-mediated denitrification decreased with increasing overlap with oxic, saline water, rates of reactions that require seawater-derived reactants, such as sulfate reduction, may conversely be amplified. Transience of POC deposition, dissolved reactant movement, and heterogeneous distribution of POC combined would therefore create complex dynamics in POC utilization in the intertidal zones of beach aquifers.

4.4.2 Model Assumptions of POC Chemical Characteristics

This study explored the impacts of various physical and chemical parameters to POC and beach reactivity, and in doing so, made various assumptions in the

chemical behavior of carbon infiltration, transport, and degradation. Consideration of the various chemical characteristics of POC and DOC would increase the transience and complexity of POC contributions to beach biogeochemistry.

While a static concentration of POC was used in the model for the duration of the simulation, surface water productivity, the source of POC to the beach aquifer, varies over seasons. This implies that the total amount of POC within the aquifer continuously changes with infiltrating concentrations, retardation, and transport.

Although the model eliminated zero-order POC degradation to ensure a steady-state distribution of POC, degradation of POC in beach sediments is undoubtedly expected. This would increase the transience of POC contributions to beach reactions, as pools form and disappear within some time of formation. The timescale of POC relevance to a system would depend on the degradation, utilization, and replenishment rate of POC. Reactivity of POC is also expected to vary from DOC and over time, contingent on the molecular quality of POC [Seidel et al., 2015]. In times of low surface water DOC and high DOC degradation rates, the more refractory POC may become the relatively more important source of carbon for beach reactions. Further work is required at various timescales to better resolve the relationship between transient POC distributions and beach biogeochemical reactions.

Field investigations of POC pools show that POC not only directly supports biogeochemical redox reactions, but is also a source of DOC and other nutrients (particulate nitrogen, phosphate, particulate phosphorus) via degradation and leaching [Kim et al., 2019]. Though the model assumed that no additional nutrients were released from the pool of POC, in environmental settings, the POC may be a source, rather than a sink, of nitrogen. While freshwater contributions of terrestrial nutrients

would generally far surpass the contributions from POC, POC pools as a potential repository of nutrients may be an important consideration for settings with abundant organic matter. After its release from POC, these nutrients may be spatially linked to the pool of POC [Kim et al., 2019], or be transported with groundwater for utilization down the flow gradient.

Therefore, POC is a potentially important, but intermittently utilized, reactant, that creates complex, transient reaction patterns within the intertidal zone during its interaction with dissolved, mobile reactants.

4.5 Conclusions

The contributions of particulate organic carbon to beach biogeochemical reactions and the conditions that increase its relative importance were explored using numerical simulations of groundwater flow and reactive transport. POC formed a pool near the infiltration zone due to its retarded transport relative to groundwater advection. Higher retardation values and higher tidal amplitude during POC deposition increased POC contributions to nitrate removal. Unlike DOC-supported denitrification that occurs along groundwater flowpaths, POC supported nitrate removal at its infiltrated location, upland of the groundwater discharge zone. Due to the necessity of spatial overlap between with anoxic, nitrate-rich water for POC-supported denitrification, POC intermittently created nitrogen gas hotspots near the landward edge of the saline circulation cell. The nitrate removal magnitude of systems responded to changes in saline circulation cell extent, which subsequently altered the areal extent of POC and nitrate-rich groundwater contact. Decreased extent of the circulation cell due to freshwater fluctuations and higher hydraulic conductivity (during neap tide) subsequently increased nitrate removal. In contrast, an excessively-

large circulation cell developed during tidal amplitude larger than conditions used during POC deposition dampened the utilization of POC by denitrification, by preventing its exposure to anoxic freshwater. The deposition concentration, location, and pattern of POC varies over time and space, creating complex interactions with dissolved reactants. In highly transient beach systems, POC may be a previously-ignored, but sporadically-important source of carbon for intertidal biogeochemical reactions.

REFERENCES

- Abarca, E., H. Karam, H. F. Hemond, and C. F. Harvey (2013), Transient groundwater dynamics in a coastal aquifer: The effects of tides, the lunar cycle, and the beach profile, *Water Resources Research*, 49, 1–16.
<https://doi.org/10.1002/wrcr.20075>.
- Andersen, M. S., L. Baron, J. Gudbjerg, J. Gregersen, D. Chapellier, R. Jakobsen, and D. Postma (2007), Discharge of nitrate-containing groundwater into a coastal marine environment, *Journal of Hydrology*, 336 (1-2), 98-114,
<https://doi.org/10.1016/j.jhydrol.2006.12.023>.
- Anschutz, P., T. Smith, A. Mouret, J. Deborde, S. Bujan, D. Poirer, and P. Lecroart (2009), Tidal sands as biogeochemical reactors, *Estuarine, Coastal, and Shelf Science*, 84, 84-90, doi:10.1016/j.ecss.2009.06.015.
- Anwar, N., C. Robinson, and D. A. Barry (2014), Influence of tides and waves on the fate of nutrients in a nearshore aquifer: Numerical simulations, *Advances in Water Resources*, 73, 203-213,
<http://dx.doi.org/10.1016/j.advwatres.2014.08.015>.
- Bacon, M. P., R. A. Belostock, and M. H. Bothner (1994), ²¹⁰Pb balance and implications for particle transport on the continental shelf, US Middle Atlantic Bight, *Deep Sea Research Part II: Topical Studies in Oceanography*, 41(2-3), 511-535, [https://doi.org/10.1016/0967-0645\(94\)90033-7](https://doi.org/10.1016/0967-0645(94)90033-7).
- Bardini, L., F. Boano, M. B. Cardenas, R. Revelli, and L. Ridolfi (2012), Nutrient cycling in bedform induced hyporheic zones, *Geochimica et Cosmochimica Acta*, 84, 47–61. <http://doi.org/10.1016/j.gca.2012.01.025>.
- Beck, A. J., Y. Tsukamoto, A. Tovar-Sanchez, M. Huerta-Diaz, H. J. Bokuniewicz, and S.A. Sanudo-Wilhelmy (2007), Importance of geochemical transformations in determining submarine groundwater discharge-derived trace metal and nutrient fluxes, *Applied Geochemistry*, 22(2), 477-490,
<https://doi.org/10.1016/j.apgeochem.2006.10.005>.

- Beck, M., A. Reckhardt, J. Amelsberg, A. Bartholomä, H. Brumsack, H. Cypionka, T. Dittmar, B. Engelen, J. Greskowiak, H. Hillebrand, M. Holtappels, R. Neuholz, J. Köster, M. Kuypers, G. Massmann, D. Meier, J. Niggemann, R. Paffrath, K. Pahnke, S. Rovo, M. Striebel, V. Vandieken, A. Wehrmann, and O. Zielinski (2017), The drivers of biogeochemistry in beach ecosystems: A cross-shore transect from the dunes to the low water line, *Marine Chemistry*, 190, 35-50, <http://dx.doi.org/10.1016/j.marchem.2017.01.001>.
- Briggs, M. A., F. D. Day-Lewis, J. P. Zarnetske, and J. W. Harvey (2015), A physical explanation for the development of redox microzones in hyporheic flow, *Geophysical Research Letters*, 42: 4402–4410, <https://doi.org/10.1002/2015GL064200>.
- Burak, S. A., E. Dogan, and C. Gazioglu (2004), Impact of urbanization and tourism on coastal environment, *Ocean & Coastal Management*, 47 (9-10), 515-527, <https://doi.org/10.1016/j.ocecoaman.2004.07.007>.
- Carter, R.W.G. (1988), *Coastal environments: an introduction to the physical, ecological, and cultural systems of coastlines*. London: Academic Press Limited.
- Chaillou, G., F. Lemay-Borduas, and M. Couturier (2016), Transport and transformations of groundwater-borne carbon discharging through a sandy beach to a coastal ocean, *Canadian Water Resources Journal*, 41(4): 455-468, <https://doi.org/10.1080/07011784.2015.1111775>.
- Charbonnier, C., P. Anschutz, D. Poirier, S. Bujan, and P. Lecroart (2013), Aerobic respiration in a high-energy sandy beach, *Marine Chemistry*, 155, 10-21, <http://dx.doi.org/10.1016/j.marchem.2013.05.003>.
- Charette, M. A., and E. R. Sholkovitz (2002), Oxidative precipitation of groundwater-derived ferrous iron in the subterranean estuary of a coastal bay, *Geophysical research letters*, 29(10), 85-1–85-4, doi:10.1029/2001GL014512.
- Charette, M.A., E.R. Sholkovitz, and C. M. Hansel (2005), Trace element cycling in a subterranean estuary: Part 1. Geochemistry of the permeable sediments, *Geochimica et Cosmochimica Acta*, 69(8): 2095-2109, <https://doi.org/10.1016/j.gca.2004.10.024>.
- Cloern, J. E. (2001), Our evolving conceptual model of the coastal eutrophication problem, *Marine Ecology Progress Series*, 210: 223-253, doi:10.3354/meps210223.

- Costanza, R., R. d'Arge, R., De Groot, S. Farber, M. Grasso, B. Hannon, K. Limburg, S. Naeem, R. V. O'Neill, J. Paruelo, and R. G. Raskin (1997), The value of the world's ecosystem services and natural capital, *Nature*, 387 (6630), 253-260.
- Davis, H. (2000), Fate and transport modeling of selected chlorinated organic compounds at operable unit 3, US Naval Air Station, Jacksonville, Florida, Department of the Interior, Washington D.C., USGS-OFR-00-255, <https://apps.dtic.mil/dtic/tr/fulltext/u2/a442391.pdf>
- Diaz, R. J. and A. Solow (1999), Ecological and economic consequences of hypoxia, Silver Spring, Maryland: NOAA Coastal Ocean Program.
- Doney, S. C. (2010), The growing human footprint on coastal and open-ocean biogeochemistry, *Science*, 328(5985), 1512-1516, doi: 10.1126/science.1185198.
- El-Farhan, Y.H., N.M. DeNovio, J.S. Herman, and G.M. Hornberger (2000), Mobilization and transport of soil particles during infiltration experiments in an agricultural field, Shenandoah Valley, Virginia, *Environmental science & technology*, 34(17), 3555-3559, doi: 10.1021/es991099g.
- Gu, C. H., G. M. Hornberger, A. L. Mills, J. S. Herman, and S. A. Flewelling (2007), Nitrate reduction in streambed sediments: Effects of flow and biogeochemical kinetics, *Water Resources Research*, 43, W12413. <https://doi.org/10.1029/2007WR006027>.
- Hays, R. L., and W. J. Ullman (2007), Direct determination of total and fresh groundwater discharge and nutrient loads from a sandy beachface at low tide (Cape Henlopen, Delaware), *Limnology and oceanography*, 52(1), 240-247, doi:10.4319/lo.2007.52.1.0240.
- Heiss, J. W., and H. A. Michael (2014), Saltwater-freshwater mixing dynamics in a sandy beach aquifer over tidal, spring-neap, and seasonal cycles, *Water Resour. Res.*, 50, 6747–6766, doi:10.1002/2014WR015574.
- Heiss, J. W., V. E. Post, T. Laattoe, C. J. Russoniello, and H. A. Michael (2017), Physical controls on biogeochemical processes in intertidal zones of beach aquifers, *Water Resources Research*, 53(11), 9225-9244, <https://doi.org/10.1002/2017WR021110>.
- Huettel, M., and A. Rusch (2000), Transport and degradation of phytoplankton in permeable sediment, *Limnology and Oceanography*, 45(3), 534-549, <https://doi.org/10.4319/lo.2000.45.3.0534>.

- Huettel, M., P. Berg, and J. E. Kostka (2014), Benthic exchange and biogeochemical cycling in permeable sediments, *Annu. Rev. Mar. Sci.*, 6: 23–51, doi:10.1146/annurev-marine-051413-012706.
- Jiao, L., J. Wu, X. He, X. Wen, Y. Li, and Y. Hong (2018), Significant microbial nitrogen loss from denitrification and anammox in the land-sea interface of low permeable sediments, *International Biodeterioration & Biodegradation*, 135: 80-89, <https://doi.org/10.1016/j.ibiod.2018.10.002>.
- Johannes, R. E. (1980). Ecological significance of the submarine discharge of groundwater, *Marine ecol. prog. ser.*, 3(4), 365-373.
- Kim, T.H., E. Kwon, I. Kim, S. A. Lee, and G. Kim (2013), Dissolved organic matter in the subterranean estuary of a volcanic island, Jeju: Importance of dissolved organic nitrogen fluxes to the ocean, *Journal of sea research*, 78: 18-24, <https://doi.org/10.1016/j.seares.2012.12.009>.
- Kim, T.H., H. Waska, E. Kwon, I. G. N. Suryaputra, and G. Kim (2012), Production, degradation, and flux of dissolved organic matter in the subterranean estuary of a large tidal flat, *Marine Chemistry*, 142: 1-10, <https://doi.org/10.1016/j.marchem.2012.08.002>.
- Kim, K. H., J. W. Heiss, H. A. Michael, W. J. Cai, T. Laattoe, V. E. Post, and W. J. Ullman (2017), Spatial patterns of groundwater biogeochemical reactivity in an intertidal beach aquifer, *Journal of Geophysical Research: Biogeosciences*, 122(10), 2548-2562, <https://doi.org/10.1002/2017JG003943>.
- Kroeger, K. D., M. L. Cole, and I. Valiela, (2006), Groundwater-transported dissolved organic nitrogen exports from coastal watersheds, *Limnology and Oceanography*, 51(5), 2248-2261, <https://doi.org/10.4319/lo.2006.51.5.2248>.
- Kroeger, K. D., and M. A. Charette (2008), Nitrogen biogeochemistry of submarine groundwater discharge, *Limnology Oceanography*, 53(3), 1025–1039, doi:10.4319/lo.2008.53.3.1025.
- Krupka, K. M., D. I. Kaplan, G. Whelan, R. J. Serne, and S. V. Mattigod (1999), Understanding variation in partition coefficient, K_d , values, Volume II: Review of Geochemistry and Available K_d Values, for Cadmium, Cesium, Chromium, Lead, Plutonium, Radon, Strontium, Thorium, Tritium (3H), and Uranium, EPA, Washington D.C., <https://www.epa.gov/sites/production/files/2015-05/documents/402-r-99-004b.pdf>.

- Lamontagne, S., F. Cosme, A. Minard, and A. Holloway (2018), Nitrogen attenuation, dilution and recycling in the intertidal hyporheic zone of a subtropical estuary, *Hydrology and Earth System Sciences*, 22(7): 4083-4096, <https://doi.org/10.5194/hess-22-4083-2018>.
- Martínez, M. L., A. Intralawan, G. Vázquez, O. Pérez-Maqueo, P. Sutton, and R. Landgrave (2007), The coasts of our world: Ecological, economic and social importance, *Ecological Economics*, 63(2-3), 254-272, <https://doi.org/10.1016/j.ecolecon.2006.10.022>.
- McAllister, S.M., J.M. Barnett, J.W. Heiss, A.J. Findlay, D.J. MacDonald, C. L. Dow, G.W. Luther, H. A. Michael, and C.S Chan (2015), Dynamic hydrologic and biogeochemical processes drive microbially enhanced iron and sulfur cycling within the intertidal mixing zone of a beach aquifer, *Limnology and Oceanography*, 60, 329-345, doi: 10.1111/lno.10029.
- McDowell-Boyer, L.M., J.R. Hunt, and N. Sitar, (1986), Particle transport through porous media, *Water Resources Research*, 22(13), 1901-1921, <https://doi.org/10.1029/WR022i013p01901>.
- McLachlan, A., I. G. Eliot, and D. J. Clarke (1985), Water filtration through reflective microtidal beaches and shallow sublittoral sands and its implications for an inshore ecosystem in Western Australia, *Estuarine, Coastal and Shelf Science*, 21(1), 91-104.
- Michael, H. A., A. E. Mulligan, and C. F. Harvey (2005), Seasonal oscillations in water exchange between aquifers and the coastal ocean, *Nature*, 436(7054), 1145-1148, doi:10.1038/nature03935.
- Moore, W. S. (1999), The subterranean estuary: a reaction zone of ground water and sea water. *Marine Chemistry*, 65(1), 111-125, [http://dx.doi.org/10.1016/S0304-4203\(99\)00014-6](http://dx.doi.org/10.1016/S0304-4203(99)00014-6).
- Ocampo, C. J., C. E. Oldham, and M. Sivapalan (2006), Nitrate attenuation in agricultural catchments: Shifting balances between transport and reaction, *Water Resources Research*, 42, W01408. <https://doi.org/10.1029/2004WR003773>.
- O'Connor, A. E., J. L. Krask, E. A. Canuel, and A. J. Beck (2018), Seasonality of major redox constituents in a shallow subterranean estuary, *Geochimica et Cosmochimica Acta*, 224, 344-361, <https://doi.org/10.1016/j.gca.2017.10.013>.

- Oh, Y.H., Y. W. Lee, S. R. Park, and T. H. Kim (2017), Importance of dissolved organic carbon flux through submarine groundwater discharge to the coastal ocean: Results from Masan Bay, the southern coast of Korea, *Journal of Marine Systems*, 173: 43-48, <https://doi.org/10.1016/j.jmarsys.2017.03.013>.
- Pilditch, C. A. and D. C. Miller (2006), Phytoplankton deposition to permeable sediments under oscillatory flow: Effects of ripple geometry and resuspension, *Continental Shelf Research*, 26(15), 1806-1825, <https://doi.org/10.1016/j.csr.2006.06.002>.
- Pronk, M., N. Goldscheider, J. Zopfi, and F. Zwahlen (2009), Percolation and particle transport in the unsaturated zone of a karst aquifer, *Groundwater*, 47(3), 361-369, <https://doi.org/10.1111/j.1745-6584.2008.00509.x>.
- Reckhardt, A., M. Beck, M. Seidel, T. Riedel, A. Wehrmann, A. Bartholomä, and H. J. Brumsack (2015), Carbon, nutrient and trace metal cycling in sandy sediments: A comparison of high-energy beaches and backbarrier tidal flats, *Estuarine, Coastal and Shelf Science*, 159, 1-14, <http://dx.doi.org/10.1016/j.ecss.2015.03.025>.
- Robinson, C., B. Gibbes, and L. Li (2006), Driving mechanisms for groundwater flow and salt transport in a subterranean estuary, *Geophys. Res. Lett.*, 33, L03402, doi:10.1029/2005GL025247.
- Roy, M., J. B. Martin, J. Cherrier, J. E. Cable, and C. G. Smith (2010), Influence of sea level rise on iron diagenesis in an east Florida subterranean estuary, *Geochimica et Cosmochimica Acta*, 74(19): 5560-5573, <https://doi.org/10.1016/j.gca.2010.07.007>.
- Roy, M., J. B. Martin, J. E. Cable, and C. G. Smith (2013), Variations of iron flux and organic carbon remineralization in a subterranean estuary caused by inter-annual variations in recharge, *Geochimica et Cosmochimica Acta*, 103, 301-315. <https://doi.org/10.1016/j.gca.2012.10.055>.
- Rusch, A. and M. Huettel (2000), Advective particle transport into permeable sediments—evidence from experiments in an intertidal sandflat, *Limnology and Oceanography*, 45(3), 525-533, <https://doi.org/10.4319/lo.2000.45.3.0525>.
- Rusch, A., M. Huettel, and S. Forster (2000), Particulate organic matter in permeable marine sands—dynamics in time and depth, *Estuarine, Coastal and Shelf Science*, 51(4), 399-414.

- Seidel, M., M. Beck, T. Riedel, H. Waska, I. G. Suryaputra, B. Schnetger, J. Niggemann, M. Simon, and T. Dittmar (2014), Biogeochemistry of dissolved organic matter in an anoxic intertidal creek bank, *Geochimica et Cosmochimica Acta*, 140, 418-434, <https://doi.org/10.1016/j.gca.2014.05.038>.
- Seidel, M., M. Beck, J. Greskowiak, T. Riedel, H. Waska, I. G. N. A. Suryaputra, B. Schnetger, J. Niggemann, M. Simon, and T. Dittmar (2015), Benthic-pelagic coupling of nutrients and dissolved organic matter composition in an intertidal sandy beach, *Marine Chemistry*, 176, 150-163, <http://dx.doi.org/10.1016/j.marchem.2015.08.011>.
- Slomp, C. P., and P. Van Cappellen (2004), Nutrient inputs to the coastal ocean through submarine groundwater discharge: controls and potential impact. *Journal of Hydrology*, 295(1), 64-86, <http://dx.doi.org/10.1016/j.jhydrol.2004.02.018>.
- Spiteri, C., C. P. Slomp, K. Tuncay, and C. Meile (2008a), Modeling biogeochemical processes in subterranean estuaries: Effect of flow dynamics and redox conditions on submarine groundwater discharge of nutrients, *Water Resources Research*, 44(2), doi:10.1029/2007WR006071.
- Spiteri, C., C. P. Slomp, M. A. Charette, K. Tuncay, and C. Meile (2008b), Flow and nutrient dynamics in a subterranean estuary (Waquoit Bay, MA, USA): Field data and reactive transport modeling, *Geochim. Cosmochim. Acta*, 72(14): 3398–3412, doi:10.1016/j.gca.2008.04.027.
- Ullman, W. J., B. Chang, D. C. Miller, and J. A. Madsen (2003), Groundwater mixing, nutrient diagenesis, and discharges across a sandy beachface, Cape Henlopen, Delaware (USA), *Estuarine, Coastal and Shelf Science*, 57(3), 539-552, [http://dx.doi.org/10.1016/S0272-7714\(02\)00398-0](http://dx.doi.org/10.1016/S0272-7714(02)00398-0).
- Valiela, I., J. McClelland, J. Hauxwell, P.J. Behr, D. Hersh, and K. Foreman (1997), Macroalgal blooms in shallow estuaries: Controls and ecophysiological and ecosystem consequences. *Limnology and Oceanography*, 42(5/2): 1105–1118, https://doi.org/10.4319/lo.1997.42.5_part_2.1105.
- van der Meulen, F., T. W. M. Bakker, and J. A. Houston (2004), The costs of our coasts: examples of dynamic dune management from Western Europe, In *Coastal Dunes: Ecology and Conservation* (259-278), Berlin: Springer-Verlag.
- Vandenbohede, A. and L. Lebbe (2006), Occurrence of salt water above fresh water in dynamic equilibrium in a coastal groundwater flow system near De Panne, Belgium, *Hydrogeology Journal*, 14(4): 462-472, doi: 10.1007/s10040-005-0446-5.

- Vitousek, P.M., J. D., Aber, R W. Howarth, G. E. Likens, P. A. Matson, D. W. Schindler, W. H. Schlesinger, and D. G. Tilman (1997), Human alteration of the global nitrogen cycle: sources and consequences, *Ecological applications*, 7(3), 737-750, [https://doi.org/10.1890/1051-0761\(1997\)007\[0737:HAOTGN\]2.0.CO;2](https://doi.org/10.1890/1051-0761(1997)007[0737:HAOTGN]2.0.CO;2).
- Zarnetske, J. P., R. Haggerty, S. M. Wondzell, V. A. Bokil, and R. González-Pinón (2012), Coupled transport and reaction kinetics control the nitrate source-sink function of hyporheic zones, *Water Resources Research*, 48, 1–15, <https://doi.org/10.1029/2012WR011894>.

Chapter 5

CONCLUSIONS

These studies focus on the spatiotemporal dynamics of biogeochemical reactions within the intertidal zone of a beach aquifer, controlled by fresh-saline groundwater mixing and reactant delivery.

Results from field sampling, laboratory experiments, and numerical models show the complex and dynamic relationship between biogeochemical reactions within the beach aquifer. Field and laboratory methods investigated the relationship between spatial patterns of reaction rates and dynamic distributions of reactants (oxygen, nitrate, carbon) in response to transient hydrology. Divergent transport between particulate (POC) and dissolved organic carbon (DOC) was found to deviate reaction and nutrient distribution patterns from concurrent groundwater flowpaths. Numerical modeling was used to further examine the biogeochemical impacts within beach aquifers of particulate carbon transport divergent from that of aqueous solutes and identified conditions that increase the relative contributions of POC to biogeochemical transformations in beach sediments. These studies collectively illustrate the complex interplay between hydrologic transience, reactant delivery and transport, and sediment-hosted biogeochemical reactions.

5.1 Spatial Characteristics of Beach Aquifer Reactions

The infiltration of saline seawater onto the seaward-discharging fresh groundwater creates an intertidal circulation cell in coastal aquifers. Seawater delivers

oxygen and reactive marine carbon into the beach aquifer, two key reactants that are otherwise depleted in fresh groundwater. Fresh groundwater is often elevated in nutrients such as nitrate, which can serve as alternative electron acceptors during carbon remineralization after oxygen has been depleted.

Groundwater flowpaths control the delivery and movement of these reactants within the aquifer. Reaction rates for aerobic respiration and denitrification were spatially correlated to patterns of groundwater flow. Aerobic respiration rates were highest near the point of seawater infiltration and along the groundwater flowpath in the landward freshwater-seawater interface. Conversely, nitrogen gas production rates along the freshwater-seawater mixing zone increased towards the discharge point. High aerobic respiration rates did not correspond to elevated concentrations of particulate organic carbon and chlorophyll, indicating that aerobic respiration is limited by the presence of O₂ rather than carbon.

The intertidal circulation cell is highly dynamic in time and space, responding to various hydrologic factors such as freshwater flux, tidal amplitude, and tidal stage. Reaction rates and biogeochemical patterns within the intertidal zone, controlled by reactant delivery, are therefore equally dynamic in time and space as patterns of groundwater flow change. Although the spatial extent and geometry of the intertidal circulation cell shifts due to seasonal hydrologic changes, aerobic respiration rates were consistently elevated along the landward freshwater-seawater interface. This highlights the link between physical patterns of groundwater flow, reactant transport, and reaction rates within the beach aquifer.

5.2 Reactive Particulate Organic Carbon Dynamics within Beach Aquifers

Unlike aerobic respiration rates that were spatially coupled to oxic seawater infiltration, distributions of denitrification, phosphate, and dissolved organic carbon were less coupled to groundwater flow patterns. This deviation was due to the distribution of particulate organic carbon (POC) within the aquifer, which was retarded in its movement relative to groundwater advection.

POC and other mobile solutes (oxygen, salt) were delivered to the aquifer by infiltrating seawater. Once delivered, the POC was mobile within the sediments, responding to groundwater flow. However, due to flow retardation, filtration, and entrapment, elevated pools of POC formed in various locations that did not necessarily correspond to concurrent groundwater flowpaths. This spatially-variable distribution of POC contributed to the deviation between biogeochemical activity and hydrologic flow patterns, by actively supporting biogeochemical transformations and leaching other nutrients (nitrogen, dissolved organic carbon, phosphate). As hydrologic conditions change and mobile solutes move relative to the pool of POC, there are distinct changes in the biogeochemical patterns. This highlights that particulate forms of carbon, while often ignored in previous studies of beach biogeochemistry, are also important contributors to the bulk biogeochemical reactivity of beach sediment systems.

5.3 Particulate Carbon Contributions to Beach Biogeochemical Reactions

A numerical variable-density, groundwater flow model with a retardation factor simulated various distributions of POC pools within the intertidal zone. The POC supported aerobic respiration and denitrification within the beach aquifer,

producing CO₂ and N₂ which traveled with groundwater flow towards the discharge zone.

Because the less mobile POC pool had to spatially coincide with inflow of NO₃⁻-rich, anoxic water to support denitrification, the spatial relationship between the extent of the POC pool and the saline circulation cell (controlling the location of the freshwater-saltwater mixing zone) was central to the viability of such redox reactions. Greater retardation of POC transport promoted a more expansive distribution of the POC pool. Compared to cases with a lower retardation factor, this wider areal distribution of POC lead to increased nitrate removal. Similarly, a higher tidal amplitude during POC deposition increased the spatial extent of POC distribution and thereby promoted increased nitrate removal.

Conditions that allowed smaller saline circulation cells further increased the utilization of POC by increasing the contact area between POC and fresh groundwater. Higher hydraulic conductivity, higher tidal amplitudes, and larger range of freshwater fluctuations increased the geometrical transience of the saline circulation cell, increasing the contribution of POC to overall beach sediment reactivity.

Pools of POC resulting from retarded transport relative to groundwater are important contributors to beach biogeochemical reactions. Due to transient hydrologic patterns and its intermittent usage, POC increases spatial variations in reaction zone dynamics within intertidal zones of coastal aquifers.

5.4 Implications

Biogeochemical reactions in the intertidal zone of coastal aquifers control the fluxes of solutes to the marine system, by transforming terrestrial nutrients or altering the redox conditions. Therefore, these reactions directly impact the health of coastal

environments [Slomp and Van Cappellen, 2004]. Groundwater mixing patterns in the intertidal zone of coastal aquifers are highly dynamic in time and space, responding to various hydrologic factors such as freshwater flux, spring-neap cycles, and seasonal tidal amplitude variations, and climate [Heiss and Michael, 2014]. In turn, the biogeochemical reactions that occur as a result of freshwater-seawater mixing are also highly dynamic. This makes quantifying the reactions in time and space difficult, as reaction location and magnitudes are constantly altered over time. While site-specific field investigations are useful, they are often limited to the distinct hydrologic characteristics found at the site. Therefore, linkages between different processes must be explored to increase the applicability of site-specific field measurements to more global problems. This study, by showing the linkages between groundwater flow, reactant transport, and reaction rates, takes a critical step toward constraining beach reaction characteristics in space and time.

Sandy shorelines are found in 16% of the coastal areas [Burke et al., 2001; Martínez et al., 2007], and fresh groundwater discharge along the contiguous U.S. coastline is universal [Sawyer et al., 2016]. While specifics of groundwater flow [Evans and Wilson, 2016; Heiss and Michael, 2014], carbon retardation, carbon reactivity [Heiss et al., 2017], and reactant (dissolved/particulate carbon, oxygen, nitrate, etc.) concentrations [Anwar et al., 2014; Buesen et al., 2013] are expected to vary across sites, the relationship between groundwater flowpaths and aerobic respiration rates is likely to endure. Reactions intermittently supported by particulate organic carbon within beach systems provide key insight to interpreting diverging physical and chemical characteristics. Further, while this study primarily focused on the movement and distributions of particulate organic carbon and its impact on mobile

nitrate, it can analogously serve as an example for any setting or reaction that involves reactants that move at different rates. Such reactions include the movement and degradation of BTEX [Robinson et al., 2009], hydrocarbons [Geng et al., 2015], and bacteria [Gast et al., 2015]. This study, using interdisciplinary approaches, demonstrates the oxygen- and carbon-dependent characteristics of beach reactions and indicates a system that is more reactive, dynamic, and incongruous with salinity than previous thought.

5.5 Recommendations for Future Work

Many research questions concerning the spatiotemporal characteristics of beach biogeochemical reactions remain unanswered. Further studies of: 1) carbon characteristics, 2) particle transport 3) geologic heterogeneity, 4) reaction transience, 5) beach typology, and 6) climate change and human interactions, will be needed to more fully describe the contrasting patterns of groundwater flow and biogeochemical reactions.

The approaches used to characterize reactive organic carbon were overly simplistic in this study, treating carbon as only two forms and assuming similar reactivity between them. Refractory terrestrial organic carbon was disregarded. However, carbon delivered to the intertidal system from both terrestrial and marine sources are highly diverse in its molecular structure and complexity [Seidel et al., 2015], and therefore would display a wide range of reactivity. Integrating advanced information on the reactivity, nutrient leaching, and sorption behavior of carbon will help constrain the large range of carbon-related parameters and denitrification efficiency presented in Chapter 4. Further, understanding the reactivity difference

between POC, seawater DOC, and leached DOC from *in-situ* POC will allow better constraints on the relative contributions of POC in a hydrologically transient system.

Particulate transport dynamics within beach aquifers over various timescales may be further explored. This information will serve to improve the simulations presented in Chapter 4 to better reflect the proposed transport processes in Chapter 3. Vast literature exists in particle transport within porous media [El-Farhan et al., 2000; Gast et al., 2015; McDowell-Boyer et al., 1986; Pronk et al., 2009], as well as on colloidal and bacterial behavior [Bradford et al., 2003; de Siewes et al., 2016; Harter et al., 2000; Johnson et al., 1996; Ryan and Gschwend, 1990]. POC occurs in various size and reactivity fractions, and therefore will display far more complex transport dynamics and heterogeneous distributions than depicted in this study. How changing hydrologic vectors influence and control POC transport within the aquifer is a critical question that would benefit from further efforts at quantification.

Both particulate and dissolved reactant transport are undoubtedly controlled by groundwater flowpaths, which are direct functions of geologic heterogeneity. While field sediment sampling in Chapter 3 indicated that Cape Shores had interfingering of high-K layers with lower-K layers, the aquifer was mostly homogeneous and POC distributions did not correlate with grain size. However, in highly heterogeneous systems, the filtration and retardation effect of POC would be heightened, increasing spatial variability of POC pools. Further, as flowpaths change due to the heterogeneous K-field, the flowpaths and residence times of mobile reactants would be altered in turn. As shown in Chapter 4, changes to hydraulic conductivity and residence times modify the Damköhler value for a given location accordingly. Even if chemical reaction rates are constant, some beach conditions with varying geologic

heterogeneity have the potential to drive an advection-limited system ($Da > 1$) to a rate-limited system ($Da < 1$). More work is needed in heterogeneous systems, both modeled and real, to understand how geologic configurations alter the distributions and asynchronous movements of particulate and dissolved reactants.

Similarly, the applicability of this study would be greatly increased when repeated across various beaches spanning different typologies and topographies. The extent and geometry of the saline circulation cell is dependent on beach slope and other aquifer properties [Evans and Wilson, 2016; Heiss and Michael, 2014; Reckhardt et al., 2015], which in turn would alter groundwater flow patterns and reaction characteristics [Heiss et al., 2017]. Beach configurations that allow increased lateral movement of the circulation cell and faster groundwater flowrate would increase the relative contributions of POC over time, while tidal flats with finer sands may display less divergence between biogeochemistry and groundwater flow due to slower flowrates. Investigating the biogeochemical characteristics in rocky beaches, mangroves, and coastal lagoons are areas for potential expansion of this study.

In addition to hydrologic transience, biogeochemical conditions and end-member concentrations are also dynamic in time. While models presented in Chapter 4 used a constant POC distribution, end-member concentrations, and reaction rates over model time, all of these variables are temporally dynamic in natural environmental settings. Distributions of POC and mobile reactants are spatially variable over time, influenced by changing hydrology. Concentration and infiltration rates of POC and DOC also vary depending on seasonal primary productivity, while biogeochemical reaction rates are influenced by ambient temperature and stage of degradation. Therefore, incorporating the transience of biogeochemical conditions over various

timescales would improve our understanding of the intertidal beach system. High-frequency (15 minutes) field measurements of redox conditions and salinity at Cape Shores show rapid, asynchronous fluctuations in both redox and salinity conditions at a given location. This further indicates that a better constraint of the relationships between hydrological and biogeochemical conditions will be necessary in finer timescales.

Lastly, how these sandy beach systems evolve with climate change, rising sea-levels, and increased frequency of extreme climate events is a major frontier that must be explored. Warmer ocean conditions alter not only the temperature of the infiltrating seawater, but also its pH, gas dissolution capacity, and primary production potential. As sea-level encroaches the coastline, the width and extent of the beach where reactions are hosted decreases. Also, extreme events such as storms and tsunamis have the potential to quickly alter the salt, oxygen, and carbon flux into the aquifer, leading to lasting changes to beach biogeochemistry. It is further recommended that the results of this study be reassessed in a beach system with high human activity. Beach restoration and management practices differ, due to reasons recreational, economical, ecological, or political. A long-term observational study of shifts in biogeochemical reactions at a site with frequent human interactions of various forms may be useful to determine how changes to coastal aquifers, climatic or anthropogenic, will impact the overall patterns of reactions and ultimately the health of coastal environments.

Biogeochemical reactions within beach aquifers are contingent on various chemical, geological, and hydrological factors, and are highly variable in time and space. Constraining the relationship between these interconnected processes is critical to accurately quantifying coastal solute concentrations along its flowpath, and

preserving marine ecosystems. In current times of intensified coastal activity and progressive climate change, it is imperative that these relationships are well-defined for versatile applications across diverse beach aquifer settings.

REFERENCES

- Anwar, N., C. Robinson, and D. A. Barry (2014), Influence of tides and waves on the fate of nutrients in a nearshore aquifer: Numerical simulations, *Advances in Water Resources*, 73, 203-213, <http://dx.doi.org/10.1016/j.advwatres.2014.08.015>.
- Beusen, A.H.W., C. P. Slomp, and A. F. Bouwman (2013), Global land–ocean linkage: direct inputs of nitrogen to coastal waters via submarine groundwater discharge, *Environmental research letters*, 8(3): 034035, doi:10.1088/1748-9326/8/3/034035.
- Bradford, S. A., J. Simunek, M. Bettahar, M. van Genuchten, and S. R. Yates (2003), Modeling colloid attachment, straining, and exclusion in saturated porous media, *Environmental Science & Technology*, 37(10): 2242-2250, doi:10.1021/es025899u.
- Burke, L., Y. Kura, K. Kassem, C. Revenga, M. Spalding, D. McAllister, and J. Caddy (2001), *Coastal ecosystems*, Washington, DC: World Resources Institute.
- de Sieyes, N. R., T. L. Russell, K. I. Brown, S. K. Mohanty, and A. B. Boehm (2016), Transport of enterococci and F+ coliphage through the saturated zone of the beach aquifer, *Journal of Water and Health*, 14(1): 26-38, <https://doi.org/10.2166/wh.2015.290>.
- El-Farhan, Y.H., N.M. DeNovio, J.S. Herman, and G.M. Hornberger (2000), Mobilization and transport of soil particles during infiltration experiments in an agricultural field, Shenandoah Valley, Virginia, *Environmental science & technology*, 34(17), 3555-3559, doi: 10.1021/es991099g.
- Evans, T. B. and A. M. Wilson (2016), Groundwater transport and the freshwater–saltwater interface below sandy beaches, *Journal of hydrology*, 538: 563-573, <https://doi.org/10.1016/j.jhydrol.2016.04.014>.
- Gast, R.J., S. Elgar, and B. Raubenheimer (2015), Observations of transport of bacterial-like microspheres through beach sand, *Continental Shelf Research*, 97, 1-6, <https://doi.org/10.1016/j.csr.2015.01.010>.

- Geng, X., M. C. Boufadel, K. Lee, S. Abrams, and M. Suidan (2015), Biodegradation of subsurface oil in a tidally influenced sand beach: Impact of hydraulics and interaction with pore water chemistry, *Water Resources Research*, 51(5): 3193-3218, [dx.doi.org/10.1002/2014WR016870](https://doi.org/10.1002/2014WR016870).
- Harter, T., S. Wagner, and E. R. Atwill (2000), Colloid transport and filtration of *Cryptosporidium parvum* in sandy soils and aquifer sediments, *Environmental Science & Technology*, 34(1): 62-70, doi: 10.1021/es990132w.
- Heiss, J. W., and H. A. Michael (2014), Saltwater-freshwater mixing dynamics in a sandy beach aquifer over tidal, spring-neap, and seasonal cycles, *Water Resour. Res.*, 50, 6747–6766, doi:10.1002/2014WR015574.
- Heiss, J. W., V. E. Post, T. Laattoe, C. J. Russoniello, and H. A. Michael (2017), Physical controls on biogeochemical processes in intertidal zones of beach aquifers, *Water Resources Research*, 53(11), 9225-9244, <https://doi.org/10.1002/2017WR021110>.
- Johnson, P. R., N. Sun, and M. Elimelech (1996), Colloid transport in geochemically heterogeneous porous media: Modeling and measurements, *Environmental Science & Technology*, 30(11): 3284-3293, doi: 10.1021/es960053+.
- Martínez, M. L., A. Intralawan, G. Vázquez, O. Pérez-Maqueo, P. Sutton, and R. Landgrave (2007), The coasts of our world: Ecological, economic and social importance, *Ecological Economics*, 63(2-3), 254-272, <https://doi.org/10.1016/j.ecolecon.2006.10.022>.
- McDowell-Boyer, L.M., J.R. Hunt, and N. Sitar, (1986), Particle transport through porous media, *Water Resources Research*, 22(13), 1901-1921, <https://doi.org/10.1029/WR022i013p01901>.
- Pronk, M., N. Goldscheider, J. Zopfi, and F. Zwahlen (2009), Percolation and particle transport in the unsaturated zone of a karst aquifer, *Groundwater*, 47(3), 361-369, <https://doi.org/10.1111/j.1745-6584.2008.00509.x>.
- Reckhardt, A., M. Beck, M. Seidel, T. Riedel, A. Wehrmann, A. Bartholomä, and H. J. Brumsack (2015), Carbon, nutrient and trace metal cycling in sandy sediments: A comparison of high-energy beaches and backbarrier tidal flats, *Estuarine, Coastal and Shelf Science*, 159, 1-14, <http://dx.doi.org/10.1016/j.ecss.2015.03.025>.
- Robinson, C., A. Brovelli, D.A. Barry, and L. Li (2009), Tidal influence on BTEX biodegradation in sandy coastal aquifers, *Advances in Water Resources*, 32(1), 16–28, doi:10.1016/j.advwatres.2008.09.008.

- Ryan, J. N., and P. M. Gschwend (1990), Colloid mobilization in two Atlantic Coastal Plain aquifers: Field studies, *Water Resources Research*, 26(2): 307-322, <https://doi.org/10.1029/WR026i002p00307>.
- Sawyer, A. H., David, C. H., and J. S. Famiglietti (2016), Continental patterns of submarine groundwater discharge reveal coastal vulnerabilities, *Science*, 353(6300): 705-707, [10.1126/science.aag1058](https://doi.org/10.1126/science.aag1058).
- Seidel, M., M. Beck, J. Greskowiak, T. Riedel, H. Waska, I. G. N. A. Suryaputra, B. Schnetger, J. Niggemann, M. Simon, and T. Dittmar (2015), Benthic-pelagic coupling of nutrients and dissolved organic matter composition in an intertidal sandy beach, *Marine Chemistry*, 176, 150-163, <http://dx.doi.org/10.1016/j.marchem.2015.08.011>.
- Simmons, G. M. (1992), Importance of submarine groundwater discharge (SGWD) and seawater cycling to material flux across the sediment/water interfaces in marine environments, *Mar. Ecol. Prog. Ser.*, 84, 173–184.
- Slomp, C. P., and P. Van Cappellen (2004), Nutrient inputs to the coastal ocean through submarine groundwater discharge: controls and potential impact. *Journal of Hydrology*, 295(1), 64-86, <http://dx.doi.org/10.1016/j.jhydrol.2004.02.018>.

Appendix A

SUPPLEMENTARY MATERIALS FOR CHAPTER 2

This document includes Table A-1, table with field and laboratory data used for the main text.

Table A-1. Data from the Cape Shores, Lewes, DE site, collected 08 and 10 September 2014. Data is organized by multi-level porewater sampler locations (A~G, refer to Figure 2.1), numbered by depth. x indicates distance from benchmark, y height above mean sea level. Abbreviated parameters are as follows: oxidation-reduction potential (ORP), dissolved oxygen (DO), particulate carbon (PC), dissolved inorganic carbon (DIC), particulate nitrogen (PN), and particulate phosphorus (PP). Refer to Section 2. Methods for details on data collection.

Port	x (m)	y (m)	Salinity	pH	ORP (mV)	DO (%)	Chloro phyll- <i>a</i> (µg/L)	PC (mg/L)	DIC (µmol/kg sw)
A-1	128.4	-0.5	1.23	7.62	74.20	3.66	0.51	0.03	1190.10
A-2	128.4	-1.2	21.63	6.83	103.60	12.15	0.41	0.03	1435.85
A-3	128.4	-2.0	22.39	6.70	101.00	9.70	0.07	0.08	1576.82
B-1	136.5	-0.2	11.64	6.87	85.40	2.39	0.13	0.02	1881.72
B-2	136.5	-1.5	0.94	8.42	52.40	9.27	0.04	0.01	1064.61
B-3	136.5	-2.6	11.54	7.16	102.50	3.65	0.25	0.03	1124.01
C-1	142.4	-0.4	12.66	7.76	37.80	33.48	0.03	0.02	1934.03
C-2	142.4	-1.2	13.22	7.57	16.70	3.35	0.14	0.02	1767.89
C-3	142.4	-2.0	15.83	7.11	31.90	2.12	0.10	0.03	1690.34
C-4	142.4	-2.8	13.11	6.79	19.10	1.68	0.25	0.03	1378.09
D-1	148.3	-0.6	29.00	7.51	81.70	77.42	0.21	0.02	2042.92
D-2	148.3	-1.4	28.16	7.46	76.00	52.90	0.64	0.03	2082.42
D-3	148.3	-2.2	19.99	7.42	74.00	7.30	0.64	0.04	2081.94
D-4	148.3	-3.0	17.73	7.50	78.10	5.72	0.09	0.04	2058.35
E-1	152.1	-1.0	29.34	7.55	52.60	81.37	0.37	0.03	2065.55
E-2	152.1	-1.6	28.85	7.35	37.70	7.47	2.00	0.07	2041.17
E-3	152.1	-2.3	27.62	7.14	23.20	7.39	52.90	0.11	2025.52
E-4	152.1	-3.1	25.68	7.09	42.80	4.60	0.90	0.22	2042.24
E-5	152.1	-3.8	14.32	7.05	17.30	4.70	3.42	0.03	1471.26
F-1	158.6	-2.5	23.37	7.12	-6.10	16.55	1.78	0.27	1917.81
F-2	158.6	-4.0	6.47	7.26	-63.10	4.87	1.64	0.03	1727.89
G-1	161.6	-1.2	7.07	6.88	-49.20	4.67	0.07	0.05	2036.10
G-2	161.6	-1.8	7.99	6.89	-52.00	3.43	1.26	0.04	1874.52
G-3	161.6	-2.5	7.89	7.05	-44.90	0.46	0.18	0.07	1756.28
G-4	161.6	-3.3	12.05	7.16	-52.40	4.05	0.36	0.02	1731.34
G-5	161.6	-4.0	6.06	7.60	-76.80	4.46	0.54	0.03	1951.20

Table A-1 continued.

Port	O ₂ consumption ($\mu\text{M}/\text{d}$)	N ₂ production ($\mu\text{M}/\text{d}$)	NO ₃ ⁻ (μM)	NH ₄ ⁺ (μM)	PN (mg/L)	PP (μM)	PO ₄ ³⁻ (μM)	Si (μM)
A-1	2.47	0.01	44.73	0.36	0.0049	7.68	6.07	51.87
A-2	1.15	0.00	52.63	0.71	0.0062	55.16	8.06	122.75
A-3	0.00	0.00	20.00	0.93	0.0098	2.51	1.13	76.09
B-1	0.49	0.08	38.71	0.29	0.0040	4.63	5.74	107.30
B-2	0.00	0.00	20.21	0.57	0.0034	9.20	1.08	61.82
B-3	0.00	0.00	19.19	0.64	0.0056	6.35	4.26	55.43
C-1	3.13	0.05	177.35	0.29	0.0034	1.72	3.62	79.64
C-2	1.86	0.03	8.01	1.79	0.0040	7.48	5.40	110.06
C-3	0.59	0.05	0.11	3.29	0.0054	7.48	6.05	77.05
C-4	1.16	0.04	8.47	2.21	0.0040	3.44	3.34	70.55
D-1	0.00	0.00	24.84	0.50	0.0029	5.36	3.65	38.52
D-2	0.00	0.00	58.30	0.21	0.0037	8.47	3.90	69.53
D-3	3.63	0.12	82.24	2.71	0.0065	11.45	3.64	75.37
D-4	0.91	0.00	64.20	0.29	0.0045	5.42	3.34	74.19
E-1	2.12	0.02	92.80	0.29	0.0054	6.95	2.77	20.13
E-2	0.00	0.00	20.63	0.29	0.0114	15.42	2.26	41.85
E-3	0.00	0.00	5.97	0.46	0.0218	18.07	0.81	39.52
E-4	2.56	0.00	12.96	0.64	0.0287	11.45	0.23	50.40
E-5	1.15	0.04	0.12	1.50	0.0049	16.28	2.05	68.91
F-1	0.00	0.00	0.15	2.36	0.0351	10.99	2.15	78.80
F-2	0.31	0.19	0.09	24.90	0.0078	10.59	0.07	52.24
G-1	0.18	0.00	0.14	36.40	0.0107	8.67	0.76	59.30
G-2	0.20	0.00	0.09	37.10	0.0086	22.58	0.29	55.53
G-3	0.45	0.00	0.14	26.90	0.0151	4.43	0.99	54.89
G-4	0.14	0.19	0.25	11.70	0.0045	5.16	1.65	58.73
G-5	0.84	0.00	0.10	6.29	0.0042	5.69	5.60	64.64

Appendix B

SUPPLEMENTARY MATERIALS FOR CHAPTER 3

This document includes supporting table for sediment grainsize analysis and oxygen consumption rates for vibracore samples, and supporting figure for dissolved silica production.

Table B-1. Grainsize, D10 grainsize (10% percentile particle diameter), organic matter content, and oxygen consumption rates for Core C and Core F samples from July 2015 (location highlighted in Figure 3.3). Grainsize description from: Folk, R. L., and W. C. Ward [1957], Brazos River bar (Texas); a study in the significance of grain size parameters, *Journal of Sedimentary Research*, 27(1), 3-26, <https://doi.org/10.1306/74D70646-2B21-11D7-8648000102C1865D>.

Core	Section	Depth [cm]	Mean grainsize ^a [μm]	D10 grainsize [μm]	Organic matter content [mg OM / g sed]	Oxygen consumption rates [ΔO ₂ μM/d]	Color	Description ^b
C	1	0-24	579.8	292.6	3.33	9.23	Light brown	Coarse sand
	2	25-74	579.3	294.9	2.55	29.35	Light brown with black coating	Coarse sand
	3	75-88	942.1	360.7	4.02	28.52	Light brown	Coarse sand
	4	89-110	334.5	195.1	1.95	31.95	Light brown	Medium sand
F	1	0-31	1046.6	294.7	3.43	39.10	Light brown	Very coarse
	2	32-63	508.4	245.6	3.73	34.29	Transition zone between light brown sand to black silt, Fe-oxides	Coarse sand
	3	64-113	238.4	128.4	7.00	77.90	Black	Fine sand
	4	114-192	295.9	197.8	4.01	65.19	Grayish black	Medium sand

^aFolk and Ward [1957] grainsize ^bFolk and Ward [1957] mean description

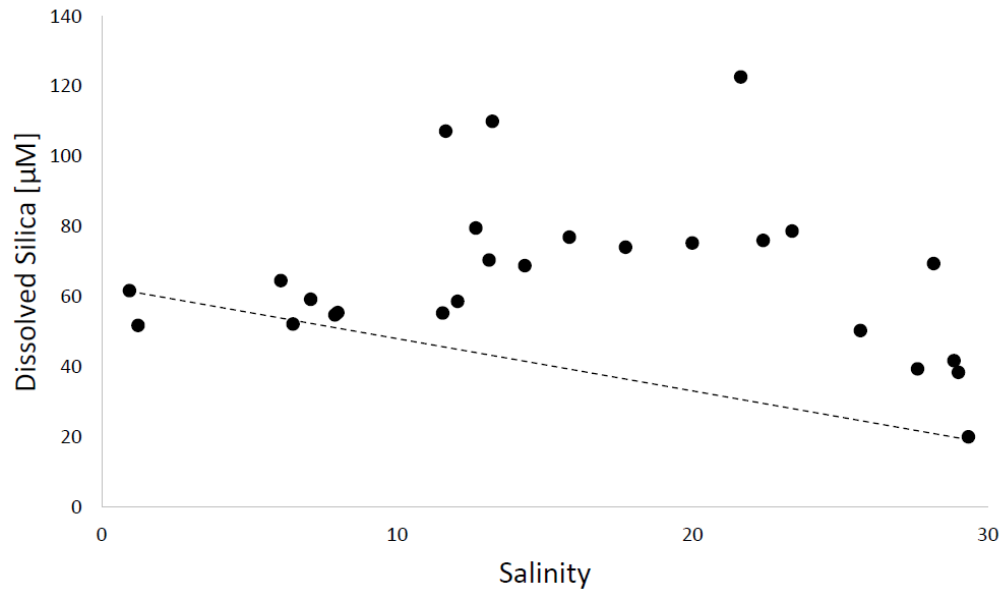


Figure B-1. Salinity vs. Dissolved Silica for September 2014. Silica production via dissolution occurs over a range of higher salinities.

Appendix C

SUPPLEMENTARY MATERIALS FOR CHAPTER 4

This document includes Table C-1, table of tidal constituents used for fully transient circulation cell case, and Table C-2, table of parameters used to calculate the retardation factor. Text explains the retardation factor and justifies the parameters used in the calculating retardation.

Table C-1. Tidal constituents used for fully transient circulation cell case.

Name	Amplitude (m)	Phase (rad)	Frequency (rad s ⁻¹)	Description
M ₂	0.616	0.543	1.41 × 10 ⁻⁴	Principle lunar semidiurnal
S ₂	0.108	0.991	1.45 × 10 ⁻⁴	Principle solar semidiurnal
N ₂	0.134	0.185	1.38 × 10 ⁻⁴	Larger lunar elliptic semidiurnal
K ₁	0.103	3.520	7.29 × 10 ⁻⁵	Lunar diurnal
O ₁	0.083	2.073	6.75 × 10 ⁻⁵	Lunar diurnal

Table C-2. Parameters used for retardation equation. $K_d = 0.1$ is used in the base case simulation, but is varied across cases to increase the retardation factor.

Parameter	Description and source	Value	Units
ρ_b	Bulk density of sand aquifer, average value measured from vibrocore sediment samples	1.25	g/cm ³
θ	Porosity, Heiss and Michael (2014)	0.3	unitless
K_d	Distribution coefficient, average ratio of particulate to dissolved organic carbon from July 2015 porewater samples.	0.1	cm ³ /g

The retardation factor is a measure of the groundwater velocity relative to the velocity of the retarded constituent (Krupka, 1999; Davis, 2000). In this paper, the retardation factor of 1.416 therefore indicates that groundwater is moving 1.416 times faster than the particulate organic carbon. While the bulk density and porosity used in the retardation equation was easily obtained empirically, estimation of K_d values are not as straightforward. EPA (Krupka, 1999) defines K_d to be a ratio between a chemical's sorbed concentration (mg/kg) to the dissolved concentration (mg/L). K_d is often estimated via batch or flow-through tests in the laboratory, where a solute spiked with a contaminant of interest is forced through a porous medium, and quantified for

adsorbed fractions (Krupka, 1999). However, because the retarded movement of porewater POC in the beach aquifer is not strictly analogous to such movements of organic contaminants, we used previous field measurements of POC (Kim et al., 2017 & 2019) to estimate K_d . *In-situ* concentrations of POC near the infiltration zone was compared with surface water POC. Fraction of POC found in-situ was taken to be the solid, “adsorbed” fraction, and the remaining was assumed to behave like dissolved carbon, moving with porewater and transported out of its original infiltration location. Near-surface sampling locations often had up to 10% of the surface water POC, resulting in a K_d of 0.1.

The other method to approximate K_d could be by comparing the ratio between POC and leached DOC at a given location. Within the aquifer, POC leached DOC to the adjacent porewater, elevating DOC concentrations beyond surface water DOC values. The ratio between POC and leached DOC could also be representative of a K_d value, as the POC would stay immobile while the produced DOC in the adjacent porewater represents the mobile portion of organic carbon associated with this pool of POC. In areas with active leaching (or degradation of POC to become more mobile and “dissolved”), 1 mg/L of POC was associated to up to 5-8 mg/L of excess DOC beyond surface water DOC. This yields a K_d range of 0.125~0.2, similar to the K_d estimation obtained from the above method.

A sensitivity test using a wide range of R (1-30) showed that while resulting concentrations of retarded solute within the aquifer varied between model cases, the distribution pattern remained similar overall. Because the resulting solute concentrations from SEAWAT were scaled to match field values of POC, the absolute value of R used in simulations did not therefore have a large bearing on model results

that explore the biogeochemical contributions of retarded POC. In environmental settings, due to geologic heterogeneity, sorption behavior, and filtration / transport dynamics, the retardation factor for POC is expected to be a range of values along a flowpath rather than one set value. However, limitations notwithstanding, the retardation factor used in the paper is adequate in describing the delayed transport of POC relative to seawater.

Appendix D

COPYRIGHT INFORMATION

Chapter 2 is reproduced with permission from Kim, K. H., J. W. Heiss, H. A. Michael, W. Cai, T. Laattoe, V. E. A. Post, and W. J. Ullman (2017), Spatial patterns of groundwater biogeochemical reactivity in an intertidal beach aquifer, *Journal of Geophysical Research: Biogeosciences*, 122, 2548-2562, doi: 10.1002/2017JG003943.

JOHN WILEY AND SONS LICENSE
TERMS AND CONDITIONS

Feb 25, 2019

This Agreement between Kyra H. Kim ("You") and John Wiley and Sons ("John Wiley and Sons") consists of your license details and the terms and conditions provided by John Wiley and Sons and Copyright Clearance Center.

License Number	4536111216828
License date	Feb 25, 2019
Licensed Content Publisher	John Wiley and Sons
Licensed Content Publication	Journal of Geophysical Research: Biogeosciences
Licensed Content Title	Spatial Patterns of Groundwater Biogeochemical Reactivity in an Intertidal Beach Aquifer
Licensed Content Author	Kyra H. Kim, James W. Heiss, Holly A. Michael, et al
Licensed Content Date	Oct 17, 2017
Licensed Content Volume	122
Licensed Content Issue	10
Licensed Content Pages	15
Type of use	Dissertation/Thesis
Requestor type	Author of this Wiley article
Format	Print and electronic
Portion	Full article
Will you be translating?	No
Title of your thesis / dissertation	SPATIOTEMPORAL DYNAMICS OF BIOGEOCHEMICAL REACTIONS IN AN INTERTIDAL BEACH AQUIFER: A FIELD, LABORATORY, AND NUMERICAL MODELING STUDY
Expected completion date	Aug 2019
Expected size (number of pages)	200
Requestor Location	Kyra H. Kim 700 Pilottown Rd LEWES, DE 19958 United States Attn: Kyra H. Kim
Publisher Tax ID	EU826007151
Total	0.00 USD

Figure D-1. Copyright license.